STUDY OF SECOND AND THIRD ORDER IONOSPHERIC EFFECT ON GLOBAL POSITIONING SYSTEM (GPS) SIGNALS ALONG THE EQUATORIAL REGIONS

BY:
ASMAMAW CHANIE YEHUN

A Thesis submitted to the school of Graduate studies of Addis Ababa University in partial fulfillment of the requirements for the Degree of Master of Science in Civil Engineering under Geodesy.

Addis Ababa, Ethiopia
April, 2013

Addis Ababa University
Institute of Technology
Department of Civil Engineering

The undersigned here by certify that they have read and recommend to the school of technology for acceptance a thesis entitled “study of second and third order ionospheric effect on global positioning system (GPS) signals along the equatorial regions” by Asmamaw Chanie Yehun in partial fulfillment of the requirements for the degree of Master of Science.

Date: April, 2013

Supervisor/Advisor:

1. _____ _____ _____
   Signature Date

2. _____ _____ _____
   Signature Date

Examiner(s):

1. _____ _____ _____

2. _____ _____ _____

3. _____ _____ _____
   Signature Date

Acknowledgements

First of all, I would like to express my deepest sense of Gratitude to my advisor Dr Adisu Hunegnaw. It is a privilege to work with him; his contribution to the overall results of the thesis and other technical and computational helps was tremendous. He was very friendly too.

Secondly, I would like to express my sincere gratitude to Dr. - Ing Elias Lewi and Dr Robert King. Their advises and scientific support was unforgettable.

Thirdly, I would like to express my many thanks to all Institute of Geophysics Space Science and Astronomy (IGSSA) staffs. Because they have good cooperation, positive thinking and they were helping me a lot during the thesis work.

I am very pleased to take this opportunity to express lovely gratitude from the deep of my heart to my beloved Simret Demeke for her love and moral support. Thank you Simret, my life couldn't have been as I wanted without you.

At last but not least, I want to expresses my gratefulness to my colleagues and friends Kibrom Ebuy and to all my classmates. Their friendship besides their scientific discussions was memorable.

Abstract

Ionosphere is the major source of error for geodetic applications despite the fact that it's possible to remove most of the effect using its dispersive nature. However, it's only the first order of the ionospheric effect that can be removed using dual frequencies signal observations. The second and third order ionosphere effect cannot be removed though we can model their effects on geodetic applications such as their effects on Global Positioning System (GPS) signals. The study mainly focuses on the assessment of higher order (second and third) ionosphere effects on GPS for accurate positioning along the equatorial regions. Some stations at higher latitudes were also included in our GPS data processing for comparison purposes. GAMIT/GLOBK software was used to process the GPS data including a suite of other ancillary information.

The time series of the residuals from the final GAMIT/GLOBK result were compared with the geomagnetic field effects and solar cycle (sunspot activities). High ionopheric effects on the GPS signals from stations along the equator were observed relative to stations at higher latitudes due to the fact that total electron content density is high along the equator. In addition to this, the contribution of Equatorial Electrojet (EEJ) to ionospheric disturbances is higher along the equator. Higher total electron content was also observed for the stations from the equatorial region in particular on years 2002 and 2012 as these are the years where solar activity were at maximum.

Keywords: GPS, Higher order ionosphereic effects, Total electron contents density, Geomagnetic field

Contents

Abbreviations

AFS	Atomic Frequency Standard
A-S	Anti-spoofing

ASCII	American Standard Code for Information Interchange
BIPM	Bureau of Weights and Measures
C/A	Coarse/Acquisition
CDMA	Code division multiple access
CHAMP	Challenging Minisatellite Payload (mission)
CME	Coronal Mass Ejections
CODE	Center for Orbit Determination in Europe
DoD	Department of Defense
DOP	Dilution of Precision
ECEF	Earth Center Earth Fixed
EEJ	Equatorial ElectroJet
EGNOS	European Geostationary Navigation Overlay Service
EOP	Earth Orientation Parameter
GAMIT	GPS Analysis Massanchusset Institute of Technology
GDOP	Geometric Dilution of Precision
GGSP	Galileo Geodetic Service Provider
GIM	Global Ionosphere Map
GLONASS	Global'naya Navigatsionnaya Sputnikovaya Sistema (Global Navigation Satellite System)
GNSS	Global Navigation Satellite System
GPS	Global Positioning System
GPS_TEC	GPS Total Electron Content
GST	Galileo System Time
GTRF	Galileo Terrestrial Reference Frame
HDOP	Horizontal Dilution of Precision
IAG	International Association of Geodesy

ICAO	International Civil Aviation Organization
IERS	International Earth Rotation Service
IF	Ionosphere free
IGS	International GNSS (formerly GPS) Service for Geodynamics
IMO	International Maritime Organization
IRI	International Reference of Ionosphere
ITRF	International Terrestrial Frame
JD	Julian Date
JPL	Jet Propulsion Laboratory
JPO	Joint Program Office
LEO	Low Earth Orbit (satellite)
MSAS	Multi-functional Satellite Augmentation System
MM	Milimeter
NASA	National Aeronautics and Space Administration
NAVSTAR	Navigation System with Timing and Ranging
OS	Open Service
PDOP	Position Dilution of Precision
PE-90	Parameter of the Earth 1990
PPP	Precise Point Positioning; public-Private Partnership
PPS	Precise Positioning Service
PRN	Pseudo-Random Noise Sequences
PZ-90	Parametry Zemli 1990
QC	Quality Control
RINEX	Receiver Independent Exchange (format)
RMS	Root Mean Square
SINEX	Software Independent Exchange (format)

SPS	Standard Positioning Service
TDMA	Time Division Multiple Access
TDOP	Time Dilution of Precision
TDT	Terrestrial Dynamic Time
TEC	Total Electron Content
TECU	TEC Units
TVEC	Total Vertical Electron Content
UV	Ultra Violet
VDOP	Vertical Dilution of Precision
VLBI	Very Long Baseline Interferometry
WAAS	Wide Area Augmentation System
WGS-84	World Geodetic System 1984

Chapter One

1. Introduction

1.1. Background

The Global Positioning System is the responsibility of the Joint Program Office (JPO), a component of the Space and Missile Center at El Segundo, California. In 1973, the JPO was directed by the US Department of Defense (DoD) to establish, develop, test, acquire, and deploy a space borne positioning system. The present navigation system with timing and ranging (NAVSTAR) Global Positioning System (GPS) is the result of this initial directive. GPS was conceived as a ranging system from known positions of satellites in space to unknown positions on land, at sea, in air and space. Satellite signal is continually marked with its (own) transmission time and the position of the satellite. Using this information from four satellites observed simultaneously, the observer can determine his instantaneous position and the time of the receiver clock.
The original objectives of GPS were the instantaneous determination of position and velocity (i.e., navigation), and the precise coordination of time (i.e., time transfer). A detailed definition is given by W. Wooden (1985).

"The NAVSTAR Global Positioning System (GPS) is an all-weather, space based navigation system under development by the Department of Defense (DoD) to satisfy the requirements for the military forces to accurately determine their position, velocity, and time in a common reference system, anywhere on or near the earth on a continuous basis." Since the DoD is the initiator of GPS, the primary goals were military ones.

But the US Congress, with guidance from the President, directed the DoD to promote a civilian use. This was greatly accelerated by the production of a "portable" codeless GPS receiver for geodetic surveying that could measure short baselines to millimeter accuracy and long baselines to one part per million (ppm). This instrument developed by C. Counselman and trade-named the Macrometer Interferometric Surveyor was in commercial use at the time the military was still testing navigation receivers so that the first productive application of GPS was to establish high-accuracy geodetic networks (Hofmann-Wellenhof et al., 2008).

The global positioning system is an all-weather navigation system; it provides three-dimensional positions and velocities on a 24-hour-per-day basis all around the world. The space segment consists of 24 satellites having a circular orbit and an orbital period of 12 hours. The satellites are being constantly tracked by a globally monitored network; the control center is located at the Falcon Air Force Station at Colorado Springs. The satellites carry an atomic frequency standard to generate a stable signal. They transmit at the frequencies

L1 = 1575.42 MHz and L2 = 1227.6 MHz. These carriers are modulated with two codes generally referred to as the coarse/acquisition (C/A) code and the precision (P) code. In addition, a navigation message is transmitted that allows the user to compute the position of the satellite as a function of time. GPS has been used by civilians since about 1983. Its use was, however, limited by the lack of sufficient numbers of satellites available at a given time. Because the constellation is completed, this bottleneck for the popularization of GPS is becoming less of a problem. The most simple navigation solution, i.e., determining one's three-dimensional position on the earth's surface, requires that four satellites be visible. This requirement, in addition to the 24 hour per day and worldwide coverage, determine the parameters of the orbital constellation. GPS has many characteristics that make it attractive to both the navigator and the engineer. Whereas the navigator might be interested in positional accuracy typically in the range of tenths of meters, the engineer is often looking for relative position accuracy in terms of centimeters and better. Fortunately, transmissions at the frequency of L1 and L2 penetrate the ionosphere very well. The ionospheric delay on the codes is proportional to the inverse of the frequency squared. Because the satellites circle the earth at about 20 000 km above ground, the impact of the variations in the earth's gravitational field on the orbital motions can be computed fairly accurately (Alfred Leick, 1992).

The ionosphere delay is also directly correlated to the sun spot activity which has maximum on an 11 period cycle.

1.2. Literature review

The Ionosphere is a shell of electrons and ionized atoms and molecules that envelops the earth and covers the part of the atmosphere between 50 – 1000 kilometers. The existence of the ionosphere is due to the radiation energy that comes from our sun. The radiation energy that hits the upper atmosphere breaks the atoms and resulted in large quantities of ionized atoms. These free floating ions in the ionosphere affect the propagation of radio waves by altering the refractive index of the atmosphere. Depending on the particular frequency of the radio waves the effect can be large or small on the propagation speed as the signal tries to pass through the ionosphere. For instance a radio wave with a frequency of 30 MHz the ionosphere basically stops this frequency range and acts like a mirror. As the frequency of the radio signal gets larger the propagation effect gets smaller. For GPS signal with a frequency range of 1.2 to 1.5 GHz the effect is minimal nevertheless not small and becomes larger as the number of free floating ions increases in the ionosphere. The developers of GPS system have understood the effect of ionosphere before the launch of the GPS satellite into the heaven and introduced two frequencies in order to make a linear combination possible of different signals that can minimize the effect of the ionosphere on the position measurements (see eg. Hofmann-Wellnhof et al., 2008).

However, a single frequency GPS user do not have the luxury to cancel most of the effect but rather have to rely on an ionosphere model such as Klobuchar (2001).

Previous works related to ionospheric effect on GPS signals shows the effect of ionosphere is high among other sources of errors and a number of studies have been carried out to model these effects. According to Z. G. Elmas et al (2011) for layered structure of the ionosphere; they account for the influence of the geomagnetic field on the refractive index of the (anisotropic) ionosphere and some may neglect the differential (frequency and satellite elevation angle dependent) bending effect on the GNSS signals. Different authors consider these concepts differently to estimate the contribution of higher order ionospheric effects to the GNSS error budget. In Wang et al. (2005) a multi-GNSS approach is used to estimate the higher order error terms; and the authors focused on the techniques of eliminating/estimating the ionospheric errors through new linear combinations possible with the new signal frequencies of the modernized GNSS. Kim and Tinin (2007) use perturbation theory to study the residual error in the dual frequency ionosphere free observable; they investigate in particular the 3^{rd} order ionospheric effect (Ion3) term associated with ray bending effect on the GNSS signals penetrating through an inhomogeneous ionosphere. Taking into account that Ion3 term includes not only the quadratic correction due to the refractive index but also the correction for the ray bending effect, they show that the ray bending effect may dominate the 2^{nd} order ionospheric effect (Ion2) error contribution. They consider both the regular large scale and random small scale irregularities in the ionosphere such that the latter can, at times, cause residual error comparable to or greater than that of the Ion2 term, dominating the contribution to the residual error in the ionospheric free (IF) observable. Datta-Brua et al. (2008) show that, unlike the 1st order ionospheric effect (Ion1) term which has the same magnitude but opposite signs for the group and carrier phase measurements, the Ion2 and Ion3 have different magnitudes and signs for these two types of measurements. For this reason, the authors claim that the higher order errors accumulate in the carrier smoothing of the IF (to the first order) code observable; the authors show that the errors in the carrier-smoothed code measurements are mostly due to Ion2 and Ion3. In other words the unaccounted higher order group errors contribute to the error in the carrier smoothing. Although can be neglected in many applications, these residual errors can be crucial in high precision applications (Petrie, E. J., King, M. A, Moore, P., and Lavallee, D, 2010).

1.3. Statement of the research problem

According to Hofmann-Wellnhof et al. (2008) sources of errors in GPS would be (1) satellite error, like satellite clock biased and satellite orbit error (2) signal propagation error, like Troposphere and Ionosphere errors (3) Receiver error, like receiver clock biased, multi-path error and antenna phase center variations (4) relativistic error. From these sources of errors the ionosphere causes GPS signal delays proportional to the total electron content (TEC) along the path from the GPS satellite to a receiver. Ionosphere effect is dispersive medium, it varies with frequency variation, and the effect also varies due to seasonal variations (summer and winter), Diurnal variations (day and night) and geographical locations. The upper atmosphere is ionized by solar radiation. That means the Sun's energy is so strong at this level, that it breaks apart molecules. So there ends up being electrons floating around and molecules which have lost or gained electrons. When the Sun is active, more and more ionization happens. Because of high sunspot activities along the equator the effect was expected to be high. The effect of ionosphere could be first order which is depends on total electron content density or higher order (second and third order up to infinity order). Second and third order ionosphere effect depends on slant path total electron contents densities, geomagnetic filed and the angle at the ionosphere price point and geomagnetic field. First order ionosphere effect is higher than the higher order ionosphere effect.

1.4. Objectives of the study

The overall goal of the study is to assess second and third order ionosphere effect on GPS signals for accurate positioning along the equatorial regions, especially more focus on ADIS station. Specifically the objectives of the study are,

- To understand the effect of ionosphere on GPS signals for accurate positioning
- Study of sources of errors on GPS signals.
- Study of total electron content density variations on the study areas.
- To see time series of residuals.

The research answered the following questions.

- How much the higher order ionosphere affects GPS derived position?
- What is the use of Global ionosphere map?
- How to mitigate ionosphere effect on GPS derived position?
- How geomagnetic field model could be used in GPS signal processing?

1.5. Organization of the study

Chapter two describes basic concepts, definitions and related review literature regarding ionosphere effect on GPS signals and sources of errors in GPS. Chapter three deals about mathematical models and observation equations of GPS. Chapter four includes data analysis and result of the study. The last chapter which is the fifth chapter it includes conclusion and recommendation.

Chapter Two

2. Basics of Global Navigation Satellite System (GNSS) and the Atmosphere

GNSS presently consists of four main satellite constellations. GPS, Glonass, Compass and Galileo. Each of them consists mainly of three segments: (a) space segment, (b) control segment and (c) user segment (Hofmann-Wellenhof et al**.** 2001).

2.1. GPS over view

2.1.1. Reference system of GPS

Referring to coordinates, the GPS (in section 1.1 see more details for GPS over view) terrestrial reference system is the World Geodetic System 1984 (WGS-84). This geocentric system was originally realized by the coordinates of about 1,500 terrestrial sites which have been derived from transit doppler observations. Associated to this frame is a geocentric ellipsoid of revolution, originally defined by the four parameters: semi-major axis a, normalized second-degree zonal gravitational coefficient $\overline{C}_{2,0}$, truncated angular velocity of the earth ωe, and earth's gravitational constant G. This frame has been used for GPS since 1987. The gravitational coefficient $\overline{C}_{2,0}$, can be expressed by the flattening parameter f, which is defined by the semi-axes of the ellipsoid: $f = \left(\frac{a-b}{a}\right)$.

Table 2-1Parameters of the WGS-84 Ellipsoid

Parameter and Value	Description
a = 6 378 137.0 m	Semi-major axis of the ellipsoid
f = 1/298.257 223 563	Flattening of the ellipsoid
ωe = 7 292 115 * 10^{-11} rad−1S^{-1}	Angular velocity of the earth
G = 3 986 004.418 * 10^{8} m^3 S^{-2}	Earth's gravitational constant

2.1.2. Time system

The time system is based on atomic clock and in satellite geodesy precise information is required on time and frequency. In many cases it is necessary to relate the epochs of some events which are observed at different stations, separated by large distances, with an accuracy of ±1 microsecond (1μs).

The performance of frequency standards must reach a stability of up to 1×10^{-15} seconds over several hours. These high demands can only be fulfilled with atomic clocks. The most important component of a clock is an oscillating system (oscillator). The following classes of oscillators are in use: precision quartz crystal oscillator, rubidium standard, cesium standard, and hydrogen maser.

Precision quartz crystal oscillators are completely sufficient as time generators in satellite receivers when they are continuously controlled and updated by external signals, for example by the time and frequency signals from satellites. Characteristic features of the quartz oscillators are that they are quite sensitive to temperature variations and those they are prone to a rather strong ageing process. In practice, it is of importance that the quartz runs in stable temperature conditions and without interruptions or other disturbances. The frequency stability per day may range from 10^{-9} to 10^{-13} second (s).

The characteristic feature of the rubidium frequency standard is its excellent long term stability. A rubidium standard can be used as an external oscillator for GPS observations, in particular to bridge periods with insufficient satellite coverage. A rubidium clock can reach a stability of 1×10^{-13} s per day under the best conditions.

The cesium frequency standards, because of their high short- and long-term stability, can be regarded as the atomic clocks “par excellence”. Assembled in groups, they form the core of time laboratories, and they are also present in fundamental satellite observation stations, in tracking stations for orbit control, or in laser ranging systems.

The time base in the GPS satellites is realized through cesium and rubidium standards. Cesium standards are transportable, and commercially available. Laboratory cesium beam standards can realize the second with an accuracy of 1.5×10^{-14}. Commercially available standards are less accurate, but may equal the stability of laboratory standards for periods up to about 1 year (Seidelmann et al., 1992).

Hydrogen masers are necessary to meet the highest accuracy demands, such as those required by Very Long Baseline Interferometry (VLBI). A frequency stability $\sigma \left(\frac{\Delta f}{f} \right)$ of 10^{-15} is required over time periods of 10^{2}

to 10^5 seconds. Hydrogen masers are very sensitive, and to date have only been operational under laboratory conditions (Seeber, 2003).

GPS atomic time system is referenced to coordinated universal time (UTC) as maintained by the US Naval observatory (USNO). Nominally the GPS time has a constant offset of 19 seconds with TAI, the international atomic time,

TAI = GPS time + 19.000^s (2.1)

Starting at the GPS standard epoch, the system time of GPS is counted in terms of GPS weeks and seconds within the current week. For the calculation of the GPS week,

WEEK = INT [(JD − 2 444 244.5)/7] (2.2)

Where JD indicates the Julian Date and INT is an integer operator.

2.1.3. GPS services

For point positioning and timing, GPS provides two levels of service: the standard positioning service (SPS) with access for civilian users and the precise positioning service (PPS) with access for authorized users. The SPS may be controlled by the joint program office by applying selective availability and anti-spoofing to deny the full system accuracy to nonmilitary users. GPS information services provide GPS status information, orbital and other data to the civilian users.

2.2 GLONASS

The abbreviation GLONASS derives from the Russian “Global’naya Navigatsion- naya Sputnikovaya Sistema”, translated to its English equivalent, this means Global Navigation Satellite System. In the mid 1970s, the former Union of Soviet Socialist Republics (USSR) initiated the development of GLONASS based on the experiences with the Doppler satellite system. As defined in the GLONASS interface control document released by the Co- ordination Scientific Information Center (2002), the purpose of GLONASS is to provide an “unlimited number of air, marine, and any other type of users with all weather three-dimensional positioning, velocity measuring and timing anywhere in the world or near-earth space”. On a continuous basis, meaning at any time, should be added.

2.2.1. Reference systems

The GLONASS terrestrial reference system is denoted as PE-90 (sometimes also PZ-90). The first abbreviation derives from “Parameters of the Earth 1990” and the second from its respective translation into Russian “Parametry Zemli 1990”. As specified in Roßbach (2001: p. 7), originally the Soviet Geodetic

System 1985 (SGS-85) was employed, which was later changed to the Soviet Geodetic System 1990 (SGS-90) based on the same definition. For the sake of completeness, Roßbach (2001: p. 7) mentions that for a short period the acronym SGS was changed from Soviet Geodetic System to Special Geodetic System.

As given in Coordination Scientific Information Center the reference frame as background of the PE-90 system is defined in the following way: the origin is located at the center of the earth; the Z-axis points to the conventional terrestrial pole as recommended by the International Earth Rotation Service (IERS); the X-axis results from the intersection line of the equatorial plane with the plane represented by the Greenwich meridian; the Y-axis completes a right-handed coordinate frame. Thus, the realization of the PE-90 reference frame is a geocentric system. Recall that the Cartesian coordinates related to the geocentric system are also denoted ECEF coordinates. For the realization, 26 ground stations were established from observations to a geodetic satellite, Doppler measurements, laser ranging, and satellite altimetry; also electronic and laser range measurements of GLONASS and Etalon satellites are included (Boucher and Altamimi 2001).

Associated to the PE-90 is a geocentric ellipsoid of revolution which is completely determined by four parameters. As defined in Coordination Scientific Information Center (2002: p. 16).

Table 2-2 Parameters of the PE-90 ellipsoid

Parameter and Value	Description
a = 6 378 136 m	Semi-major axis of the ellipsoid
f = 1/298.257 839 303	Flattening of the ellipsoid
ωe = 7 292 115 * 10^{-11} rad−1S^{-1}	Angular velocity of the earth
μ = 3 986 004.4 * 10^{8} m^3 S^{-2}	Earth's gravitational constant

2.2.2. Time system

The time system is maintained by the GLONASS central synchronizer using a set of hydrogen masers (Roßbach 2001: p. 31). The GLONASS time is closely related to the UTC but has a constant offset of three hours reflecting the difference between Moscow time and Greenwich Time. This relation implies leap seconds for the GLONASS time. Apart from the constant offset, the difference between GLONASS time and UTC shall be within 1 millisecond (Coordination Scientific Information Center 2002) arising from the keeping of the time scales by different clocks. The navigation message contains the information on this difference by the parameter τ_c. Thus, UTC can be computed from GLONASS time by,

UTC = GLONASS time + $\tau_c - 3^h$ (2.3)

The relation between UTC and TAI, the international atomic time, is given

TAI = TDT $- 32.184^s$ constant offset, Where TDT is Terrestrial dynamic time (2.4)

TAI = UTC + 1.000^s n where n is integer value variable offset as leap seconds are substituted (2.5)

2.2.3. GLONASS services

A few details on the signals are necessary here to understand the GLONASS services. Each GLONASS satellite continuously provides navigation signals: the standard-accuracy signal, i.e. the C/A-code (also denoted as S-code), and the high accuracy signal, i.e., the P-code, in two sub bands of the L-band, denoted as G1 and G2. Note that this denotation enables a better distinction from the GPS carriers L1 and L2. However, in the literature sometimes L1 and L2 are also used for GLONASS. The C/A-code is modulated onto G1 only, whereas the P-code is modulated onto G1 and G2. In the course of modernization of GLONASS, a standard accuracy signal has been added on G2 in the GLONASS-M satellites. The C/A-code of GLONASS has an effective wavelength of about 600 m and the respective value of the P-code is about 60 m.

Standard positioning service: "standard positioning service" is not an official notation. Other terms used are "standard accuracy positioning service" (United Nations 2004: p. 19), "lower accuracy service" and "GLONASS civil accuracy" (Feairheller and Clark 2006: p. 611), or the general term "GLONASS performance" (Roßbach 2001: p. 29). Talking here now of standard positioning service implies that only the standard accuracy signal the C/A-code is available. It is important to note that there are no standardized values for the standard positioning service.

A generic remark is found reading: "This GLONASS system provides accuracy that is better than GPS with SA on and worse than GPS with SA off." This translates to about 13 m ≤ horizontal error ≤ 100 m and 22 m ≤ vertical error ≤ 156 m (95% probability).

Precise positioning service: Again, this is not an official denotation. Talking here now of precise positioning service implies that the high-accuracy signal the P-code is available which a military signal is even if the P-code is on the one hand not encrypted, but it has on the other hand not been officially released. Furthermore, the Russian Ministry of Defense does not recommend its unauthorized use. There is not much known about the precise positioning service. Essentially, the same military arguments as given in for the United States in favor of the GPS precise positioning service will apply for Russia and the GLONASS precise positioning service but are not repeated here.

Anti-spoofing (A-S), which means to “turn off” the P-code or invoke an encrypted code as a means of denying access to the P-code to all but authorized users might be an issue. So far no activation of A-S is reported. However, since the P-code may be changed without prior notice to unauthorized users, the option of activating A-S is available.

2.3. Galileo

Europe early recognized the strategic, economic, social, and technological importance of satellite-based navigation. A European strategy and major actions in the field of satellite positioning and navigation have become necessary to establish trans-European networks in the fields of transport, telecommunications, and energy infrastructures in accordance with the European Community (EC) treaty (European Council 1994).
In 1994, the European Council requested from the European Commission (European Council 1994) in a resolution to respond to the challenges of information technology and take necessary initiatives to contribute to satellite navigation. Europe envisaged a two-step approach: the first step headed for the augmentation of the existing first generation GNSS (i.e., GPS and GLONASS). This action finally resulted in the development and deployment of the European geostationary navigation overlay service (EGNOS). In the second step, the European Union (EU) requested to “initiate and support the preparatory work needed for the design and organization of a global navigation satellite system for civil use”.

At the same time the European Council fostered the need to cooperate with the private sector for cost and risk sharing whilst maximizing the benefits. Europe also emphasized the need to closely cooperate with the International Civil Aviation Organization (ICAO) and the International Maritime Organization (IMO) in order to develop and implement a system in accordance with international standards. The EU headed at first for a close cooperation with the US in the development of the next-generation GPS and an active participation in the control and development of it. Negotiations with the US revealed the interest of both parties in a cooperation but also brought up the reservations of the US. GPS has always been considered as safety-critical infrastructure. A participation of foreign countries in the definition and control of GPS was not acceptable for the US. Europe, in contrast, headed for a maximum of control to guarantee its own sovereignty, autonomy, and competitiveness. Europe also considered too closely cooperate with Russia but finally took the decision to develop its own GNSS.
In 1999, the European contribution to satellite navigation has been provisionally named Galileo, but meanwhile Galileo has become the synonym for the European GNSS. As a matter of fact, Galileo is not an acronym. The European satellite navigation system has been named after the Italian scientist and astronomer

Galileo Galilei (1564–1642). In 1610, he discovered the first four satellites of the planet Jupiter, later named Io, Europa, Ganymede, and Callisto. Galileo Galilei furthermore described how the regular movement of the four satellites could be used for longitude determination by observing their eclipses.

2.3.1 Reference systems

Referring to coordinates, Galileo relies on a geocentric Cartesian reference frame as defined by the Galileo terrestrial reference frame (GTRF). GTRF will be related to the international terrestrial reference frame (ITRF), which has been established by the International Earth Rotation Service (IERS) (Hein and Pany 2002). The GTRF is specified to differ from the latest version of ITRF by no more than 3 centimeters (2σ). This will be ensured by the Galileo geodetic service provider (GGSP). Furthermore, the GGSP is responsible for the involvement of the geodetic community during the definition, implementation, and maintenance of GTRF (Swann 2006).

2.3.2. Time system

The Galileo system time (GST) is a continuous atomic time scale with a nominal constant offset (i.e., integer number of seconds) with respect to the international atomic time (TAI). With respect to the coordinated universal time (UTC), the modulo 1 second offset is variable due to the insertion of leap seconds.
GST will be maintained by an ensemble of atomic frequency standards (AFS), where active hydrogen maser clocks will serve as the master clock (Hahn 2005). Galileo will use the steering correction parameters provided by an external time service provider in order to steer GST towards TAI. Therefore, the external time service provider will interface to the International Bureau of Weights and Measures (BIPM), which maintains UTC time.

2.3.3. Galileo services

Europe has chosen a service-oriented approach for the design of Galileo. During the definition phase, the user requirements have been categorized into four different service levels. (1) The satellite-only service relies solely on the signals from the Galileo satellites. This service will be available worldwide and independent from other systems. (2) Enhancing the performance of the satellite-only service by local augmentation or assistance information is summarized by the Galileo locally assisted services. (3) The EGNOS service concentrates on the combined use of Galileo and a future evolution of EGNOS to provide a maximum of integrity.

(4) Finally, the combined-service level describes the use of Galileo in combination with other GNSS or other means of navigation systems.

Open and commercial service; The open service (OS) is accessible to all users free of charge. Since no integrity information is included and therefore no service guarantee or liability provided, the receiver may apply RAIM techniques to derive integrity information. The OS is primarily intended for the mass market providing simple positioning and timing services. Six unencrypted signals are modulated onto three different carrier frequencies to provide a competitive navigation service compared to other GNSS. The usage of several signals and frequencies increases the performance and interference resistance but at the same time increases technological requirements, if these advantages want to be exploited. The frequency bands partly overlap with the frequency bands of other GNSS to increase compatibility and interoperability. Galileo single-frequency receivers will provide a performance comparable to GPS C/A-code receivers.

The commercial service (CS) is intended to generate a revenue stream for the GOC. Therefore, the CS will rely on data included in the navigation message in all frequency bands. The data messages will be encrypted and broadcast with a data rate of up to 500 bits per second providing an added value compared to the OS. Additionally, a service guarantee is envisaged for the CS. The access to the data message as well as to the encrypted ranging data will be controlled by the Galileo concessionaire. The Galileo ground segment will provide an interface to external service providers in order to forward any information from them to the users via the satellite signal.

2.4 Compass

The People's Republic of China carries out space activities since the 1970s, when it started its first satellite. The idea of satellite navigation has been pursued since the early 1980s, following a regional system concept similar to the one proposed and build by the US GEOSTAR Corporation. The concept foresees two geostationary satellites to determine position in a two-way ranging method. In 1989, two communication satellites have been successfully used for first tests under the Twin-Star program. In 1993, China decided to implement an independent navigation system called Beidou. The name Beidou denotes the seven-star constellation also known as Ursa Major, Great Cart, or Big Dipper. This constellation has been used for centuries to identify the star Polaris, which indicates the north direction on the northern hemisphere.

Little official information is publicly available about Beidou. Interface specification documents are not provided, therefore most of the system parameters are still to be considered preliminarily. A two-step approach has been chosen for the development of Beidou. In its first step, Beidou-1, the regional system concept of the Twin-Star program has been realized. In a second step, the satellites of Beidou-1 should have

been complemented by a number of additional satellites to provide higher performances. Various design options have been studied for Beidou-2, incorporating geostationary as well as medium earth orbit (MEO) satellites. Meanwhile, China extended its original concepts by planning to gradually build up its own global system like GPS, GLONASS, and Galileo.

Beidou-2 will be a global passive one-way downlink ranging system. In its first development step, it will provide service to China and parts of neighboring countries by 2008. In the latest iteration of the Beidou system, referred to as Compass, the Chinese navigation satellite system will provide global coverage.

Beidou-2 will be a dual-use system. The civilian open service is designed to provide position accuracy of 10 m, velocity accuracy of 0.2 ms^{-1}, and timing accuracy of 50 ns. No detailed performance parameters have been published for the authorized service. However, it has been announced that it will provide a higher integrity level (Hofmann-Wellenhof et al**.,** 2001).

2.5. Sources of errors in GNSS

Apart from the inaccuracy of the clock in the GPS receiver, there are other factors that affect the quality of the GPS signal and cause calculation errors. These are ionosphere and troposphere disturbances. These cause the satellite signal to slow down as it passes through the atmosphere. However, the GPS system has a built in model that accounts for an average amount of these disturbances. Signal reflection the signal hits and is reflected off objects like tall buildings, rocks etc. This causes the signal to be delayed before it reaches the receiver. Ephemeris errors: Ephemeris errors are also known as orbital errors. These are errors in the satellite's reported position against its actual position. Clock errors: The built in clock of the GPS receiver is not as accurate as the atomic clocks of the satellites and the slight timing errors leads to corresponding errors in calculations. Visibility of Satellites: The more the number of satellites a GPS receiver can lock with, the better its accuracy. Buildings, rocks and mountains, dense foliage, electronic interference, in short everything that comes in the line of sight cause position errors and sometimes make it unable to take any reading at all. GPS receivers do not work indoors, underwater and underground. Satellite Shading: For the signals to work properly the satellites have to be placed at wide angles from each other. Poor geometry resulting from tight grouping can result in signal interference. Intentional degradation: This was used till May 2000 by the US Department of Defense so that military adversaries could not use the GPS signals. This has been turned off since May 2000, which has improved the accuracy of readings in civilian equipment (www.roseindia.net/software-tutorials/detail/19656).

2.6 Atmospheric Errors

Atmospheric errors are the most significant source of errors of GPS. With the satellites orbiting at about 20,000km above the earth, the GPS signals have to travel through the ionosphere and the troposphere layers before reaching the receiver antenna. Ionosphere is the collective term for the various layers of ionized particles and electrons found at altitudes of 80–250 km in the atmosphere. Ionization is caused primarily by short-wavelength (Xray and ultraviolet) solar radiation during the daytime. Ionospheric activities have the biggest impact on GPS accuracy.

2.7 The Earth Atmosphere Layers

The Earth's atmosphere is a mixture of different gases and small particles. The atmosphere can roughly be defined as the region from sea level to about 1000 km altitude above the Earth's surface, where neutral gases can be detected, although traces of atmospheric gases have been detected far into space. 99% of the mass of the atmosphere lies below about 30 km altitude. Above 80 km altitude the atmosphere contains ionized molecules and free electrons.

The Earth's atmosphere can be coarsely subdivided in several concentric spherical layers based on different characteristic features such as temperature, ionization, and propagation. Based on the vertical variation of temperature the Earth's atmosphere is subdivided into four layers: troposphere (from sea level to about 10 km), stratosphere (from 10 km to about 50 km), mesosphere (from 50 km to about 80 km) and thermosphere (from 80 km to about 400 km). In general, the temperature in the troposphere decrease with height and increases in the stratosphere, but decreases again in the mesosphere. In the thermosphere the temperature increases again. Above the thermosphere, the temperature is constant, is the exosphere which gradually merges into space. The exosphere is the uppermost layer of the Earth' atmosphere that the particles can escape to space.

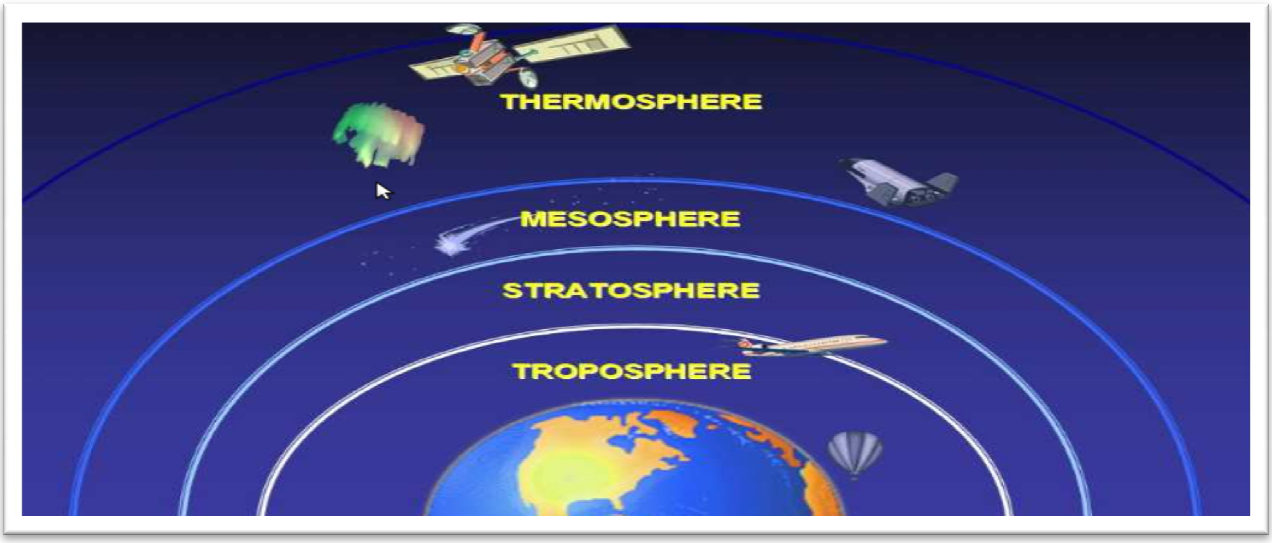

Figure 2-1 Atmosphere layers (**www.srh.noaa.gov/jetstream/atmos/layers.htm**)

The temperature variation through the atmosphere layers is shown in the above figure with respect to signal propagation, the atmosphere is subdivided into two main layers of troposphere (also referred to as neutral atmosphere) and ionosphere. The troposphere, the lower part of the atmosphere, extends from the sea level to about 40 km which is non-dispersive medium (the propagation delay is not frequency dependent). In the troposphere, signal propagation depends mainly on the water vapor content and on temperature. The ionosphere, the upper part of Earth's atmosphere, is a dispersive medium which starts about 50 km altitude. In the ionosphere, signal propagation is mainly affected by free charged particles (Memarzadeh, Y. 2009).

2.8 Ionospheric Error

The effects of the ionosphere generally change slowly, and can be averaged over time. Therefore, any particular geographical area the ionospheric effect can be easily calculated by comparing the GPS-measured position to a known surveyed location. This correction is also valid for other receivers in the same general location. Several systems send this information over radio or other links to allow L1-only receivers to make ionospheric corrections. The ionospheric data are transmitted via satellite in Satellite Based Augmentation Systems (SBAS) such as Wide Area Augmentation System (WAAS) (available in North America and Hawaii), EGNOS (Europe and Asia) or Multi-functional Satellite Augmentation System (MSAS) (Japan), which transmits it on the GPS frequency using a special pseudo-random noise sequence (PRN), so only one receiver and antenna are required (http://en.wikipedia.org/wiki/Error_analysis_for_the_Global_P) .

The ionosphere is electrically charged component of the higher atmosphere. It is characterized by its free, neutral, and charged particles, where diversity varies as a function of the time of day. The ionosphere is categorized into several layers, in particular into *D*, *E*, and *F* in ascending height order. The maximal electron density can be found in the *F*2-layer. The ionospheric delay typically ramps up rapidly around 10 hr local times and peaks around 14 hr local time (Hofmann-Wellenhof B, Lichtenegger, 2008).

2.8.1. The D-Layer

The D-layer is found between 50 to 90 km; Pressure: 2Pa; Temp.: -76° C; electron concentration: $10^7 - 10^{10}\ \frac{e^-}{m^3}$

Characteristics: D layer ionization is a function of the solar flow. The ions are formed by the ionization of atmospheric neutrals by X-ray radiation and solar Lyman α radiation. This region vanishes at night due to the combination of the ions and electrons. HF radio waves are not reflected by this region, the main impact of which is absorption of high-frequency radio waves.

2.8.2. The E-Layer

The E-layer is found beteween 90 to 150 km; Pressure: 0.01Pa; Temp.: -50° C; electron concentration: $10^{11}\ \frac{e^-}{m^3}$

Characteristics: Similarly to the D layer, the E layer shows a diurnal behavior with a maximum of ionization at local noon. In this region, ions consist primarily of O^+ produced by the absorption of solar radiation, and NO^+ formed by charge transfer collisions with other ions ionized by coronal X-rays. In aurora region, solar particle precipitation can produce radio scintillation effects in the E layer.

2.8.3. The F-Layer

The F-layer is found between 150 to 1000 km; Pressure: 4-10 Pa; Temp.: 1000° C; electron concentration: $10^{11}\ \frac{e^-}{m^3}$

Characteristics: This layer is formed by ionization of atomic oxygen by Lyman emissions and emissions from Helium (He). This region is sometimes divided into F1 and F2 sub-layers. The maximum electron concentration of the F1 region is close to 150 - 200km. This layer, in which O^+ ions transfer charge to neutrals to form NO^+, disappears at night due to dissociative recombination. F2 layer is found from 200 to

1000 km and the peak of the F2 layer electron concentration is at approximately 350km. during the night F1 and F2 layers become F layer. In this layer, O+ remains the principal ion species. The F layer is the most important part of the ionosphere in terms of HF communications.

2.9 Satellite Geometry and Orbit error

Since a receiver uses trilateration from the GPS signals to determine its location on the earth, the better the geometry of the satellites in the sky, the better (neater) the trilateration result. The effect of the satellite geometry on the position error is called Dilution of Precision, commonly referred to as DOP. A GPS receiver constantly computes a DOP value based on the satellites being used for the computation of the position (or fix). The better the geometry (satellites properly spread in the sky), the lower the DOP value. With all satellites confined in one part of the sky or blocked by buildings, mountains, etc, the geometry will be poor and the computed DOP value will be high. HDOP, VDOP, PDOP, TDOP and GDOP are respectively Horizontal, Vertical, Position (3D), Time and Geometric Dilution of Precision. There is no fixed indication of what is considered a “good” or “bad” DOP. Knowing that the ideal DOP value is 1, different applications will require different accuracies and allow higher DOP fixes. Usually, 1 to 2 is excellent, 3 to 4 is good, 5 to 7 is fair and 8 and above is poor. But forestry companies, requiring only about 5m accuracy and increased productivity will work with PDOP’s as high as 8-12.

Differential correction will not compensate for DOP errors. Instead, since the DOP is computed by the receiver, most GPS software will offer filters to prevent operation or recording when the DOP reaches a preset value.

GPS satellites carry very accurate atomic clocks and follow very precise orbits. But drifts in both clock and orbit are inevitable and very small amount can cause significant errors in a receiver on the ground. Even though their clocks and orbits may not be adjusted, their offsets are computed by the GPS Ground Segment then sent back to the satellites. The satellites then broadcast the clock and ephemeris message to the end-user. There is some latency between the actual occurrence of the offsets and the time they are computed and broadcasted.

International GPS Service for Geodynamics: International service of the IAG (International Association of Geodesy) is Coordinates data archiving and processing of a global control network of dual-frequency permanent GPS stations test campaign in 1992, routine operations since 1994. It provides precise GPS satellite orbits to the scientific community, Satellite clock corrections, Earth rotation parameters; Precise coordinates of control stations and Atmospheric parameters.

2.10 Multipath

Multipath phenomenon that results in radio signals reaching the receiving antenna by two or more paths. Causes of multipath include atmospheric ducting, ionospheric reflection and refraction, and reflection from water bodies, mountains, trees and buildings. Differential correction will not compensate for multipath errors. Certain precautions will minimize GPS antenna sensitivity to these reflected signals, like operating away from large reflective structures such as buildings. A high-end receiver/antenna combination will be more robust in rejecting multipath, whereas a consumer-level receiver will tolerate a higher amount of multipath.

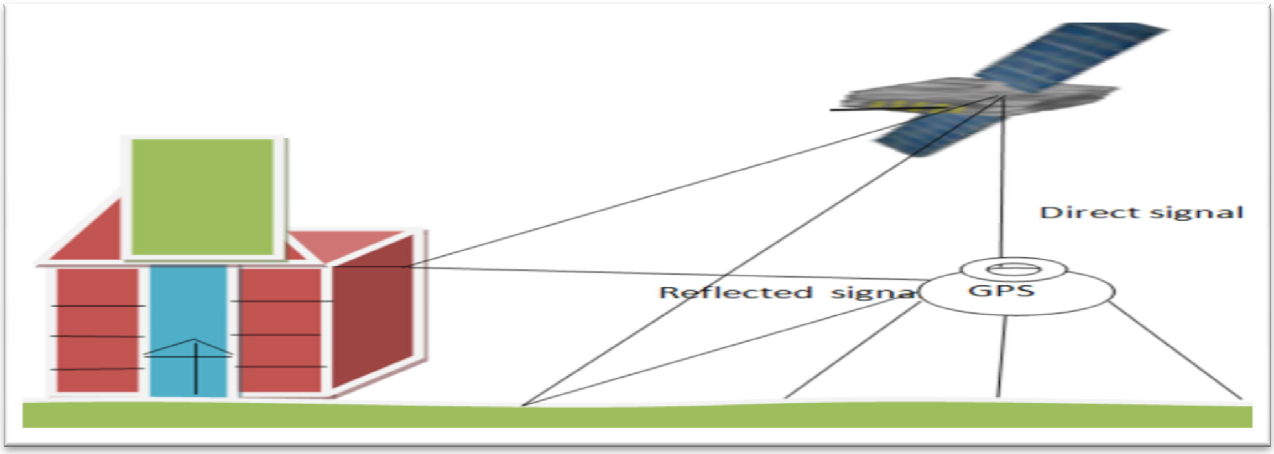

Figure 2-2 Multi-path effect plot

2.11. Sources of User Equivalent Range Errors (UERE)

The term user equivalent range error (UERE) refers to the error of a component in the distance from receiver to a satellite. These UERE errors are given as ± errors thereby implying that they are unbiased or zero mean errors. These UERE errors are therefore used in computing standard deviations. The standard deviation of the error in receiver position is computed by multiplying PDOP (Position Dilution of Precision) by, the standard deviation of the user equivalent range errors is computed by taking the square root of the sum of the squares of the individual component standard deviations. User equivalent range errors (UERE) are shown in the table 3. There is also a numerical error with an estimated value, of about 1 meter. The standard deviations, for the coarse/acquisition and precise codes are also shown in the table 2.3. These standard deviations are computed by taking the square root of the sum of the squares of the individual components (i.e., RSS for root sum squares). To get the standard deviation of receiver position estimate, these range errors must be multiplied by the appropriate dilution of precision terms and then root sum squared with the numerical error. Electronics errors are one of several accuracy-degrading effects outlined in the table 3. When taken together, autonomous

civilian GPS horizontal position fixes are typically accurate to about 15 meters (50 ft). These effects also reduce the more precise P(Y) code's accuracy. However, the advancement of technology means that today, civilian GPS fixes under a clear view of the sky are on average accurate to about 5 meters (16 ft) horizontally.

Table 2-3 User Equivalent Range Errors (UERE)

Source	Effect (m)
Signal arrival C/A	±3
Signal arrival P(Y)	±0.3
Ionospheric effects	±5
Ephemeris errors	±2.5
Satellite clock errors	±2
Tropospheric effects	±0.5
Multipath distortion	±1
C/A	±6.7
P(Y)	±6.0

(http://en.wikipedia.org/wiki/Error_analysis)

2.11. The Sun

The Sun is the largest object in the solar system. The Sun with a radius of 696 000 km contains more than 99.8% of the total mass of the solar system. The Sun is composed mainly of hydrogen and helium. The Sun emits huge amounts of energy and mass (roughly 4×10^{33}erg/sec) that is produced by nuclear fusion reactions (Hydrogen converted to Helium + gamma rays) in its interior. The Sun consists of the solar interior (core), the visible surface (photosphere), the lower solar atmosphere (chromosphere), and outer solar atmosphere (corona). The upper layers of the Sun rotate with an angular velocity which depends on the heliocentric latitude. In the photosphere the rotation is faster at the solar equator. The rotation period at the solar equatorial latitudes is about 27 days. The temperature at the Sun's core is about 15×10^6 Kelvin and decreases toward the Sun' surface. Temperature in the photosphere is about 5800 K, but there are regions with lower temperature (4000 K) which are seen by observers on the Earth as dark sunspots (Memarzadeh, Y., 2009).

2.12 Solar cycle and causes of Solar Cycle

The solar cycle (or solar magnetic activity cycle) is the periodic change in the sun's activity (including changes in the levels of solar radiation and ejection of solar material) and appearance (visible in changes in the number of sunspots, flares, and other visible manifestations). Solar cycles have duration of about 11 years. They have been observed (by changes in the sun's appearance and by changes seen on Earth, such as auroras) for hundreds of years. Solar variation causes changes in space weather and to some degree weather and climate on Earth. It causes a periodic change in the amount of irradiation from the Sun that is experienced on Earth. It is one component of solar variation, the other being periodic fluctuations.

The solar cycle was discovered in 1843 by Samuel Heinrich Schwabe, who after 17 years of observations noticed a periodic variation in the average number of sunspots seen from year to year on the solar disk. Rudolf Wolf compiled and studied these and other observations, reconstructing the cycle back to 1745, eventually pushing these reconstructions to the earliest observations of sunspots by Galileo and contemporaries in the early seventeenth century. Starting with Wolf, solar astronomers have found it useful to define a standard sunspot number index, which continues to be used today.

Until recently it was thought that there were 28 cycles in the 309 years between 1699 and 2008, giving an average length of 11.04 years, but recent research has showed that the so that the average longest of these (1784–1799) seems actually to have been two cycles, length is only around 10.66 years. Cycles as short as 9 years and as long as 14 years have been observed, and in the double cycle of 1784-1799 one of the two component cycles had to be less than 8 years in length. Significant variations in amplitude also occur. Solar maximum and solar minimum refer respectively to epochs of maximum and minimum sunspot counts. Individual sunspot cycles are partitioned from one minimum to the next.

The basic causes of the solar variability and solar cycles are still under debate, according to (H. Schwentek and W. Elling ,1984)) and (Attila Grandpierre, 2004) researchers suggesting a link with the tidal forces due to the gas giants Jupiter and Saturn, or due to the solar inertial motion (Charvátová I. 2000) and (Charvatova, Hejda ,2008-9). Another cause of sun spots can be solar jet stream "torsional oscillation".

2.13 Solar Flare

A solar flare is a sudden brightening observed over the Sun's surface or the solar limb, which is interpreted as a large energy release of up to 6×25^{10} joules of energy. The flare ejects clouds of the flare prominence electrons, ions, and atoms through the corona of the sun into space. These clouds typically reach Earth a day or two after the event (Menzel, 1970).

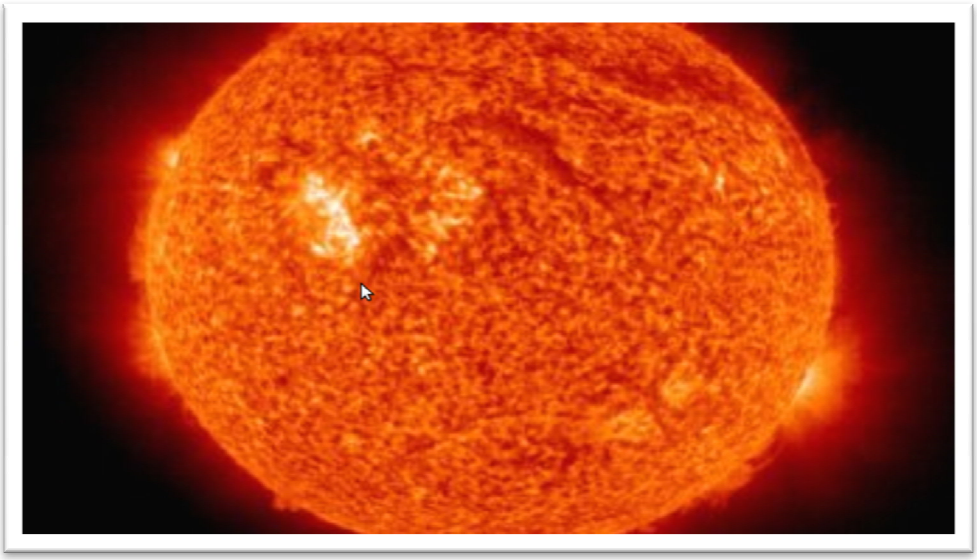

Figure 2-3 Solar Flare (http://en.wikipedia.org/wiki/Solar_flare)

Solar flares affect all layers of the solar atmosphere (photosphere, chromosphere, and corona), when the medium plasma is heated to tens of millions of Kelvin electrons, protons, and heavier ions are accelerated to near the speed of light. They produce radiation across the electromagnetic spectrum at all wavelengths, from radio waves to gamma rays, although most of the energy goes to frequencies outside the visual range and for this reason the majority of the flares are not visible to the naked eye and must be observed with special instruments. Flares occur in active regions around sunspots, where intense magnetic fields penetrate the photosphere to link the corona to the solar interior. Flares are powered by the sudden (timescales of minutes to tens of minutes) Evolution of magnetism on release of magnetic energy stored in the corona. The same energy releases may produce coronal mass ejections (CME), although the relation between CMEs and flares is still not well established.

X-rays and UV radiation emitted by solar flares can affect Earth's ionosphere and disrupt long-range radio communications. Direct radio emission at decimeter wavelengths may disturb operation of radars and other devices operating at these frequencies.

Flares occur when accelerated charged particles, mainly electrons, interact with the plasma medium. Scientific research has shown that the phenomenon of magnetic reconnection is responsible for the acceleration of the

charged particles. On the Sun, magnetic reconnection may happen on solar arcades – a series of closely occurring loops of magnetic lines of force. These lines of force quickly reconnect into a low arcade of loops leaving a helix of magnetic field unconnected to the rest of the arcade. The sudden release of energy in this reconnection is in the origin of the particle acceleration. The unconnected magnetic helical field and the material that it contains may violently expand outwards forming a coronal mass ejection. This also explains why solar flares typically erupt from what are known as the active regions on the Sun where magnetic fields are much stronger on average.

Although there is a general agreement on the flares' causes, the details are still not well known. It is not clear how the magnetic energy is transformed into the particle kinetic energy, nor is it known how the particles are accelerated to energies as high as 10 MeV (mega electron volt) and beyond.

There are also some inconsistencies regarding the total number of accelerated particles, which sometimes seems to be greater than the total number in the coronal loop. We are unable to forecast flares, even to this day (http://www.scientificamerican.com/article.cfm?id=the-mysterious-origins-of).

2.14 Ionospheric scintillations

Ionospheric scintillation is the term given to irregularities in the ionosphere caused by so-called “space weather”. Key sources of ionospheric scintillation include solar winds and magnetic storms. Historically, the level of scintillation has been seen to follow the 11-year solar cycle and peak at the time of maximum sunspot activity. Therefore the past peak was due in 2012 after 2002. Scintillation occurs most frequently at tropical latitudes at night. It occurs less frequently at high latitudes or mid-latitudes. Scintillation has a significant effect of scattering GNSS signals so that a receiver would perceive a satellite as irregularly moving around its actual position. It causes fluctuations in both the amplitude and phase of the carrier. And it is only recently that these effects have been adequately modeled.

High levels of scintillation, such as those experienced during the peak of the solar cycle, have traditionally caused problems for GNSS receivers. However, GNSS receivers can now be tested using newly developed scintillation models available in Spirent's SimGEN software. This means that the latest generations of receivers will be far better equipped to handle the high levels of scintillation due to occur in 2012 (www.spirent.com).

2.15 Geomagnetic or ionospheric storms

Within the earth, there exists a small solid inner core and an electrically conducting liquid outer core that is in steady thermal convective motion. It is believed that the rotation of the earth in combination with this convective motion generates the main part of the geomagnetic field via a dynamo-like mechanism (C.A.Onwumechili, 1997).

Besides the presence charged particles due to photo-ionization, at all times the Sun ejects a stream of high-energy particles, which is known as the solar wind. This solar wind interacts with the geomagnetic field (this may get compressed). Sometimes this charged particle stream increases enormously, caused by explosions(solar flares) which occur at the Sun's "surface". Other enormous particle originates in the Sun's atmosphere, the Corona, and is referred to as Coronal Mass Ejections. Some of these CMEs are able to compress the Earth's magnetic field enormously, causing a so-called geomagnetic storm which may (but do not automatically have to) disturb the ionosphere. When it does disturb the ionosphere, the free electron density may rapidly change. Geomagnetic or ionospheric storms especially occur in the northern auroral regions, lasting for several hours (Klobuchar, 1991).

Earth's field changes over time because it is generated by the motion of molten iron alloys in the Earth's outer core (the geodynamo). The Earth's magnetic field is mostly caused by electric currents in the liquid outer core, which is composed of highly conductive molten iron. A magnetic field is generated by a feedback loop: current loops generate magnetic fields (Ampère's circuital law); a changing magnetic field generates an electric field (Faraday's law); and the electric and magnetic fields exert a force on the charges that are flowing in currents (the Lorentz force) (http://en.wikipedia.org/wiki/Earth's_magnetic_field).

2.16 Geomagnetic regions

The Earth acts like a great spherical magnet, in that it is surrounded by a magnetic field. This magnetic field changes both with time and with location on the Earth and resembles field generated by a dipole magnet (i.e., a straight magnet with a north and South Pole) located at the center of the Earth. The axis of the dipole is offset from the axis of the Earth's rotation by approximately 11 degrees. This means that the north and south geographic poles and the north and south magnetic poles are not located in the same place. The ionospheric electron density has a large dependence on the geomagnetic latitude. The ionosphere may be divided broadly into three regions that have rather different properties and features according to their geomagnetic latitudes: the Equatorial, Mid-latitude, and Polar (or Auroral) regions.

Equatorial region: This region spanning about 20◦ either side of the geomagnetic equator. Due to horizontal geomagnetic field geometry (I = 0◦) at the dip equator, the electromagnetic drift and associated plasma fountain, results in a large variability of the electron density in low latitudes which makes it complication to model.

Mid-Latitude region: The mid latitude region of the ionosphere includes geomagnetic latitudes from about 20◦ to about 60◦. It is out of the direct influence from phenomena associated with the plasma fountain. In this region, only solar photon radiation is responsible for the ionization process and the electron density is generally not affected by the particle radiation. The mid latitude ionosphere is the best understood of all regions.

The day to day changes in the E, F1, and F2-regions show regular variations and little irregular variations associated to changes in the neutral atmosphere density and winds. The peak electron density occurs at the height where three photochemical processes are of comparable importance.

Polar region: The polar region consists of the high latitudes, which are divided in the auroral zone (approximately 60◦-70◦ geomagnetic latitudes) and the polar cap (poleward of the auroral zone). At high latitudes the geomagnetic field runs nearly vertical, and this leads to the existence of an ionosphere that is considerably more complex than that in the middle and low latitudes. This complexity is also because the geomagnetic field lines connect the high latitudes to the outer part of the magnetosphere which is driven by the solar wind, whereas the ionosphere at mid latitude is connected to the inner magnetosphere, which essentially rotates with the Earth and so is less sensitive to external influence. In the mid and low latitude regions, the primary source of ionization is the solar photon radiation, but at high latitudes, solar proton radiation produces additional ionization particularly in the E-region (Yahya Memarzadeh, 2009).

2.17 Geomagnetic field representation and Dynamo theory

At any location, the Earth's magnetic field can be represented by a three-dimensional vector. A typical procedure for measuring its direction is to use a compass to determine the direction of magnetic North. Its angle relative to true North is the declination (D) or variation. Facing magnetic North, the angle the field makes with the horizontal is the inclination (I) or dip. The intensity (F) of the field is proportional to the force it exerts on a magnet. Another common representation is in X (North), Y (East) and Z (Down) coordinates.

The intensity of the field is greatest near the poles and weaker near the Equator. It is often measured in gausses (G) but is generally reported in nanoteslas (nT), with 1 G = 100,000 nT. A nanotesla is also referred to as a gamma (γ). The field ranges between approximately 25,000 and 65,000 nT (0.25–0.65 G).

The inclination is given by an angle that can assume values between -90° (up) to 90° (down). In the northern hemisphere, the field points downwards. It is straight down at the North Magnetic Pole and rotates upwards as

the latitude decreases until it is horizontal (0°) at the magnetic equator. It continues to rotate upwards until it is straight up at the South Magnetic Pole. Inclination can be measured with a dip circle.

Declination is positive for an eastward deviation of the field relative to true north. It can be estimated by comparing the magnetic north/south heading on a compass with the direction of a celestial pole (http://en.wikipedia.org/wiki/Earth's_magnetic_field).

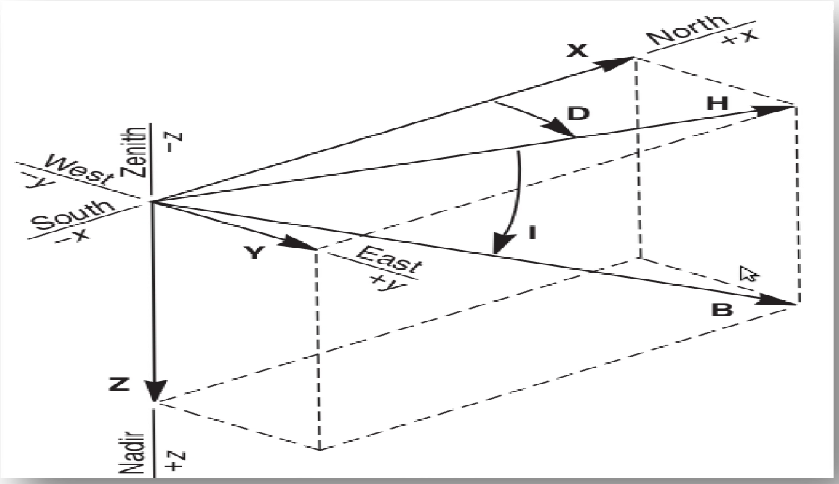

B: total field ($\sqrt{X^2 + Y^2 + Z^2}$)
H: horizontal component
($H = \sqrt{X^2 + Y^2}$)
X: northward component
Y: eastward component
Z: vertical component
D: declination ($tan^{-1}\left(\frac{Y}{X}\right)$)
I: inclination ($tan^{-1}\left(\frac{Z}{H}\right)$)

Figure 2-4 Geomagnetic field Parameters

Dynamo theory proposes a mechanism by which a celestial body such as the Earth or a star generates a magnetic field. The theory describes the process through which a rotating, convecting, and electrically conducting fluid can maintain a magnetic field over astronomical time scales.

This theory is used to explain the presence of anomalously long-lived magnetic fields in astrophysical bodies. The conductive fluid in the geodynamo is liquid iron in the outer core, and in the solar dynamo is ionized gas at the tachocline. Dynamo theory of astrophysical bodies uses magnetohydrodynamic equations to investigate how the fluid can continuously regenerate the magnetic field.

It was actually once believed that the dipole, which comprises much of the Earth's magnetic field and is misaligned along the rotation axis by 11.3 degrees, was caused by permanent magnetization of the materials in the earth. This means that dynamo theory was originally used to explain the Sun's magnetic field in its relationship with that of the Earth. However, this hypothesis, which was initially proposed by Joseph Larmo in 1919, has been modified due to extensive studies of magnetic secular variation, paleomagnetism (including polarity reversals), seismology, and the solar system's abundance of elements. Also, the application of the theories of Carl Friedrich Gauss to magnetic observations showed that Earth's magnetic field had an internal, rather than external, origin. There are three requisites for a dynamo to operate: An electrically conductive

fluid medium, kinetic energy provided by planetary rotation, an internal energy source to drive convective motions within the fluid (E. Pallé, 2010).

2.18 Equatorial Electrojet

In the dayside ionosphere, the neutral winds set up a polarization electric field which usually points into the eastward direction. At the magnetic dip equator, where the magnetic field is exactly horizontal, this electric field has an interesting effect. The resulting upward E x B (E- is Electric field and B- is geomagnetic field) drift of the electrons generates a negative charge at the top and a positive charge at the bottom of the ionospheric E-region (about 90 to 130 km altitude). The resulting electric field prevents the further upward drift of electrons. Instead, they are now propelled westward by the eastward electric field. This westward movement of the electrons constitutes an eastward electric current which is called the Equatorial Electrojet.
The motion of the ions is largely inhibited at this altitude, due to their collisions with the neutral gas.

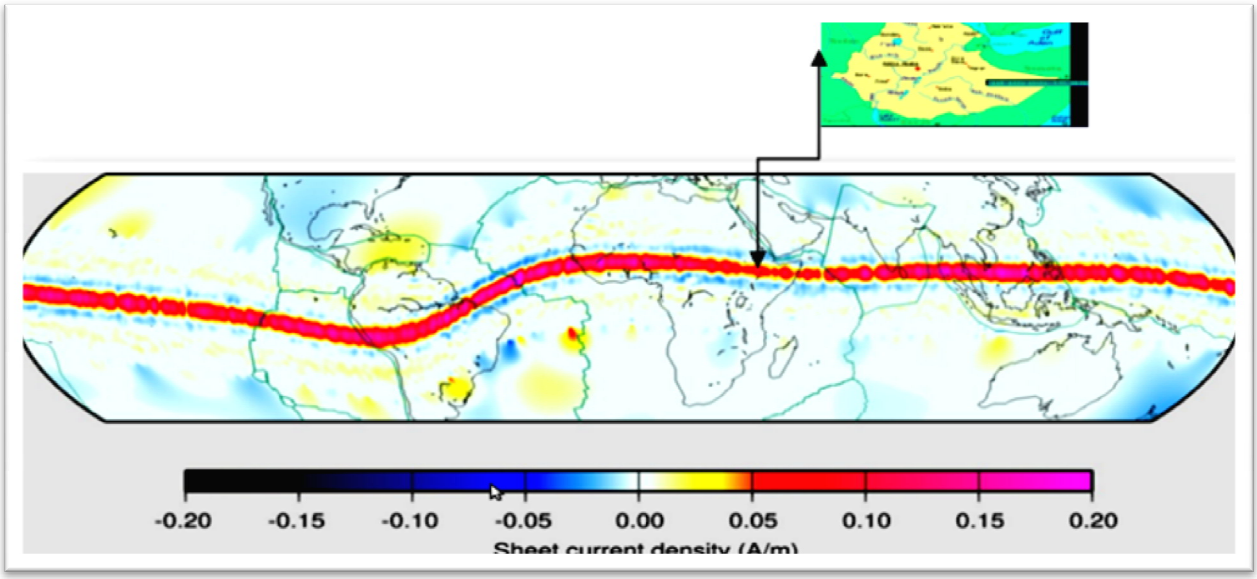

Figure 2-5 Electrojet current densities (http://info.geomag.us/equatorial_electrojet.html)

The causes of equatorial electrojet are: The sun and the 'moon produce tidal forces in the atmosphere, which result in air motion that is primarily horizontal. The motion of the air across the geomagnetic field induces electromotive forces, which drive electric currents at altitudes in the ionosphere where the air is electrically conducting, causing daily variations in the geomagnetic field. This has been referred to as the atmospheric dynamo theory.

Solar particles emitted from the sun also interact with the magnetosphere of the earth to produce additional perturbations in the geomagnetic field, referred to as geomagnetic disturbance. On a quiet day when the geomagnetic disturbance is negligible, the dominant part of the observed geomagnetic variation is a function of solar time, referred to as the geomagnetic solar quiet daily variation.

Chapter Three

3. GPS signal observables and mitigation techniques of ionosphere effect

3.1. GPS Signal Structure

When GPS became fully operational in 1995, the system started to emit primarily two main signals on the radio band, L1 and L2 carrier frequencies. Transmitting radio signals at these frequencies is a compromise between ionosphere dispersion and space-loss. Dispersion is inversely proportional to the square of the radio frequency. Single frequency users will experience up to 30 m of range delay at zenith on L1 during night time, and a small portable antenna is sufficient to track both GPS L1 and L2 signals. The separation between selected frequencies is sufficiently wide for dual frequency users to remove the first-order ionosphere dispersion effect accounting for 99% and narrow enough that only a single receiving antenna is needed (Langley, 1998a).

GPS is a one-way ranging system, that is, GPS signals are passively transmitted from satellites to an unlimited number of users. The L1 and L2 carriers are pure sinusoidal waves, which by themselves are not sufficient to fix a position in real-time because of the ambiguous phase cycles and unknown satellite positions. Therefore, additional signals are multiplexed on two L1/L2 carriers using the binary biphase modulation technique and spread out over a bandwidth of 20 MHz for direct ranging and positioning. Modulated signals are the precise-code (P-code), and coarse ranging information coarse/acquisition-code (C/A-code). The ranging data are in a binary sequence of pseudo-random numbers (PRN) generated by mathematical algorithms present in hardware device referred as the tapped feedback registers. Although the sequence appears random, a receiver can duplicate it. All GPS satellites transmit signals on the same L1/L2 frequencies. And each individual PRN signal is orthogonal to each other and can be extracted using the Code Division Multiple Access (CDMA) technique that relies on the strong auto-correlation properties (Spilker, 1996).

The C/A-code sequence has a chip length of 1,023 bits at a clock rate of 1.023 MHz, and repeats itself every 1 ms. The C/A-code sequence is unique for each satellite. In contrast, the P-code sequence has a chip length of 15,345,000 bits at a clock rate of 10.23 MHz that does not repeat itself for 266.4 days. Each satellite shares the same P-code sequence, but each is assigned with a one-week segment. The faster clock rate of P-code provides better resolution than the C/A-code by a factor of 10. Using a standard code correlation technique found in most receivers provides standard deviations of typically 1 m for the C/A-code and 0.1 m for the P-code. The broadcast message contains the satellite orbit ephemeris, constellation almanac, satellite clock corrections, satellite status, and ionosphere corrections. The message is transmitted at 50 bps data stream added to the C/A-code and P-code using a modulo-2 addition and requires 30 seconds to complete the

transmission of information necessary for an initial position fix. However, a complete message requires 12.5 minutes to transmit. The L1 carrier wave is multiplexed with two spread spectrum C/A-code and P-code signals through phase-quadrature, where the C/A-code is modulated on the in-phase component of the L1 carrier, while the P-code is modulated on a 90 degrees rotated quadrature phase. Only the P-code is modulated on the L2 carrier wave. Current activation of Anti-Spoofing (AS) denies civilian access to the P-code by encrypting it with an additional secret W-code sequence.

3.2. GPS observation models

The basic GPS observables are code pseudoranges and carrier phases as well as Doppler measurements. The principle of the GPS measurements and their mathematical expressions are described below.

3.2.1. Code pseudoranges

The pseudorange is a measure of the distance between the satellite and the receiver's antenna. The distance is measured through measuring the GPS signal transmitting time from the satellite to the GPS receiver's antenna. Therefore, such a distance is referred to the distance between the satellite at the time of the GPS signal emission and the GPS antenna at the time of GPS signals reception. The transmitting time is measured through maximum correlation analysis of the receiver code and the GPS signal. The receiver code is derived from the clock used in the GPS receiver. The GPS signal is, of course, generated by the clock used in the GPS satellite. The measured pseudorange is different from the geometric distance between the satellite and the receiver's antenna because of the errors of the both clocks and the influences of the signal transmitting mediums.

It is also notable that the path of the signal transmission differs slightly from the geometric path. The transmitting medium not only delays the transmitting of the signal, but also bends the transmitting path of the signal. The GPS signal emission time of the satellite is denoted by t_e and the GPS signal reception time of the receiver is t_r.

In case of vacuum medium and error-free situation, the measured pseudorange is equal to the geometric distance and can be presented by:

$$R_r^s(t_r, t_e) = (t_r - t_e)c \tag{3.1}$$

Where c denotes the speed of light, and subscript r and superscript s denote the receiver and satellite, respectively.

On the left-hand side, t_r denotes the epoch at which the pseudorange is measured. t_e and $t_r$are considered true emission time and reception time of the GPS signal. Taking the satellite and receiver clock errors into account, the pseudorange can be represented as

$$\mathbf{R_r^s(t_r, t_e = (t_r - t_e)c - (\delta t_r - \delta t_s)c} \quad (3.2)$$

Where $\boldsymbol{\delta t_r}$and $\boldsymbol{\delta t_s}$ denote the clock errors of the receiver and satellite, respectively. The GPS satellite clock error term $\boldsymbol{\delta t_s}$is indeed known through GPS satellite orbit determination. The clock errors are usually modeled by polynomials of time. The constant term represents the bias and the linear term the drift of the clocks. These coefficients are transmitted along with the navigation message to the users. More precisely, the satellite clock error corrections can be also obtained from all IGS data centers (*www.gfz-potsdam.de*). They are determined along with the precise IGS orbits and have higher resolution in time. The geometric distance of the first term on the right-hand side in the above equation is given by

$$\boldsymbol{\rho_r^s(t_r, t_e) = \sqrt{((x_s - x_r)^2 + (y_s - y_r)^2 + (z_s - z_r)^2)}} \quad (3.3)$$

Where the satellite coordinate vector ($\mathbf{x_s}$, $\mathbf{y_s}$, $\mathbf{z_s}$) is a vector function of the time t_e, and the receiver coordinate

$\mathbf{(x_r, y_r, z_r)}$ is a function of the time t_r. Therefore, the geometric distance is indeed a function of two time variables.

Furthermore, the emission time t_e is unknown in practice. Denoting the transmitting time as Δt, there is

$$\Delta t = t_r - t_e \quad (3.4)$$

For illustrating the transmitting time computation, the geometric distance can be generally written as

$$\boldsymbol{\rho_r^s(t_r, t_e) = \rho_r^s(t_r, t_r - \Delta t)} \quad (3.5)$$

Taking the ionospheric effects, tropospheric effects, Earth tide and loading tide effects, multipath and relativistic effects as well as remaining errors into account, the pseudorange model can be written as follows

$$\boldsymbol{R_r^s(t_r, t_e) = \rho_r^s(t_r, t_e) - (\delta t_r - \delta t_s)c + \delta_{ion} + \delta_{tro} + \delta_{tid} + \delta_{mul} + \delta_{rel} + \epsilon} \quad (3.6)$$

Where the measured pseudorange is on the left-hand side, it equals to the geometric distance between the satellite at the emission time and the antenna at the reception time plus or minus several corrections. The clock error corrections are scaled by the velocity of light *c*. $\boldsymbol{\delta_{ion}}$ and $\boldsymbol{\delta_{tro}}$ denote the ionospheric and tropospheric effects of the station. $\boldsymbol{\delta_{tid}}$ denotes the Earth tide and ocean loading tide effects, $\boldsymbol{\delta_{mul}}$denotes the multipath effects, and $\boldsymbol{\delta_{rel}}$ denotes the relativistic effects. The remaining errors are denoted by ε. For convenience, unit meter is used for all terms and instrumental biases are omitted here. The height of the GPS satellite is about 20 200 km; thus, the GPS signal transmitting time is about 0.07 sec. The Earth rotates during the signal transition. The angular velocity of the Earth rotation is about 15 arcsec sec^{-1} . The related Earth

rotation correction is about 1 arcsec (cf., Goad 1996) .The effects of such a correction depend on the latitude of the station. At the equator, 1 arcsec rotation is equivalent to about 31 meters position displacement. The clock errors could be very big. There are examples where the negative pseudoranges are observed in practice. The above-discussed pseudorange model is generally valid for both C/A code and P code. The precision of the pseudorange measurements depends on the electronic abilities. Generally speaking, it is no problem nowadays to measure with precision up to 1% of the chip length. Therefore, the C/A code has a precision of about 3 m, and the P code 30 cm. The mentioned corrections will be discussed later in detail.

3.2.2. Carrier Phases

The carrier phase is a measure of the phase of the received satellite signal relative to the receiver-generated carrier phase at the reception time. The measurement is made by shifting the receiver-generated phase to track the received phase. The number of full carrier waves between the receiver and the satellite cannot be accounted for at the initial signal acquisition. Therefore, measuring the carrier phase is to measure the fractional phase and to keep track of changes in the cycles. The carrier phase observable is indeed an accumulated carrier phase observation. The fractional carrier phase can be measured by electronics with precision better than 1% of the wavelength, which corresponds to millimeter precision. This is also the reason why the phase measurement is more precise than that of the code. A full carrier wave is called a cycle. The ambiguous integer number of cycles in the carrier phase measurement is called ambiguity. The initial measuring has correct fractional phase and an arbitrary integer counter setting at the start epoch. Such an arbitrary initial setting will be adjusted to the correct one by modeling with ambiguity parameters. In the case of a vacuum medium and an error-free situation, the measured phase can be presented by

$$\Phi_r^s(\boldsymbol{t}_r^s) = \Phi_r(t_r) - \Phi_s(t_s) + N_r^s \quad (3.7)$$

Where subscript r and superscript s denote the receiver and satellite, respectively. t_r denotes the GPS signal reception time of the receiver. Φ_r denotes the phase of receiver's oscillator. Φ_s denote the received signal phase of the satellite. N_r^s is the ambiguity related to receiver r and satellite s. There is an interesting property of the signal phase transmission, i.e., the received phase of the satellite signal at the reception time is exactly the same as the phase of the emitted satellite signal at the emission time (Remondi 1984; Leick 1995),

$$\Phi^s(t_r) = \boldsymbol{\Phi_e^s}(\mathbf{t_r} - \Delta t) \quad (3.8)$$

Where $\Phi^s(t_r)$ is geometric distance between the satellite at the emission time $\mathbf{t_e}$, and the GPS antenna at the reception time $\mathbf{t_r}$, c is the speed of light. Then Eq. 3.8 can be written as:

$$\Phi_r^s((\boldsymbol{t}_r^s) = \Phi_r(t_r) - \boldsymbol{\Phi_e^s}(\mathbf{t_r} - \Delta t) + N_r^s \quad (3.9)$$

Suppose the initial time is zero and the received satellite signal and the reference carrier of the receiver have the nominal frequency *f*. Then one has

$$\Phi_r(t_r) = \mathbf{f t_r} \quad \textbf{and} \tag{3.10}$$

$$\Phi_r^s(\mathbf{t_r} - \Delta t) = f(\mathbf{t_r} - \Delta t) \tag{3.11}$$

Taking the satellite and receiver clock errors into account, the carrier phase can be represented as

$$\Phi_r^s(\mathbf{t_r}) = \frac{\rho_r^s(\mathbf{t_r},\mathbf{t_e})f}{c} - f(\delta\mathbf{t_r} - \delta\mathbf{t_s}) + N_r^s \tag{3.12}$$

Where $\delta\mathbf{t_r}$ and $\delta\mathbf{t_s}$ denote the clock errors of the receiver and satellite, respectively. The frequency f and wavelength λ have the relation of

$$c = f\lambda \tag{3.13}$$

Taking the ionospheric effects, tropospheric effects, Earth tide and loading tide effects, multipath and relativistic effects as well as remaining errors into account, the carrier phase model can be written in the following

$$\Phi_r^s(\mathbf{t_r}) = \frac{\rho_r^s(\mathbf{t_r},\mathbf{t_e})}{\lambda} - f(\delta\mathbf{t_r} - \delta\mathbf{t_s}) + N_r^s - \frac{\delta_{\mathbf{ion}}}{\lambda} + \frac{\delta_{\mathbf{tro}}}{\lambda} + \frac{\delta_{\mathbf{tide}}}{\lambda} + \frac{\delta_{\mathbf{mul}}}{\lambda} + \frac{\delta_{\mathbf{rel}}}{\lambda} + \frac{\in}{\lambda} \tag{3.14}$$

This is equivalence to

$$\lambda\Phi_r^s(\mathbf{t_r}) = \rho_r^s(\mathbf{t_r},\mathbf{t_e}) - f(\delta\mathbf{t_r} - \delta\mathbf{t_s}) + N_r^s - \delta_{\mathbf{ion}} + \delta_{\mathbf{tro}} + \delta_{\mathbf{tide}} + \delta_{\mathbf{mul}} + \delta_{\mathbf{rel}} + \in \tag{3.15}$$

Where the measured phase on the left-hand side with a factor of λ equals the geometric distance between the satellite at the emission time and the antenna at the reception time plus or minus several corrections. The above equation is convenient to use, because all terms have units of length (meter). It is notable that the sign of the ionospheric term is negative, whereas in the pseudorange model it is positive.

3.3. Phase and group velocity

Consider a single electromagnetic wave propagating in space with wavelength λ and frequency *f*. The velocity of its phase $V_{ph} = \lambda f$ (3.16)

Where V_{ph} represents the phase velocity, λ wave length, f frequency and group velocity can be calculated as follows:

$$V_{gr} = -\lambda\frac{dv_{ph}}{d\lambda} + f\lambda \tag{3.17}$$

Where V_{gr} represents the group velocity. This differentiation tells us the ionosphere has dispersive nature, the effect depends on wave length or frequency. Phase velocity and group velocity are equal in non dispersive media and corresponds to the speed of light in vacuum. The wave propagation in a medium depends on the refractive index *n*. Generally, the propagation velocity is obtained from

$$v = \frac{c}{n} \tag{3.18}$$

Where v is the speed of light in medium and n is refractive index.

The refractive indexes of the phase and group velocities can be calculated as follow;

$$n_{gr} = n_{ph} + f\frac{dn_{ph}}{df} \tag{3.19}$$

Where n_{gr}represents the refractive index of group velocity and $n_{ph}$is refractive index of phase velocity.

3.4. Total Electron Content and Refraction index

The ionosphere extends in various layers from about 50 km to 1 000 km above earth and it is a dispersive medium with respect to the GNSS radio signal (Seeber , 2003). The refractive index can be expanded in to a series of the form,

$$n_{ph} = 1 + \frac{c_2}{f^2} + \frac{c_3}{f^3} + \frac{c_4}{f^4} + \cdots \tag{3.20}$$

Where n_{ph} approximates the phase refractive index. The coefficients c_2,c_3 c_4 do not depend on frequency but on the quantity *Ne* denoting the number of electrons per cubic meter (i.e., the electron density) along the propagation path. Using an approximation by cutting off the series expansion after the quadratic term, that is

$$n_{ph} = 1 + \frac{c_2}{f^2} \text{ and } \qquad n_{gr} = 1 - \frac{c_2}{f^2} \tag{3.21}$$

From these we can see both phase and group velocities have equal magnitude of refractive indexes but opposite signs. According (seeber, 2003) we can estimate $c_2 = -40.3N_e(m^2)$.

From the above two formulas we can easily see group refractive index is greater than phase refractive index because the electron density *Ne* is always positive. As a consequence of the different velocities, a group delay and a phase advance occur. In other words, GNSS ranging codes are delayed and the carrier phases are advanced. Therefore, the measured code pseudoranges are too long and the measured carrier phase pseudoranges are too short compared to the geometric range between the satellite and the receiver. The amount of the difference is the same in both cases.

According to Fermat's principle, the measured range *s* is defined by

$$s = \int n ds \tag{3.22}$$

Where the integral must be extended along the path of the signal. The geometric range S_o along the straight line between the satellite and the receiver may be obtained analogously by setting $n = 1$:

$$s_o = \int ds_o \tag{3.23}$$

The difference Δ^{Ion} between measured and geometric range is called ionospheric refraction and follows from

$\Delta^{Ion} = \int nds - \int ds_o$ which may be written for a phase refractive index, n_{ph} (3.24)

$$\Delta_{ph}^{Ion} = \int (1 + \frac{c_2}{f^2}) ds - \int ds_o \tag{3.25}$$

group refractive index , n_{gr}

$$\Delta_{gr}^{Ion} = \int (1 - \frac{c_2}{f^2}) ds - \int ds_o \tag{3.26}$$

A simplification is obtained when approximating the integration for the first term along the geometric range. In this case, *ds* become ds_o and the formulas;

$$\Delta_{ph}^{Ion} = \int \frac{c_2}{f^2} dso \quad and \quad \Delta_{gr}^{Ion} = -\int \frac{c_2}{f^2} ds\, o \tag{3.27}$$

This can also be written as;

$$\Delta_{ph}^{Ion} = -\frac{40.3}{f^2} \int N_e ds \quad and \quad \Delta_{gr}^{Ion} = \frac{40.3}{f^2} \int N_e dso \tag{3.28}$$

We can also make more simplified form

$$\Delta_{ph}^{Ion} = -\frac{40.3}{f^2} TEC \quad and \quad \Delta_{gr}^{Ion} = \frac{40.3}{f^2} TEC \tag{3.29}$$

Where TEC it represents total electron content and 1TECU = 10^{16} electrons per meter square. Where TECU is total electron content unit.

3.5. VTEC and STEC using GPS_TEC

GPS radio signals are subjected to effects, which degrade its accuracy in all three layers of the atmosphere (troposphere, stratosphere, Ionosphere), The effects of accuracy degradation in the ionosphere are the most significant. The largest effect that ionosphere has on GPS accuracy is group time delay which is proportional to the total electron content (TEC). Generally the ionospheric delay is of the order of 5m to 15m, but can reach over 40-60m during the periods of high sunspot activity and large space weather events such as geomagnetic and solar disturbances. Hence, the measurements of TEC have gained importance with the increasing demand for the GPS based navigation applications in trans-ionospheric communications with space borne vehicles such as satellites, aircrafts and surface transportations (Gopi ,2008).

3.6. STEC measurement from Dual frequency receiver

The ionosphere has an effect on group delays and phase advances. TEC of the group delay from pseudo-range measurements is given by;

$$\mathrm{TEC}_{\mathrm{group}} = \frac{1}{40.3}\left(\frac{1}{f_1^2 - f_2^2}\right) \mathrm{x}\ (P_1 - P_2) \tag{3.30}$$

Where f1 & f2 are L1 and L2 carrier frequencies and P1 & P2 are pseudo-range observables

TEC from carrier phase measurements is given by

$$TEC_{phase} = (C_1 - C_2)\ \mathrm{x}\ 2.852 \tag{3.31}$$

Where C_1 & C_2 are phase measurements in nano-seconds. Calculation of TEC from group delay measurement is absolute and noisy. The relative phase delay between the two carrier frequencies gives a more precise measure of relative TEC, but is ambiguous because the actual number of cycles of phase is unknown. These two estimates can be combined to form an improved estimate for absolute TEC.

3.7. Vertical TEC conversion

To calculate the VTEC, it was assumed that the ionosphere (and the protonosphere) is spatially uniform, and further it is simplified to a thin layer at an altitude of h = 350 km above the earth's surface. This is the thin shell model and its height is the effective height or centroid of the plasmasphere (ionosphere and protonosphere collectively called plasmasphere). Impact of the state of ionosphere on the propagation of waves is characterized by the Total Electron Content (TEC).

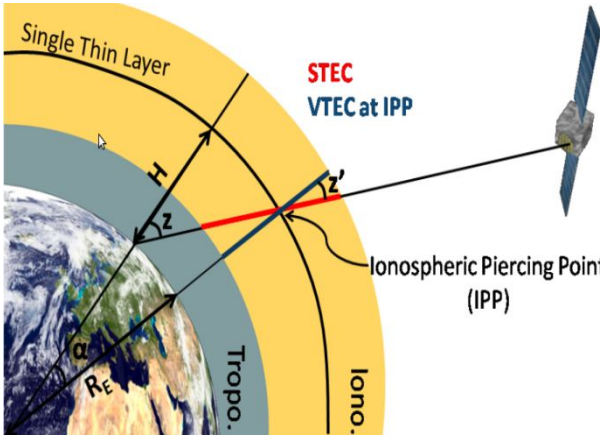

Figure 3-1 Single layer of Ionosphere (http://gnss.be/ionosphere_tutorial.php#x2-70000)

$$STEC = \int_s^r n_e(s)\,ds \tag{3.32}$$

Where STEC is slant total electron content n_e is the electron density s is satellite, r is receiver.

The integral contains the total number of electrons that are included in a column with a cross-sectional area of 1 m^2 counted along the signal path s between the satellite S and receiver R. For comparison purposes among sets of STEC data the vertical electron content VTEC is formed as:

$$VTEC = \frac{1}{\mathrm{F}} * STEC \tag{3.33}$$

Where VTEC is vertical electron content and F is obliquity factor or mapping function.

$$F = \frac{1}{\cos(\mathrm{z^i})} \tag{3.34}$$

Where z^i is zenith angle between the signal path and horizontal plane in the mean altitude h.

A frequently used model for data reduction in satellite geodesy is the single layer model. In this case the total electron content is represented by a spherical layer at the mean ionospheric height h usually 400 km on this layer IPP is the ionspheric piercing point of the single path to satellite S. RE Earth radius, and z the zenith angle of Satellite for an observer of receiver. The zenith angle z^i at IPP then is given by:

$$z^i = \arcsin\left(\frac{RE}{RE+h}\right) \text{ x } \sin(z) \tag{3.35}$$

Mapping function (F) increases with increasing zenith angle z to the satellite target. Table 3.1 (wanninger,1994) shows that for small elevation angles TEC can reach at most three times the value of VTEC. The electron density is highly variable and depends mainly on the geographic location, time of the day, season of the year and solar activity. Regions of the highest TEC are located approximately $\pm 15\, to\, \pm 20\, degrees$ each side of Earth's magnetic equator.

Table 3-1 the effect of elevation on STEC

E (degree)	Z(degree)	z^i (degree)	F (degree)	Distance (km)
90	0	0	1.00	0
60	30	28	1.13	215
30	60	55	1.73	603
20	70	62	2.14	873
10	80	68	2.66	1344
5	85	70	2.87	1712

(wanninger, 1994)

3.8. Effective mitigation of ionosphere effect in single frequency receiver

In this section four different methods of ionosphere effect mitigation are briefly described.

3.8.1. Broadcast ionospheric model

The navigation message broadcast by the satellites contains a predicted ionospheric model (four α and four β parameters) that can be used with the Klobuchar model to correct single frequency observations (Klobuchar, 1996). During normal operation, the parameters of the model are updated at least once every six days (ARINC Engineering Services, 2004). The inputs in the Klobuchar model are the user geodetic latitude, the longitude, the time of day at the intersection between the mean ionospheric layer and the receiver to satellite line of sight, as well as the relative azimuth and elevation angle of the satellite. This model can provide a correction for about 50% root-mean-squares (RMS) of the ionospheric range delay (Klobuchar, 2000).

3.8.2.Global ionospheric maps

The IGS (International GNSS Service) ionosphere working group (Iono-WG) was established in May 1998, to produce ionospheric vertical total electron content (VTEC) maps as one of the IGS products for the GNSS community. Currently, four IGS Ionosphere Associate Analysis Centers (IAACs) operated by different agencies provide their ionosphere products as two-dimensional Global Ionosphere Maps (GIMs) in IONopshere Map Exchange (IONEX) format (Schaer et. al., 1998). Each IAAC generates its daily IONEX file that has 13 GIMs at 2-h intervals. These files are contributed to the Iono-WG in order to generate the combined IGS final and rapid product. Since April 2003, the final IGS GIMs in IONEX format have become an official IGS product, which are uploaded with a delay of about 11 days for public downloading. Meanwhile, a rapid version of GIMs is available to the public since December 2003 with latency less than 24 hours. Both final and rapid IGS GIMs have a temporal resolution of 2 hours and a spatial resolution of 2.5 degrees north-south (latitude) and 5 degrees east-west (longitude). The accuracy varies from the level of 2 TEC (1 TECU corresponds to 0.163 m range error on L1 frequency) to about 8-9 TECU (IGS, 2009). The accuracy degrades for the interpolated points (vstendal, 2002).

3.8.3.Wide-Area Real Time Kinematic derived ionospheric corrections

The Wide-Area Real Time Kinematic (WARTK) is a very precise differential technique to compute ionospheric corrections in real-time using a 3-D voxel model of the ionosphere, estimated by means of a

Kalman filter, and using exclusively GNSS data gathered from fixed receivers separated several hundreds of kilometers (Hernandez-Pajares 1999, 2000).

3.8.4. GRAPHIC combination

The ionosphere-free code and phase combination (Gi) is the average of the code and phase measurement as follows:

$$G_i = \frac{P_i+\Phi_i}{2} = \rho_i + cdt + m_w ZWD + \frac{\lambda_i+N_i}{2} + \frac{\varepsilon p_i+\varepsilon\Phi_i}{2} \quad (3.36)$$

Where $G_i$is the Graphic ionosphere free combination, ρ_i is the geometric distance between satellite and receiver including geometric error, cdt is clock bias, zenith delay, λ_i is wave length, N_i is non integer ambiguity on the carrier phase, εp_i ,$\varepsilon\Phi_i$ is code and phase measurement noise including the multi-path respectively.

This combination is known also as GRAPHIC – Group and Phase Ionospheric Combination (Yunck, 1996). It is of particular interest in single-frequency space applications because it is able to eliminate all the ionospheric effect, but at the cost of having an ambiguity (from the carrier-phase measurement) and more noise than the pure carrier-phase combination. Most of the noise in this combination is due to C/A (P) code measurement error, while the noise and multipath of Li is negligible with respect to the code. According to Yunck (1996), modern, high quality receivers in optimal low multipath environments can recover code pseudorange with a precision better than 50 cm in 1 s. The GRAPHIC observable reduces this by half. With this method, the position coordinates and ambiguity parameters cannot be estimated using a single epoch of observations. Based on cumulative measurements, Heroux et al. (2004) found that the estimation process requires several hours for the float ambiguity to converge.

3.9. Linear combination in Dual frequencies receiver

Linear carrier phase or code combinations are formed by adding or subtracting carrier phase or code measurements on two or more frequencies. Such combinations are used to improve the resulting measurement in some manner relative to the original measurements. In this context, “improvement” usually implies removing/reducing certain errors so as to facilitate the ambiguity resolution process or increase the measurement. Improvement in both areas is not possible and thus a design trade-off is required. It may therefore be of advantage to use all observables, or linear combinations thereof, in the parameter estimation process. In principle, an unlimited number of possibilities exists, to combine the different observables, and to form derived observables, but only some combinations are meaningful in the context of positioning. One advantage of the use of derived observations is that errors that are present in the original observations are

eliminated or reduced when differences are formed between observables. In some cases the ambiguities of derived observations are easier to solve than for those of the original observations. On the other hand, the noise level may be considerably increased on combination.

3.10. Linear combination of phase and code in Dual frequencies receiver

If we use Wide-Lane and Narrow-Lane linear combination techniques, it is possible to make ionosphere-free linear combinations to first order ionosphere effect. This linear combination can avoid 99.9 % of first order ionosphere effect error.

3.11. Wide-Lane combination of the phase measurement

From this combination by convenient the coefficients a and b have 1 and -1 respectively. Hence,

$$\varphi_{\mathrm{a,b}} = \quad a\varphi_{\mathrm{a}} + b\varphi_{\mathrm{b}} \quad = \varphi_1 - \varphi_2 \tag{3.37}$$

The wave length of this combination is

$$\lambda w_L = \frac{\mathrm{c}}{\mathrm{af_1 + bf_2}} = \frac{\lambda_1\lambda_2}{\mathrm{b}\lambda_1 + \mathrm{a}\lambda_2} = \frac{\lambda_1\lambda_2}{\lambda_2 - \lambda_1} = 86cm \tag{3.38}$$

$$Lw_L = \frac{\mathrm{f1L1 - f2L2}}{\mathrm{f2 - f1}} \tag{3.39}$$

3.12. Narrow-Lane combination of the phase

This combination uses the coefficients a and b 1 and 1 respectively. Hence,

$$\varphi_{\mathrm{ab}} = a\varphi_{\mathrm{a}} + b\varphi_{\mathrm{b}} \quad = \varphi_1 + \varphi_2 \tag{3.40}$$

The wave length of this combination is

$$\lambda w_L = \frac{\mathrm{c}}{\mathrm{af_1 + bf_2}} = \frac{\lambda_1\lambda_2}{\mathrm{b}\lambda_1 + \mathrm{a}\lambda_2} = \frac{\lambda_1\lambda_2}{\lambda_2 + \lambda_1} = 10.7\mathrm{cm} \tag{3.41}$$

$$LN_L = \frac{\mathrm{f1L1 + f2L2}}{\mathrm{f2 + f1}} \tag{3.42}$$

Phase measurements in single frequency

$$\varphi_{\mathrm{i}} = \frac{1}{\lambda}\left(\rho + G + I_i\right) + N_i + \epsilon_i \tag{3.43}$$

Where G is the geometric errors (trop,Ion,satellite orbit,receiver clock,)

$$\mathrm{I}_i = -\frac{40.3 * \mathrm{TEC}}{\mathrm{f_i^2}} = \frac{\mathrm{K}}{\mathrm{f_i^2}} \tag{3.44}$$

Code measurements in single frequency

$$p_i = (\rho + G + I_i) + +\epsilon_i \quad (3.45)$$

$$\mathrm{I}_i = \frac{40.3*\mathrm{TEC}}{\mathrm{f_i^2}} = \frac{\mathrm{K}}{\mathrm{f_i^2}} \quad (3.46)$$

As we can see the phase and code ionosphere effect has equal magnitude but opposite sign in single frequency receiver.

3.13. Ionosphere-free combination- Code

$$R_{L1} = (\rho + c\delta t) + \Delta^{Ion}(L_1) \quad (3.47)$$

$$R_{L2} = (\rho + c\delta t) + \Delta^{Ion}(L_2) \quad (3.48)$$

Where R_{L1} is pseudorage for code and L1 is first frequency and R_{L2} is pseudorage for code and L2 is second frequency, ρ is the geometric error, δt clock error on satellite and receiver and c is the speed of light.

$\Delta^{Ion}(L_1)$ This is the ionosphere effect on L1 frequency and it is equivalence

$$\Delta_1^{ion} = \frac{40.3}{\mathrm{f_1^2}} TEC \quad and \quad (3.49)$$

$\Delta^{\mathrm{Ion(L2)}}$ this is the ionosphere effect on L2 frequensy

$$\Delta^{\mathrm{Ion(L2)}} = \frac{-40.3}{\mathrm{f_2^2}} \mathrm{TEC} \text{ or } \Delta^{\mathrm{Ion(L2)}} = -\frac{\mathrm{f_1^2}}{\mathrm{f_2^2}} \Delta_1^{\mathrm{Ion}} \quad (3.50)$$

The linear combination of the code is :

$$R_{L1L2} = a * R_{L1} + b * R_{L2} \quad here\ a = 1\ and\ b = -\frac{f_1^2}{f_2^2} \quad (3.51)$$

$$R_{L1L2} = R_{L1} - \frac{f_1^2}{f_2^2} R_{L2} \quad (3.52)$$

$$R_{L1L2} = R_{L1} = (\rho + c\delta t) + \Delta^{Ion}(L_1) - \frac{f_1^2}{f_2^2}\left((\rho + c\delta t) + \Delta^{Ion}(L_2)\right) but \quad \Delta^{Ion}(L_2) = -\frac{f_1^2}{f_2^2}\Delta_1^{Ion} \quad (3.53)$$

$$R_{L1L2} = R_{L1} = (\rho + c\delta t) + \Delta^{Ion}(L_1) - \frac{f_1^2}{f_2^2}\left((\rho + c\delta t) - \frac{f_1^2}{f_2^2}\Delta_1^{Ion}\right) = \rho + c\delta t \quad (3.54)$$

This is the ionosphere free linear combination of the code and as we can see the ionosphere delay is totally removed (Hofmann-Wellenhof et al**.**, 2008).

3.14. Ionosphere-free combination- Phase

$$\Phi_{L1} = f_1 \frac{\rho}{c} + f_1 \delta t + N_{L1} - \frac{\rho}{c} \Delta_{L1}^{Ion} \quad (3.55)$$

Where Φ_{L1} is the phase measurement on $L_1$and N_{L1} integer ambiguity.

$$\Phi_{L2} = f_2 \frac{\rho}{c} + f_2 \delta t + N_{L2} - \frac{f_{L1}^2}{c f_{L2}^2} \Delta_{L1}^{Ion} \quad (3.56)$$

Where Φ_{L2} is the phase measurement on L_2 then the linear combination of the phase is

$$\Phi_{L1,L2} = a * \Phi_{L1} + b * \Phi_{L2} \text{ here } a = 1 \text{ and } b = \frac{f_2}{f_1} \quad (3.57)$$

Where $\Phi_{L1.L2}$ is the linear combination of phase measurement on L_1 , L_2

$$\Phi_{L1,L2} = \Phi_{L1} - \frac{f_1}{f_2} \Phi_{L2} \quad (3.58)$$

From the above formulas by substitution we can get the following formula.

$$\Phi_{L1} - \frac{f_2}{f_1} \Phi_{L2} = f_1 \frac{\rho}{c} + f_1 \delta t + N_{L1} - \frac{f_2}{f_1} \left(f_2 \frac{\rho}{c} + f_2 \delta t + N_{L2} \right) \quad (3.59)$$

If we also simplifying the above formula we can get the following formula

$$\Phi_{L1} - \frac{f_2}{f_1} \Phi_{L2} = \frac{\rho}{c} \left(\frac{f_1^2 - f_2^2}{f} \right) + N_{L1} - \frac{f_2}{f_1} N_{L2} + \delta t \left(\frac{f_1^2 - f_2^2}{f} \right) \quad (3.60)$$

If we also doing more steps from the above formula we can get the following result

$$\Phi_{L1} - \frac{f_2}{f_1} \Phi_{L2} = \frac{\rho}{c} \left(\frac{f_1^2 - f_2^2}{f} \right) + N_{L1} - \frac{f_2}{f_1} N_{L2} + \delta t \left(\frac{f_1^2 - f_2^2}{f} \right) = \rho + c\delta t + \frac{N_{L1} f_{L1} - N_{L2} f_{L2}}{f_1^2 - f_2^2} \quad (3.61)$$

We can see clearly the ionosphere effect totally eliminated in first order linear combination.

3.15. First order Ionospheric-free combinations of phase in units of length

If we have L1 and L2 dual frequency receiver the phase combination can be estimated as follows,

$$\frac{c f_1 \emptyset_1 - c f_2 \emptyset_2}{f_1^2 - f_2^2} = c \frac{\rho + G}{c} + c \frac{N_1 f_1 - N_2 f_2}{f_1^2 - f_2^2} + c \frac{\epsilon_1 f_1 - \epsilon_2 f_2}{f_1^2 - f_2^2} \quad (3.62)$$

$$\frac{f_1^2 (\emptyset_1 \lambda_1) - f_2^2 (\emptyset_2 \lambda_2)}{f_1^2 - f_2^2} = \rho + G + \frac{\lambda_1 N_1 f_1^2 - \lambda_2 N_2 f_2^2}{f_1^2 - f_2^2} + \frac{\epsilon_1 \lambda_1 f_1^2 - \epsilon_2 \lambda_2 f_2^2}{f_1^2 - f_2^2} \quad (3.63)$$

$$L_3 = \frac{f_1^2 L_1^2 - f_2^2 L_2^2}{f_1^2 - f_2^2} = 2.546 L_1 - 1.546 L_2 \quad (3.64)$$

where L3 is Ionosphere free linear combination of phase

And for code measurement

$$P_3 = \frac{f_1^2 P_1 - f_2^2 P_2}{f_1^2 - f_2^2} = 2.546 P_1 - 1.546 P_2 \quad (3.65)$$

Where P_3 is linear combination of the code measurement.

If we use the third frequency (L5) we can have linear combination as follows,

$$P = a * P_1 + b * P_5 = \frac{f_1^2 P_1 - f_2^2 P_5}{f_1^2 - f_2^2} = \rho + G \frac{f_1^2 \varepsilon_1 - f_2^2 \varepsilon_5}{f_1^2 - f_5^2} \quad (3.66)$$

3.16. Second and third order ionosphere effect

The higher order ionospheric terms (I2 and I3), in particular in the second-order ionospheric term (I2), which is not totally avoided by linear combination. It basically depending on the STEC and the magnetic field projection over the propagation direction at the ionospheric pierce point**.** According to (Kim and Tinin, 2007) the common practice of eliminating the ionospheric error is by the ionosphere free (IF) observable, which is a linear combination of observables on two frequencies such as GPS L1 and L2, accounts for about 99% of the total ionospheric effect, known as the first order ionospheric effect (Ion1). The remaining 1% residual range errors (RREs) in the IF observable are due to the higher – second and third, order ionospheric effects, Ion2 and Ion3, respectively. Both terms are related with the electron content along the signal path; moreover Ion2 term is associated with the influence of the geomagnetic field on the ionospheric refractive index and Ion3 with the ray bending effect of the ionosphere, which can cause significant deviation in the ray trajectory (due to electron density gradients in the ionosphere) such that the error contribution of Ion3 can exceed that of Ion2.

$$q = 40.3 \int N d_L \quad s = 7527 * c \int N[B_o] \cos(\theta_B) d_L \quad (3.67)$$

$$q = 2437 \int N^2 N d_L + 4.74 * 10^{22} \int N B_o^2 (1 + \cos^2(\theta) dL \quad (3.68)$$

Where NdL is the total electron density along the path, B_0 is the magnitude of the geomagnetic field at the ionospheric pierce point (IPP) and θ is the angle between the signal wave vector and the geomagnetic field vector at the IPP.

Therefore; the linear combination of second and third order ionosphere effect is given as follows:

$$I_2 = -\frac{s}{2 f_1 f_2 (f_1 + f_2)} = \frac{-7527 c B_o \cos(\theta) STEC}{2 f_1 f_2 (f_1 + f_2)} = \alpha B_o \cos(\theta) STEC \quad (3.69)$$

Where $\alpha = \left[\frac{f1^2}{f1^2 - f2^2}\right]$ (3.70)

As we can see clearly second order ionospheric effect depends on the frequencies, geomagnetic field of the earth and the angle between signal wave vector and the geomagnetic field vector at the IPP.

$$I_3 = \frac{-812.47 \int N_e^2 \, dl}{f_1^4} \quad (3.71)$$

From the third order ionospheric we can see clearly also the effect depends on frequency and the slant total electron content.

3.17. High order Ionospheric-free combinations for multiple frequency (L_1, L_2, L_5)

According to different research findings the first order ionospheric term (I1) is the main contribution of the ionospheric delay to GNSS observations. But the first order ionosphere effect 99.9 % root mean square effect can be removed by using linear combination of dual frequency receiver. However, because of the increasing accuracy demand in precise GPS positioning, the study of the impact of the higher ionospheric terms contributes up to few cm in range has become relevant.

The higher order ionosphere effect can also removed by using the third frequency (L1) with L2 and L5 as follows,

$P_{L1L2L5} = (P_1 - \frac{f_2^2}{f_1^2} P_2) + \frac{f_5 f_1 - f_5}{f_1 f_2 - f_1}(P_1 - \frac{f_5}{f_1} P_5)$ For code measurement (3.73)

$$= \frac{f_1^3(f_5 - f_2)P_1 + f_2^3(f_1 - f_5)P_2 + f_5^3(f_2 - f_1)P_3}{f_1^3(f_2 - f_5) + f_2^3(f_1 - f_5)f_5^3 + (f_2 - f_1)} \quad (3.74)$$

$L_{L1L2L5} = (L_1 - \frac{f_2^2}{f_1^2} L_2) + \frac{f_5 f_1 - f_5}{f_1 f_2 - f_1}(L_1 - \frac{f_5}{f_1} P_5)$ For Phase measurement (3.75)

$$= \frac{f_1^3(f_5 - f_2)L_1 + f_2^3(f_1 - f_5)L_2 + f_5^3(f_2 - f_1)L_3}{f_1^3(f_2 - f_5) + f_2^3(f_1 - f_5)f_5^3 + (f_2 - f_1)} \quad (3.76)$$

3.18. Melbourne-Wubbena combination

This combination is done by combining Wide-Lane from the phase and Narrow-Lane from the code. The importance of this combination is it eliminates the effect of ionosphere, clock and geometry.

$$WN = L_{WL} - P_{NL} = \frac{f_1(\lambda_1 N_1) - f_2(\lambda_2 N_2)}{f_1 - f_2} + \frac{f_1(\lambda_1 \varepsilon_1) - f_2(\lambda_2 \varepsilon_2)}{f_1 - f_2} \quad (3.77)$$

Where WN is the Wide-Lane and Narrow-Lane combination, L_{WL} is Wide-Lane combination of phase and P_{NL} is Narrow-Lane combination of the code.

Chapter Four

4. Data sources and methods of data analysis

To achieve the objectives of the study, we have used daily data and products produced by the International GNSS Service (IGS) using data collected from over 200 globally distributed tracking stations and processed by seven analysis centers. The daily data has 30 second sample intervals. The IGS global system of satellite tracking stations, Data Centers, and Analysis Centers puts high-quality GPS data and data products online in near real time to meet the objectives of a wide range of scientific and engineering applications and studies. "Data" we mean raw GPS/GLONASS pseudorange and phase observations, precise ephemerides, and supporting types of raw data (such as meteorological). We use the term "products" for things like precise orbit and clock files, which are generated through analysis of the raw site data (http://igscb.jpl.nasa.gov/faqs.html#id2845337).

We have used Global Positioning System Total Electron Content Analysis (GPS_TEC), International Reference of Ionosphere (IRI-2007), Leica Quality Control (QC) software to study diurnal, spatial and cyclic effect of ionosphere on GPS signal and GAMIT/GLOBK to see the repeatability of residual time series.

4.1.1. Leica Quality Control (QC)

Leica GNSS QC is the first choice in quality monitoring software to complement the Leica GNSS Spider, Leica Spider Web or any other network reference station software. It is stand-alone software that can perform automatic quality checking and reporting of the logged RINEX data. Advanced analysis tools allow detailed site evaluation, receiver performance testing and multipath assessment and ionosphere. Combined with Leica GNSS Spider it provides online analysis of network RTK processing. GNSS QC fully supports both the GPS (including L2C and L5) and GLONASS satellite systems. Figure 9, 10 and 11 shows a plot of the vertical total electron content using Leica GNSS QC software at different time and different geographical locations. From the plots we can clearly see how the VTEC density varies with time and geographical latitude. QC software uses the following algorithm to compute VTEC.

$$VTEC = \frac{STEC}{F} \quad and\ from\ eq\ 3.64\ we\ have \qquad F = \frac{1}{cos(z^i)} \tag{4.1}$$

Where F is obliquity factor or mapping function and (z^i) is the angle between satellite and ionosphere layer. During 2012 the sunspot was expected high values and we plotted march 8th of 2012 in different Universal Time (UT) to see the density of electron contents using Leica GNNS QC software.

4.1.2. GPS_TEC

GPS_TEC software is used to calculate and plot the VTEC and other data analysis applications by using a combination of RINEX file, ephemeris from IGS navigation files and it has also the capability of downloading other ancillary files automatically if there is an internet connections. The software was developed by Goopy Krishna Seemala in 2011. An updated version is available. For this study we have used GPS_TEC 2.2 versions (Goopy Krishna, 2012).

The software works based on the following algorithms:

$$Z = [sin^{-1}(0.94792 \text{ x } \cos(elevation)] \quad (4.2)$$

Where Z is Zenith angle

$$VTEC = \frac{STEC-(b_R+b_S)}{S(E)} \quad (4.3)$$

Where STEC is slant total electron content, VTEC is vertical electron content, b_R is receiver bias, b_S is satellite bias and S (E) is projection angle. And projection angle is calculated as follows:

$$S(E) = \frac{1}{\cos(Z)} = \left(1 - \left(\frac{R_E * \cos(E)}{R_E + h_S}\right)^2\right)^{-0.5} \quad (4.4)$$

Where R_E radius of the Earth, E is elevation and h_s is the height of ionosphere.

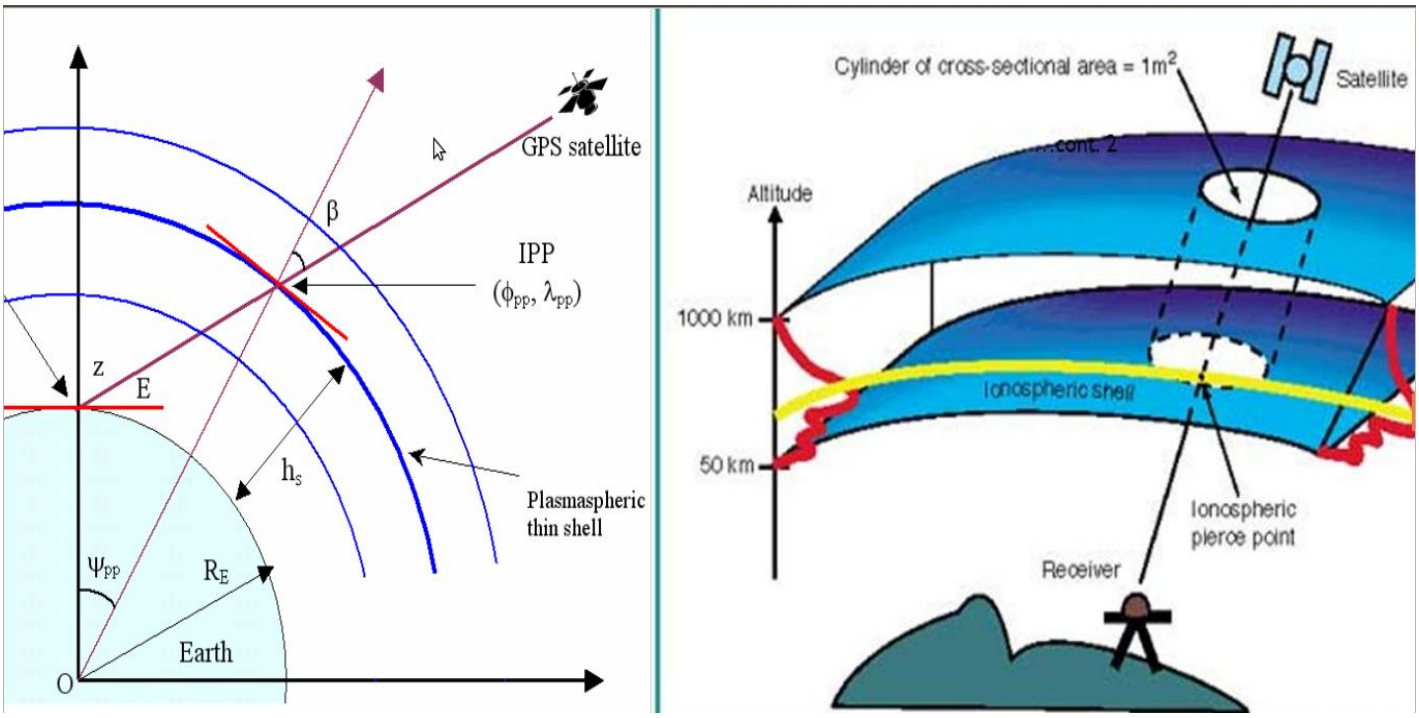

Figure 4-1Vertical total electron conversions (Goopy, 2011)

4.1.3. International Reference of Ionosphere (IRI-2007)

International Reference of Ionosphere is web design program and it enables the computation and plotting of IRI parameters: electron and ion (O+,H+, He+, O2+, NO+) densities, total electron content, electron, ion and neutral, temperatures, equatorial vertical ion drift and others (http://ccmc.gsfc.nasa.gov/modelweb/models/iri_vitmo.php) .

4.1.4. GAMIT/GLOBK

GAMIT is GPS analysis software developed by Massachusetts Institute of Technology, USA. This software estimates station position, satellite orbits parameters, initial conditions, radiation parameters, phase center offsets, earth orientation parameters (EOP), atmospheric delay parameters, time, dependent zenith delays and gradients, ionospheric delays and carrier phase ambiguities (GAMIT/GLOBK user manual, 2010).

GLOBK uses parameter estimates and full covariance matrices from different sources to combine results. Inputs from GPS, Satellite Laser Ranging (SLR), Very-long-baseline interferometry (VLBI) and Solution Independent Exchange Format (SINEX) files and can be used to estimate site velocities from series of measurements, satellite orbit improvement, EOP parameters.

4.2. Files needed to process GPS data in GAMIT/GLOBK

To solve for the position of a particular point using GPS observables does require not only mathematical modeling but also a suite of ancillary input data. These are some of the models/data that are needed to produce an accurate position or velocity of a point using software like GAMIT/GLOBK.

Nutation tables: Give position of Earth's body axis in space. Needed for transforming orbits integrated in inertial space back to Earth fixed frame.

Table of satellite types: Since the Pseudo Random Number (PRN) numbers are re-used (1-32), there could be ambiguity about the mass, size and phase center position of the satellites. There is a unique Satellite Vehicle (SV) number for each satellite.

Ephemerides of Sun and Moon: Needed for tidal forces on satellite. Can be in tabular form (most common; Harvard-Smithsonian Center for Astrophysics and JPL produce these). Ephemerides can also be used for Earth tide calculations.

Leap second table: Allows conversion from GPS time to Universal Corrected time (UTC). Offset included in broadcast ephemeris so not strictly needed if broadcast ephemeris used. Leap seconds are announced by the Inertial Earth fixed Reference System (IERS).

Polar motion/UT1 tables: Needed in the transformation from inertial to earth fixed frame and it is available through the IERS If earth-fixed orbits used not strictly necessary.

Ocean tide loading model tables: Either in the form of station dependent values or in a grid that is interpolated. Signals are diurnal and semidiurnal mainly.

Antenna phase center model tables: Give the deviations of the phase as a function of elevation angle (and possibly azimuth) relative to a fixed point on the antenna (the ARP-antenna reference point). If the same type of antenna used in a small area, then not strictly needed but with mixed antenna types or large extent networks (such that satellites are seen at different elevation angles) it is needed. The GPS processing may also need a file that translates names of antennas in RINEX files into standard names (IGS maintains list of standard names for antennas). Station information that gives position of ARP relative to ground mark. Strictly this should be in RINEX file header but is often incorrect. Getting this information correct is often the biggest problem in campaign GPS processing. Information is recorded on paper log sheets that need to be transcribed correctly. Often referred to as meta-data for RINEX file.

Apriori coordinates and velocities for sites (can extract position from RINEX header but these are often not very good)

Apriori orbit information for satellites, atmospheric and water loading files. Not normally used.

RINEX observation file: This is Receiver Independent Exchange (RINEX) file format and it contains L1 and L2 carrier beat phases and pseudo-range, signal amplitudes, initial station coordinates and antenna offsets, start and stop times, receiver and antenna type, and the identification of the satellites tracked in each receiver channels.

Sp-3 files: it contains precise igs orbits. Tabulated GPS orbits are usually distributed using "special Products 3" format developed at the U.S National Geodetic Survey.

brdc files: Broadcast Ephemeris data may be in either RINEX or other format and it contains broadcasted ephemeris.

Code IONEX files : Global ionospheric map (GIM) are generated on a daily basis at CODE using data from about 150 GPS sites of IGS and other institutions. The vertical electron content is modeled in a solar-geomagnetic reference frame using a spherical harmonics expansion up to degree and order 15.

4.3. Control files to processes GPS data

Strict information should be included in the following control files to process GPS rinex files and its ancillary data in the work flow GAMIT.

Table 4-1Control files

Control file:	Name:	Type:	Created by	Input to
1. Processing control file: Used by sh_gamit; includes directory names and some processing control	process.defaults	ASCII	User from template	Sh_gamit
1. Site processing control file: Used by sh_gamit; includes controls for use of stations.	sites.defaults	ASCII	User from template	sh_gamit
2. Session control table : Input control file for fixdrv, specifying the type of analysis and the a priori measurement errors and satellite constraints.	sestbl.	ASCII	User from template	fixdrv
3. Site control Table Input control file for fixdrv, specifying for each site the a priori coordinate constraints and optionally the clock and atmospheric models	sittbl.	ASCII	User from template	fixdrv
4. Session information or scenario file Satellites and times to be processed	session.info	ASCII	User or makexp / sh_makexp	makex, fixdrv

4.4. IGS stations of the study area

As we have described in chapter 1 our objective is to assess the effect of higher order ionosphere on GPS signals along the equatorial regions. Twenty (20) stations are selected from IGS stations where 16 stations are located along the equatorial region while 4 stations from higher latitudes are also included for comparison purposes (see Table 4.2 for details).

Table 4-2 Summary of study area.

Identification	**City**	**Location**	**Longitude (degree)**	**Latitude (degree)**	**Height (meter)**
ADIS	Addis Ababa	Ethiopia	38.7663	9.0351	2439.1540
BHR1	Manama	Bahrain	50.6081	26.2091	-13.900
BAKO	Cibinong	Indonesia	106.8500	-6.4900	158.1800
BOGT	Bogota	Colombia	285.9191	4.6401	2576.7782
CGGN	Toro	Nigeria	9.1183	10.12.13	916.683
COCO	Cocos (Keeling) Island	Australia	96.8339	-12.1883	-35.2212
DARW	Darwin	Australia	131.1327	-12.8437	125.1965
DGAR	Diego Garcia Island	U.K. Territory	72.3702	-7.2697	-64.7455
FAIR	Fairbanks	United States	212.5008	64.9780	319.1771
HOFN	Hoefn	Iceland	344.8132	64.2673	82.5000
HYDE	Hyderbad (central part of India)	India	78.5509	17.4173	441.683
KOUR	Kourou	French Guyana	307.1940	5.2522	-25.5700
MBAR	Mbarara	Uganda	30.7379	-0.6015	1337.000
MAL2	Malindi	Kenya	40.1940	-2.9960	-20.4000
NKLG	Libreville	Gabon	9.6721	0.3539	31.480
NTUS	Singapore	Republic of Singapore	103.6799	1.3458	79.000
NYAL	Ny-Alesund	Norway	11.8700	78.9300	82.0000
POVE	Porto Velho	Brazil	296.1037	-8.7093	119.6000
SALU	São Luis	Brazil	315.7875	-2.5935	18.9000
SEY1	Lamisere	Seychelles	55.4794	-4.6737	5379.230

Additional criteria for selecting the IGS station for our study is to have a longer times series with the exception of few points. Most of the stations have more than 11 years of uninterrupted time series which will help us to look an 11 years solar cycle where we expect the ionosphere effect are maxima.

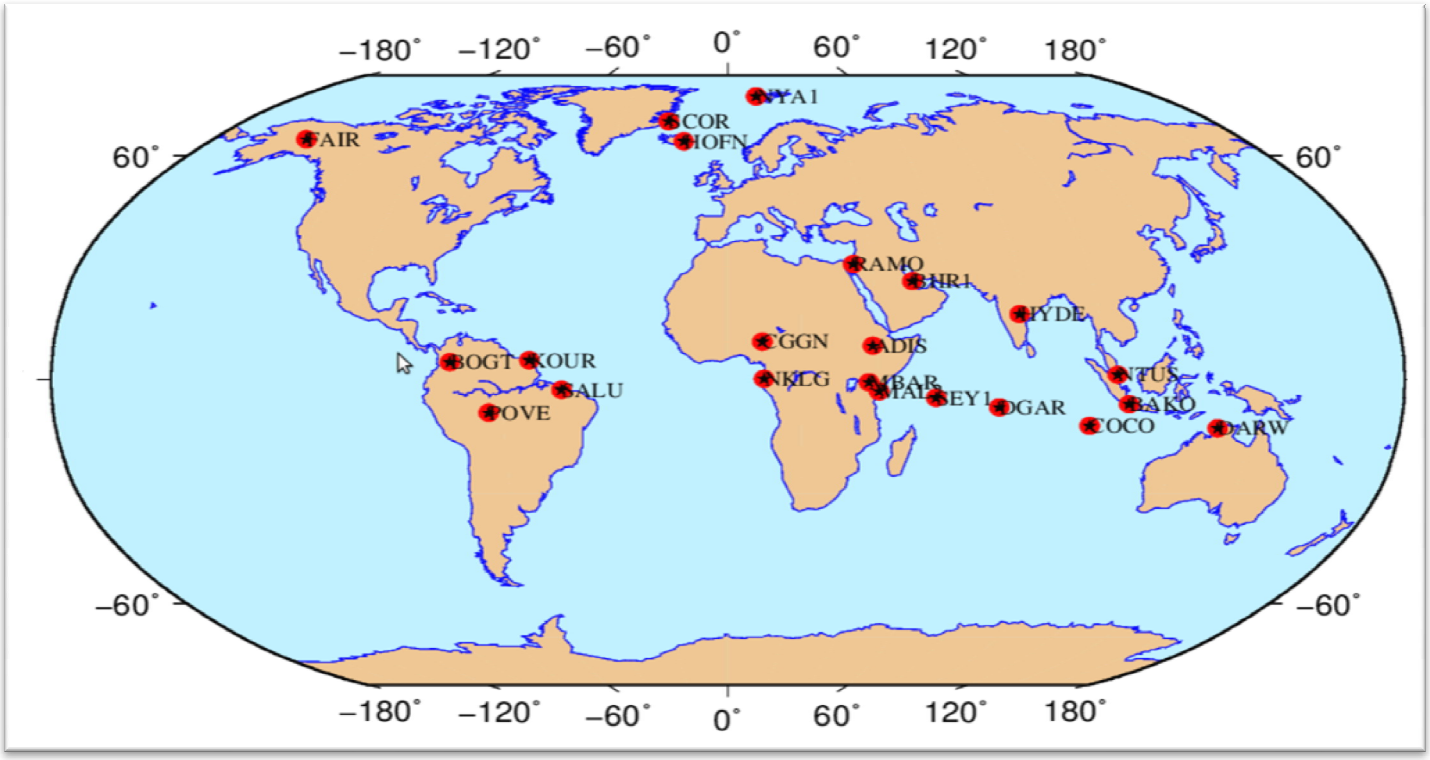

Figure 4-2 GPS sites used for this study.

4.5. Diurnal and Solar Cycle effect of ionosphere over the study areas

The density of total electron content varies due to seasonal (summer and winter), the length of the day (day and night), and geographical locations.

To show the spatial and diurnal variation of ionosphere we plotted VTEC in QC software for March, 2012.

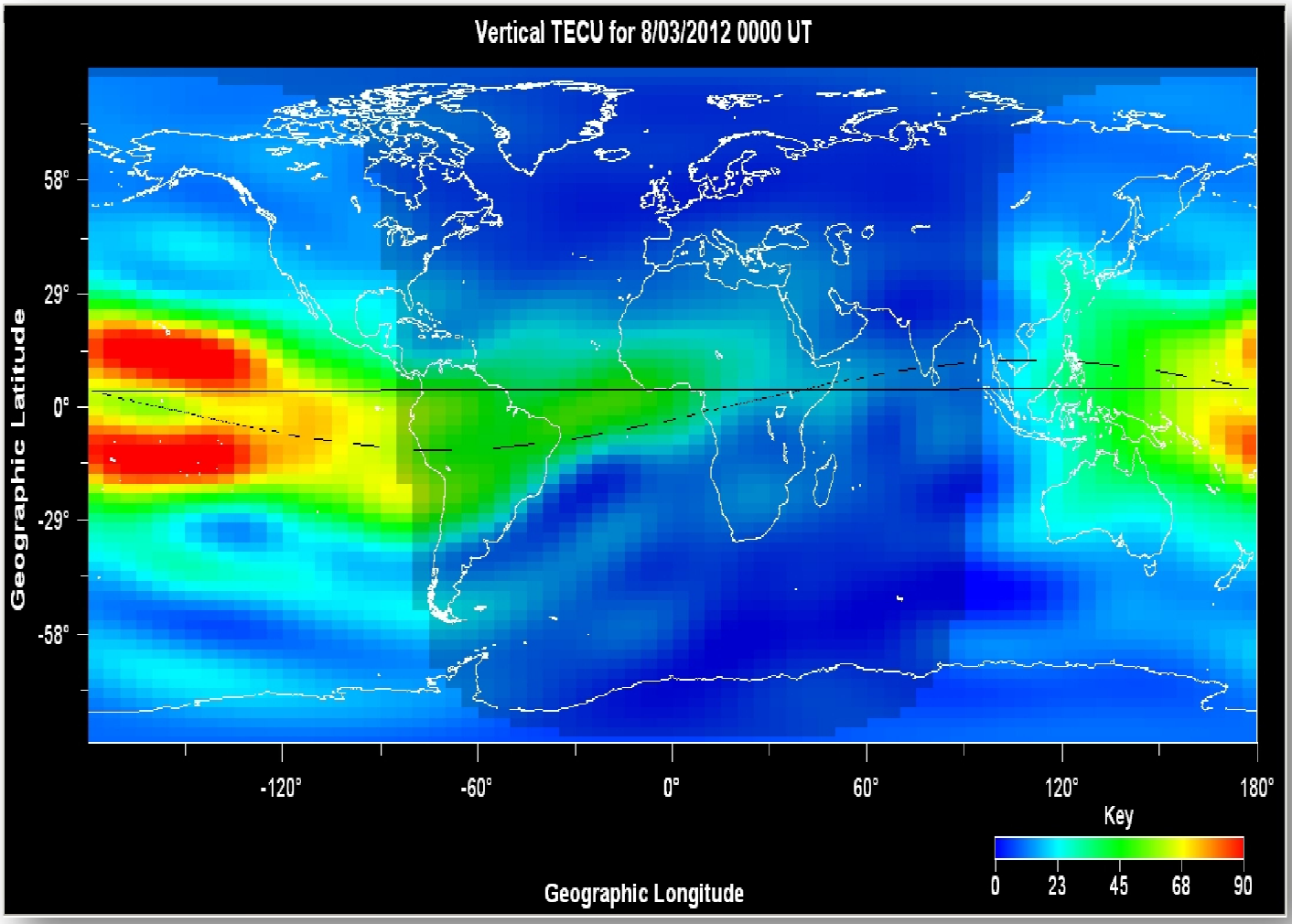

Figure 4-3 Leica GNSS QC result March, 8, 2012 at 00:00 UT

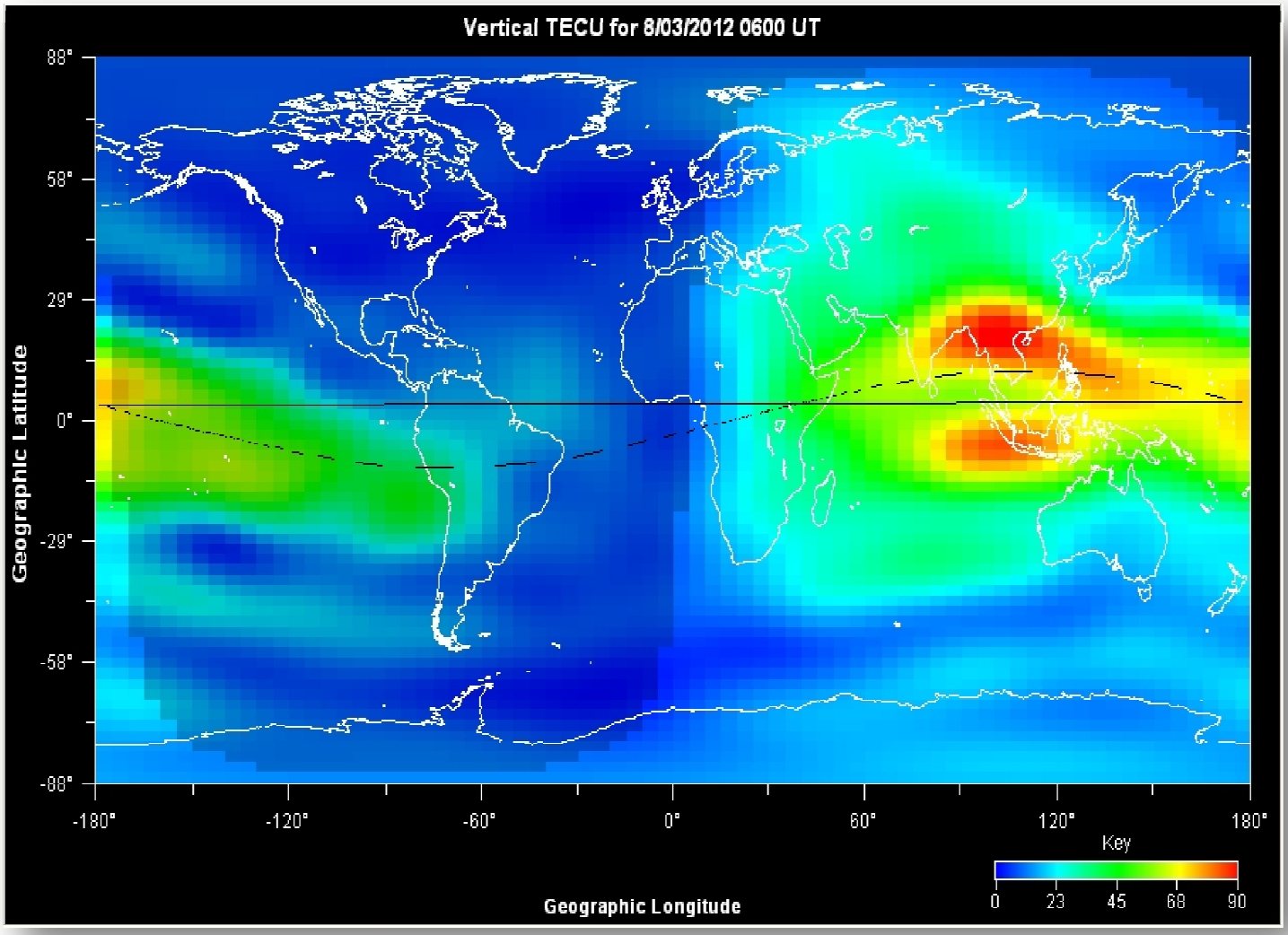

Figure 4-4 Leica GNSS QC result March, 8, 2012 at 06:00 UT

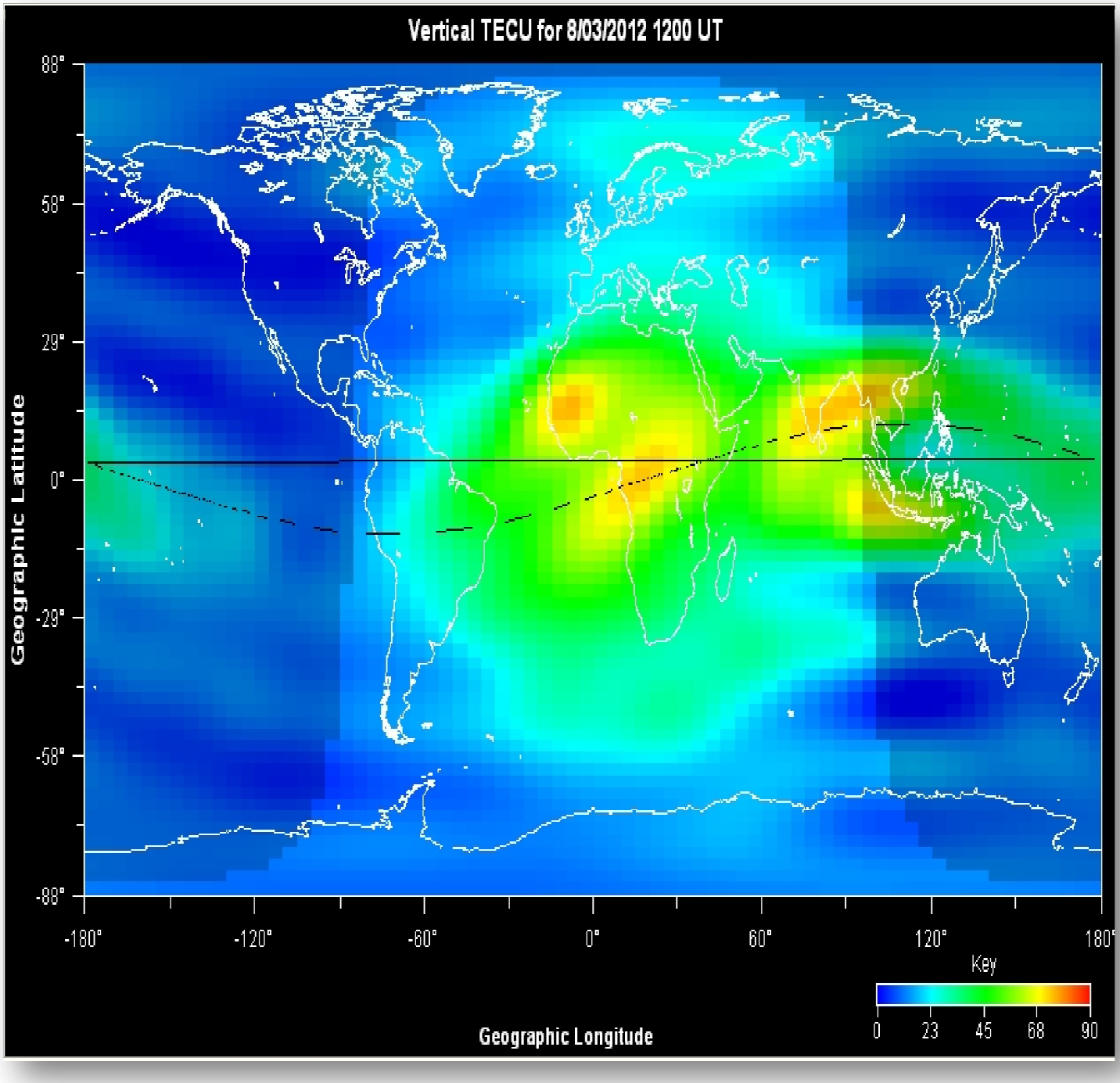

Figure 4-5 Leica GNSS QC result March 8, 2012 at 12:00 UT

Figures 4.3, 4.4 and 4.5 show the spatial and temporal (diurnal) variations of VTEC. In all figures higher values of TEC were observed in day time where the sun is active. But the values of the TEC vary spatially.

Higher values of TEC were observed on the stations from the equatorial region which indicates the spatial variation of TEC distribution.

We have used also GPS_TEC software to study diurnal effect. Figures 4.6 and 4.7 shows the diurnal effect of TEC for ADIS and BAKO stations.

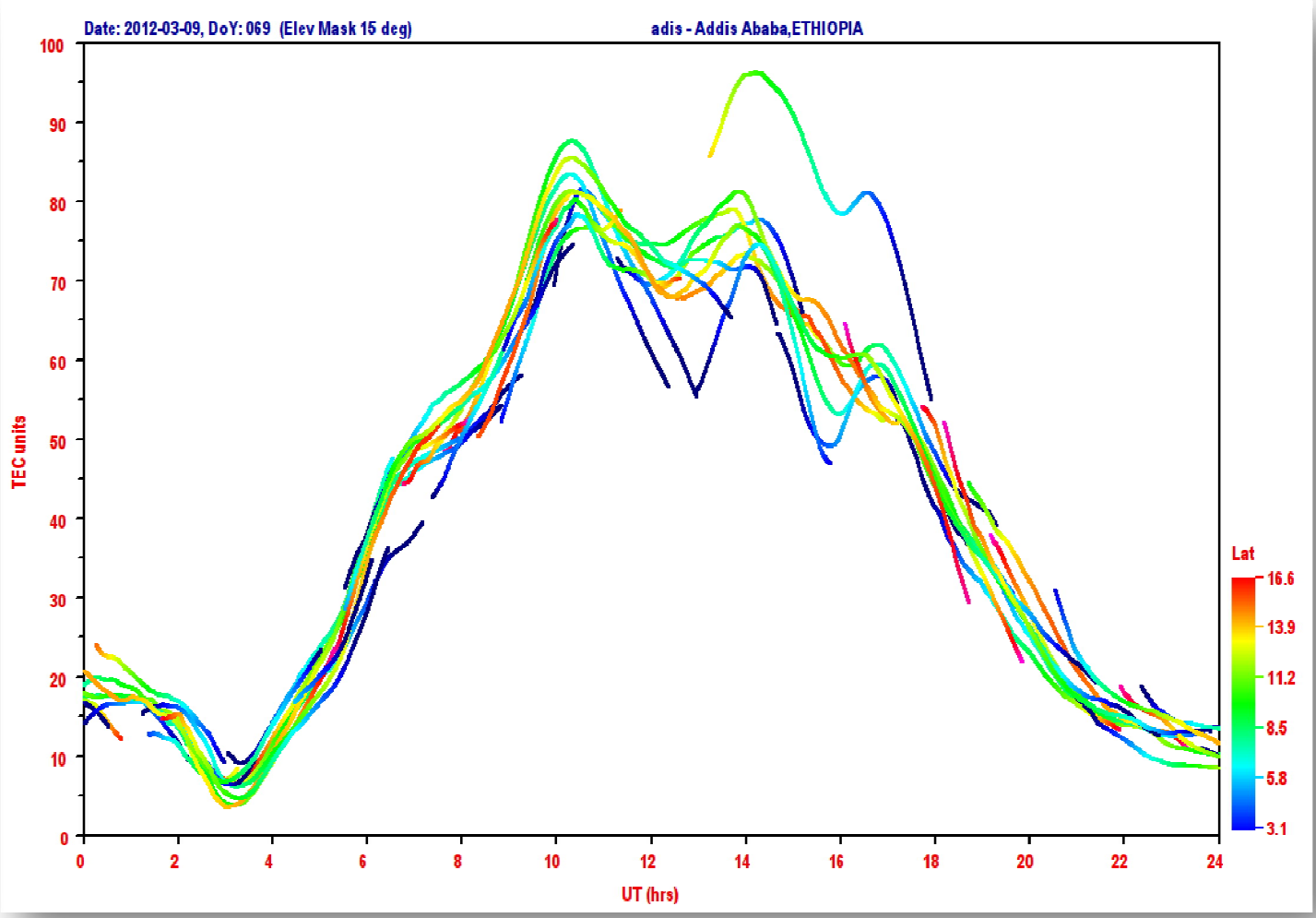

Figure 4-6 VTEC of Addis Ababa March, 9, 2012

The legends of Figures4.6 and 4.7 represent latitude variations of the satellite orbit. These different colors of the legend are the position of the satellites moves through their orbits at different latitudes and sent the signals to the stations. In general the maximum VTEC occur beteween10 to 12:00 UT and 14:00 to 16:00 UT this is because of the diurnal cycle effect of the TEC for station ADIS. The same plot is shown in Figure 13 for station BAKO were the maximum VTEC was observed at 18:00 UT.

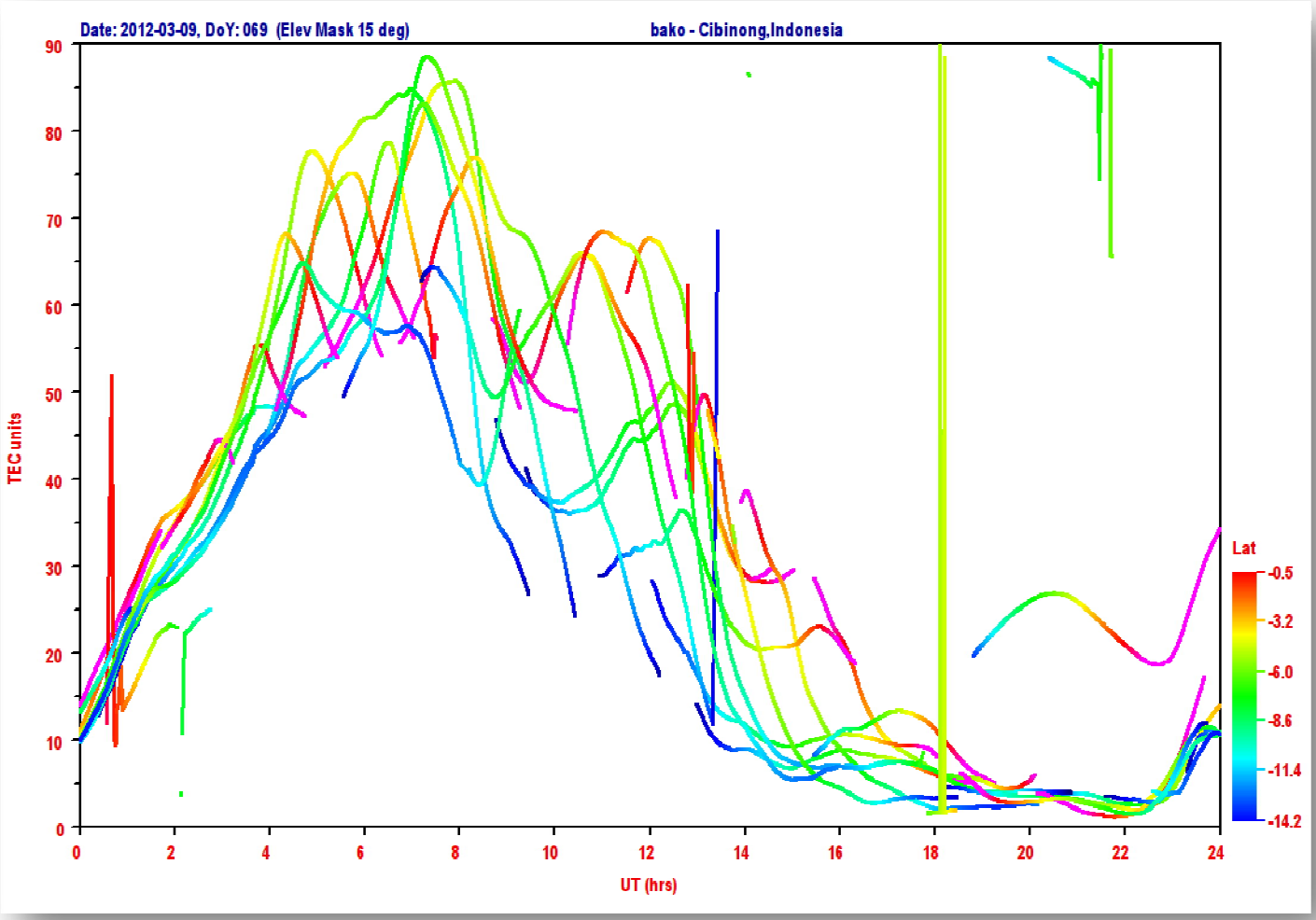

Figure 4-7 VTEC of BAKO March, 9, 2012

We also calculated the density of total electron content of the study areas at different height of the ionosphere layers by using IRI-2007 model to study the solar cycle effect.

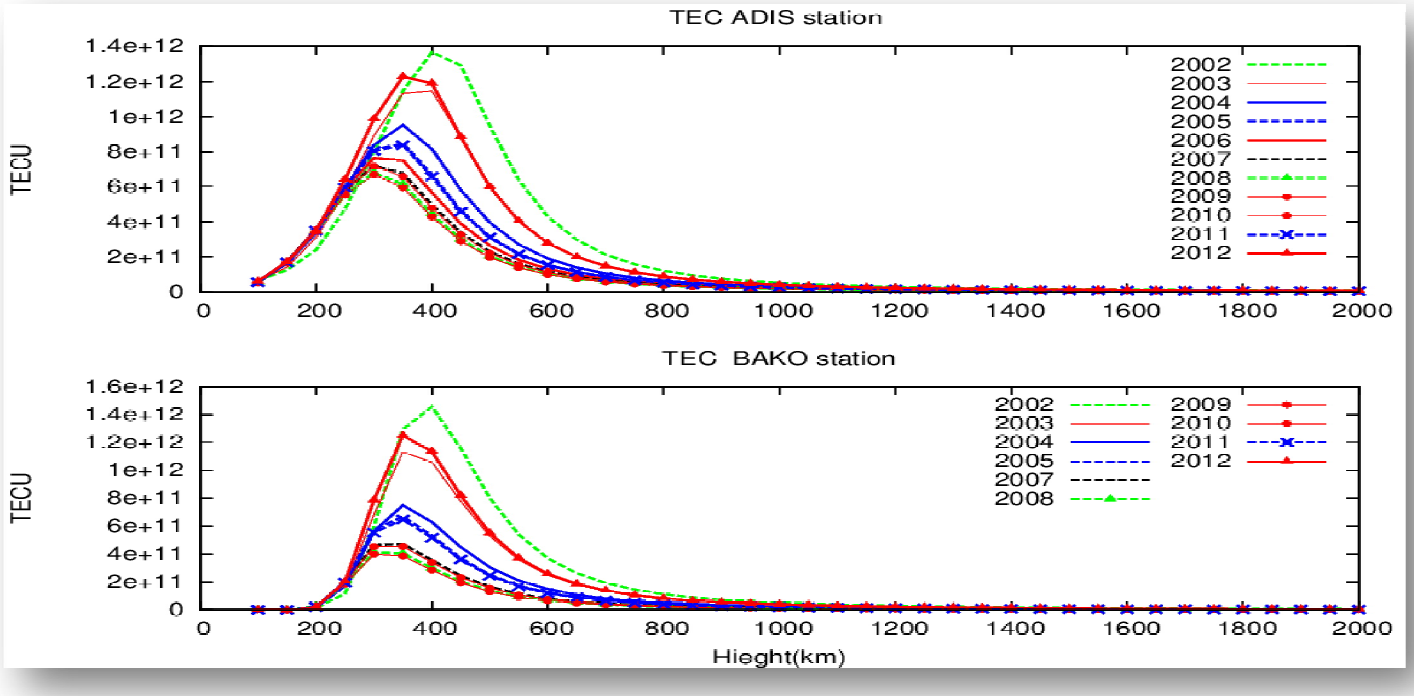

Figure 4-8 TEC of ADIS and BAKO reference station

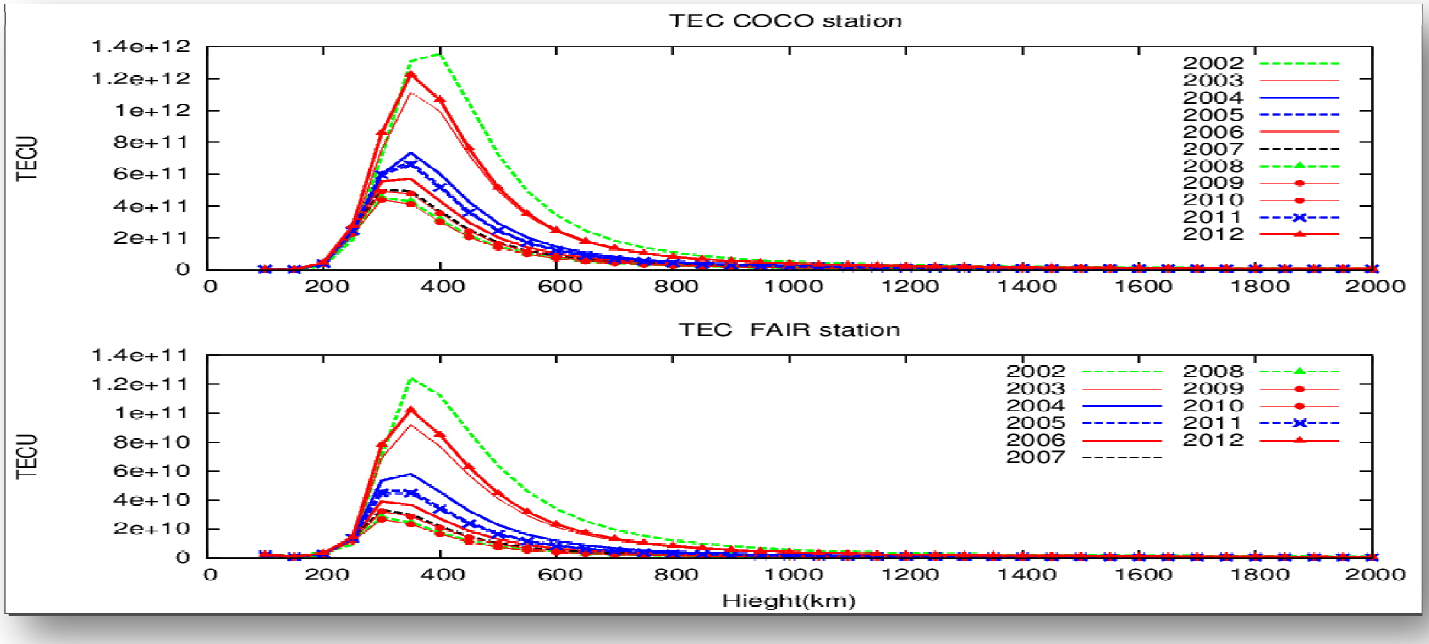

Figure 4-9 TEC of COCO and FAIR reference station

Figures 4.8 and 4.9 show higher values of TEC during 2002 and 2012 at the height of nearly from interval of 300-350 km in the ionosphere region which is the F-layer (see section 2.8.3). High values of TEC during 2002 and 2012 were because of high solar activity during these periods and this shows the solar cycle effect.

4.6. Geomagnetic field versus TEC

Geomagnetic field has an influence on second and third order ionosphere effect on GPS signal. Geomagnetic field and TEC of Addis Ababa reference station is plotted to see the correlation between geomagnetic field and TEC. In Addis Ababa University, Geophysical observatory absolute measurements of geomagnetic field are done twice a week using Declinometer-Inclinometer theodolite by the staff of Addis Ababa Ethiopia (AAU) magnetic observatory (Geophysical Observatory AAE INTERMAGNET user manual, 2001). For more details about geomagnetic field see section 2.17.

We have plotted the variation of geomagnetic field and TEC during years 2010 and 2012. We selected in March 7, 8, 9 and 10 of the year 2012 because there were high solar activity and the geomagnetic storm at these days (http://thewatchers.adorraeli.com/2012/03/24/march-solar-storms-heat-up-earths-atmosphere/).

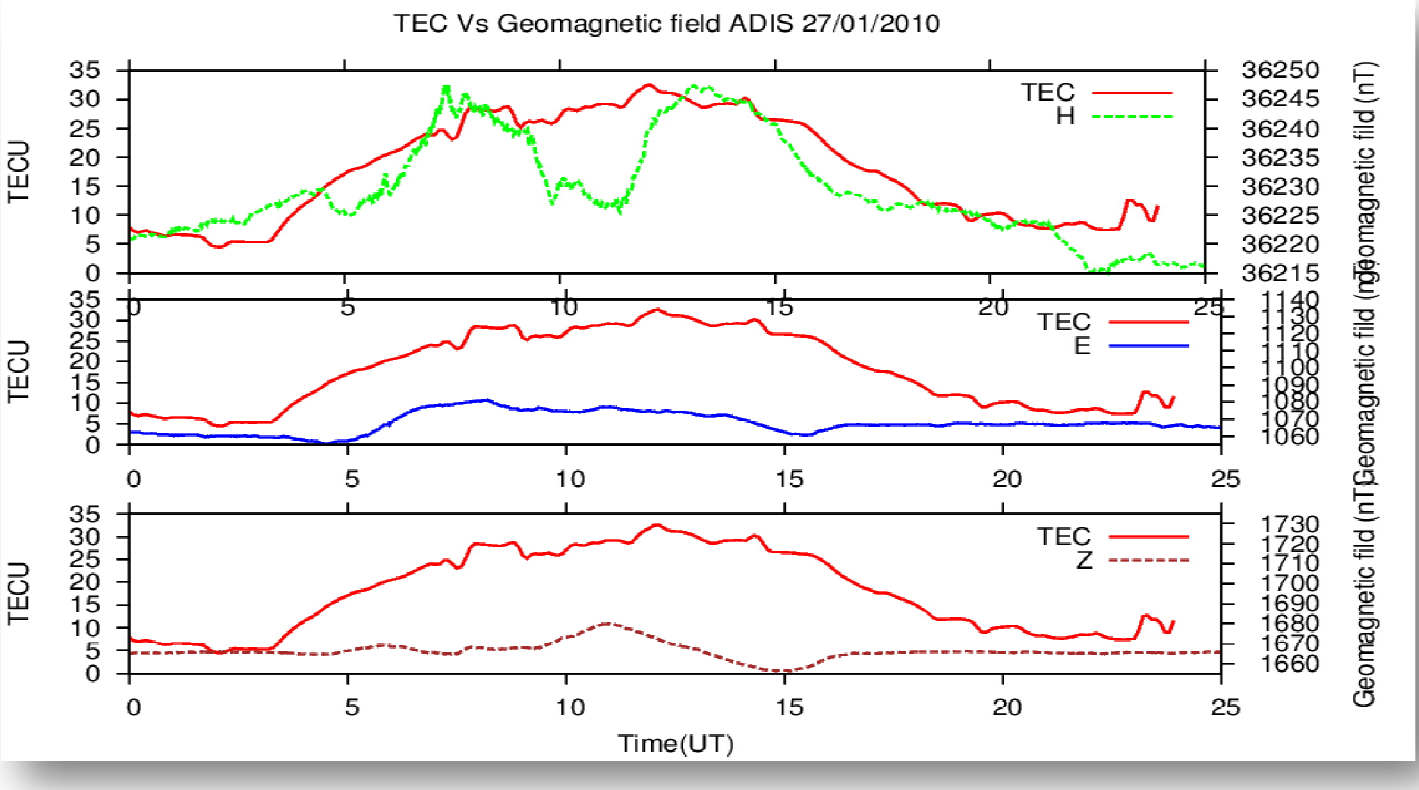

Figure 4-10 Geomagnetic field and TEC of ADIS reference station 2010

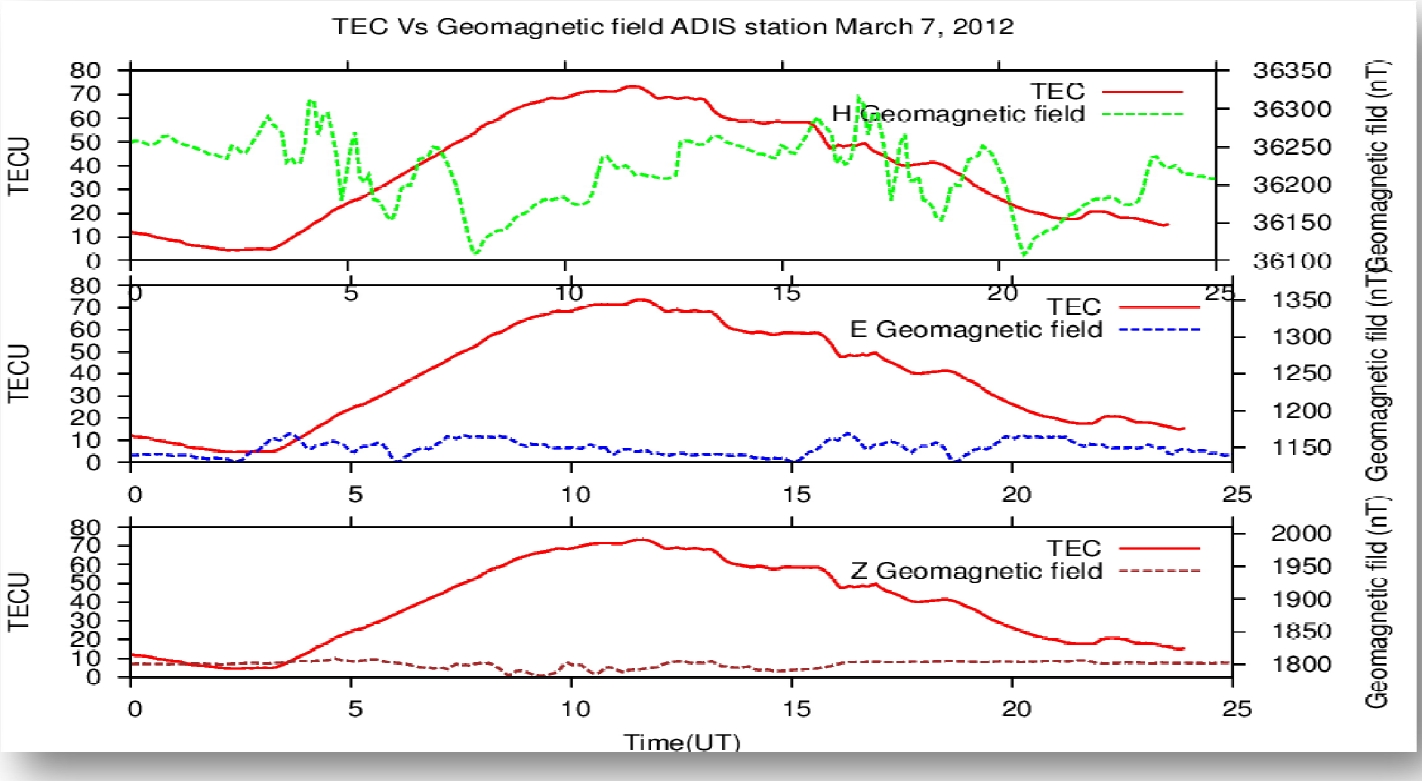

Figure 4-11 Geomagnetic field and TEC of ADIS reference station March 7, 2012

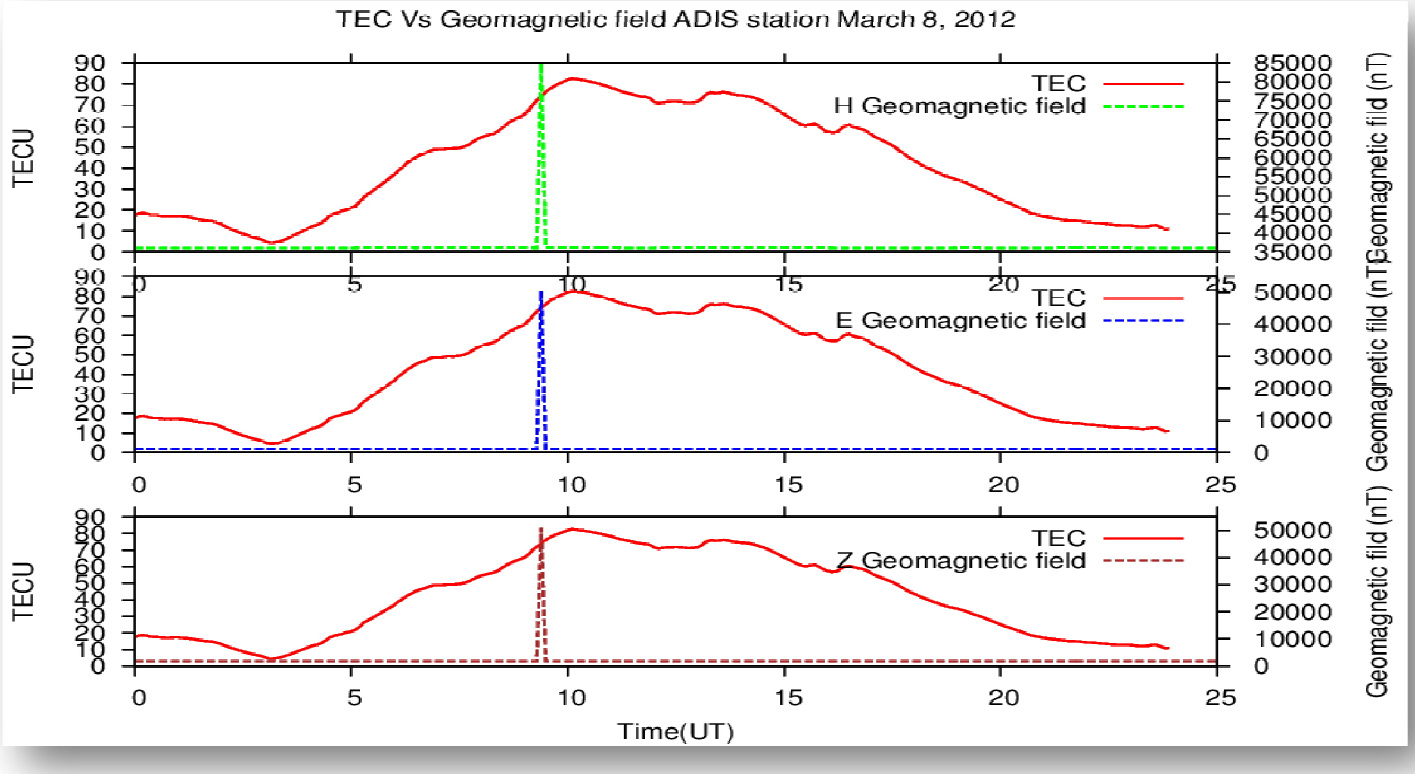

Figure 4-12 Geomagnetic field and TEC of ADIS reference station March 8, 2012

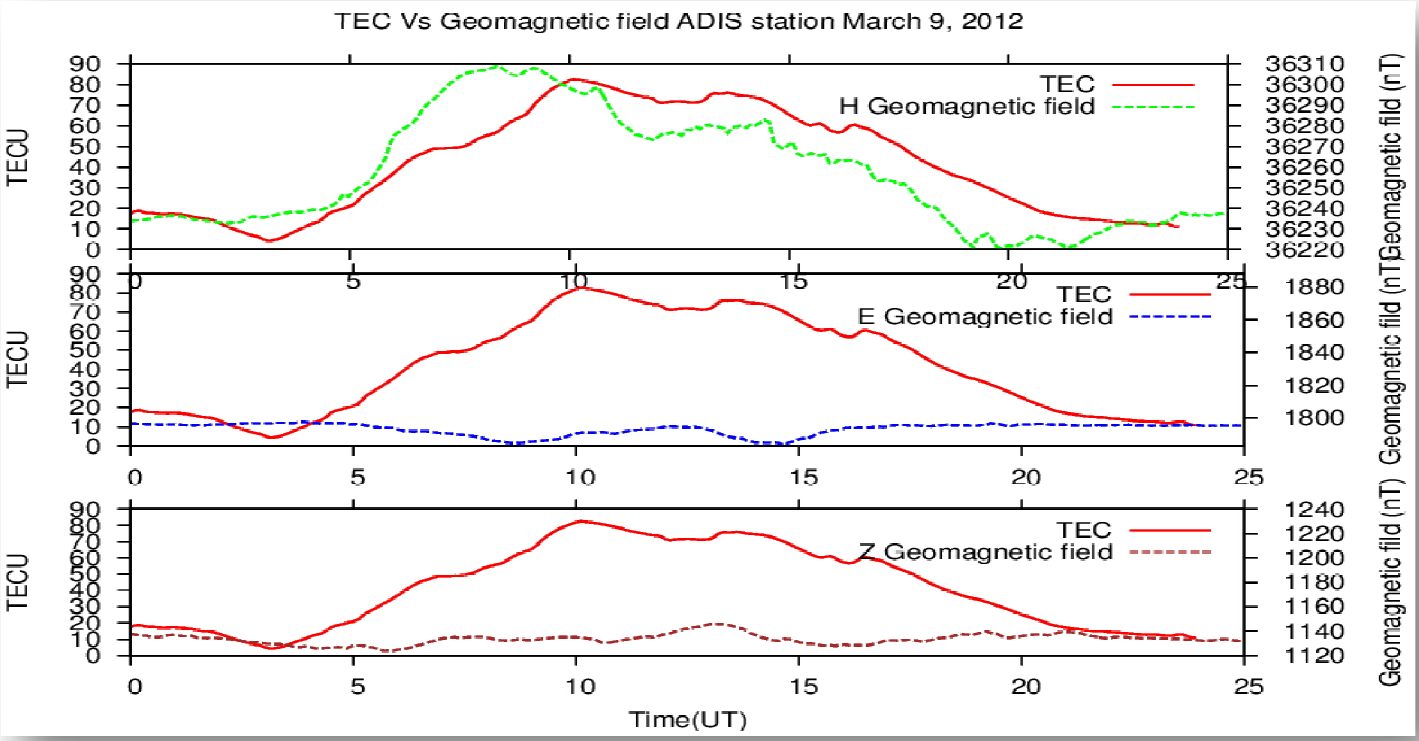

Figure 4-13 Geomagnetic field and TEC of ADIS reference station March 9, 2012

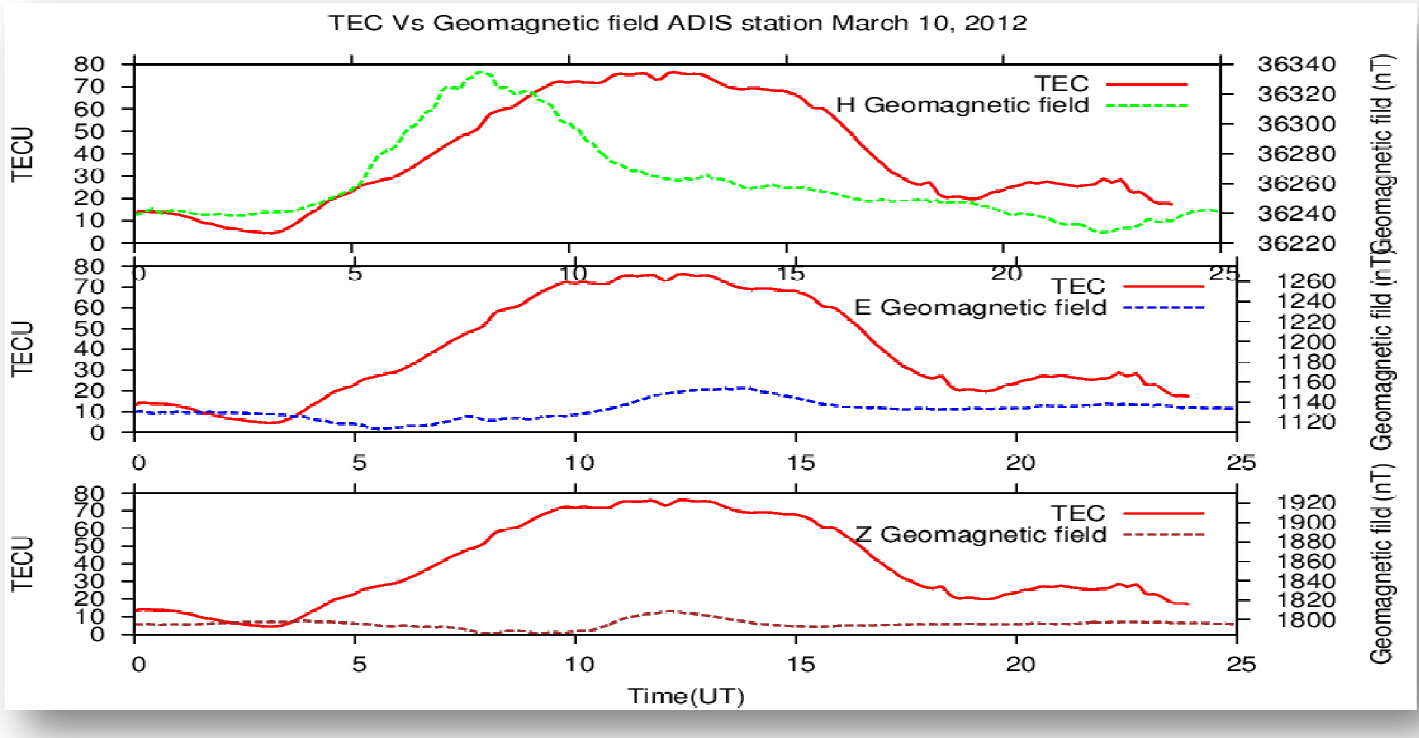

Figure 4-14 Geomagnetic field and TEC of ADIS reference station March 10, 2012

Figure 4.10, 4.11, 4.12, 4.13 and 4.14 red colors represent total electron content densities and other colors represent geomagnetic field. Figure 16 the geomagnetic field and TEC values were less than as compare to in year 2012. The reason is in 2005 to 2010 were solar minimum periods. Because of this our result shows the higher order time delay and 3D positional rms values were low during 2008 to 20011 and become high in 2012 (see the result section 4.83 and 4.93). In all Figures horizontal (H) geomagnetic field has high since it is the resultant vector of X and Y component (H = $\sqrt{X^2 + Y^2}$). This horizontal geomagnetic field is highly correlated to TEC. The reason is, along the east-west of equatorial region there is high equatorial electro-Jet flow that is affected by horizontal component of geomagnetic field. Geomagnetic field attracts the free electrons and this increase ionosphere production. Again the disturbance of ionosphere increased or decreased the geomagnetic field.

4.7. Solar cycle and Sunspot

The number of sunspots on the sun waxes and wanes over an 11-year is solar cycle. Since sunspots are associated with solar activity (i.e., flares and other rapid releases of energy that can heat localized regions of the atmosphere of the sun to many millions of degree Kelvin , the solar cycle also describes the level of activity and variability of the sun. Each snapshot of the sun shows the structure of the sun's atmosphere in X-rays at a given day, one snap- shot per year. Note that, the amount of X-rays increases and decreases over this solar cycle – with the amount of time from the most active or energetic interval (called solar maximum) to the time of least activity (solar minimum) being approximately five to six years. X-rays are very energetic electromagnetic radiation and are created when a gas is heated to about one million degree Kelvin. Notice that during solar maximum, the sun's atmosphere has many places of bright X-ray emission, whereas at solar minimum the atmosphere of the sun is essentially black in X-rays, indicating that very little heating of the upper atmosphere of the sun is taking place. Also, the X-ray emission is not coming from the surface of the sun, but from the atmosphere above the photosphere (M. Moldwin 2008).

Sunspots appear as dark spots on the surface of the Sun. Temperatures in the dark centers of sunspots drop to about 3700 K (compared to 5700 K for the surrounding photosphere). They typically last for several days, although very large ones may live for several weeks. Sunspots are magnetic regions on the Sun with magnetic field strengths thousands of times stronger than the Earth's magnetic field. Sunspots usually come in groups with two sets of spots. One set will have positive or north magnetic field while the other set will have negative or south magnetic field. The field is strongest in the darker parts of the sunspots - the umbra. The field is weaker and more horizontal in the lighter part – the penumbra (http://solarscience.msfc.nasa.gov/feature1.shtml#Sunspots).

We have plotted the sunspot number during year 2002 to 2012 to show the solar cycle.

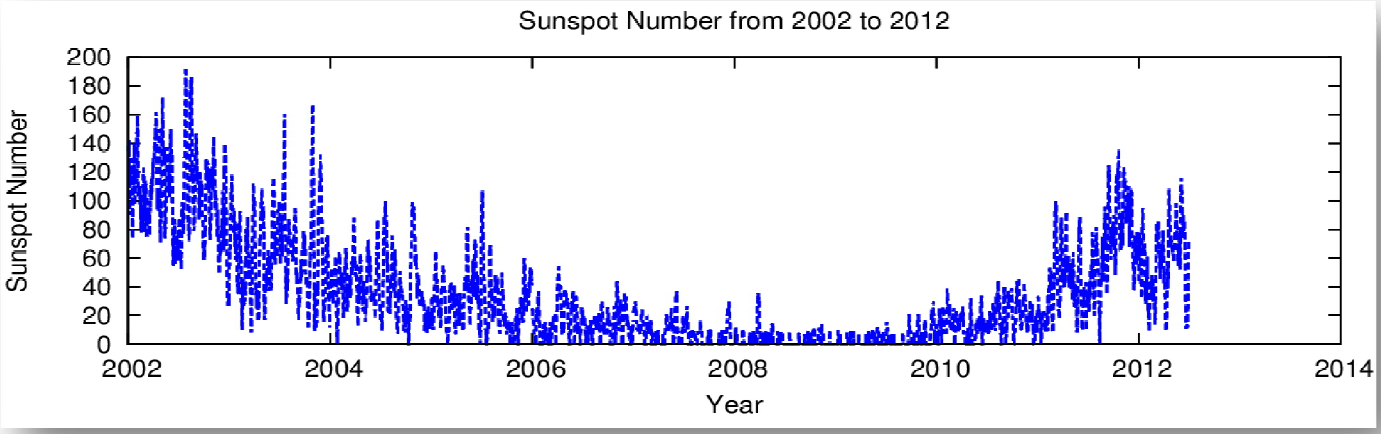

Figure 4-15 Sunspot number (solarscience.msfc.nasa.gov/predict.shtml)

4.8. Three dimensional positional accuracy with and without higher order ionospheric effects model

To obtain TEC for the computation of 2nd and 3rd order ionosphere effects we have used the global ionosphere maps (GIM) generated on a daily basis at the Center for Orbit Determination in Europe (CODE) using data from about 150 GPS sites of the IGS and other institutions. The vertical total electron content (VTEC) is modeled in a solar-geomagnetic reference frame using a spherical harmonics expansion up to degree and order 15, piece-wise linear functions are used for representation in the time domain. The time spacing of their vertices is 2 hours, conforming to the epochs of the VTEC maps. Instrumental biases, so-called differential P1-P2 code biases (DCB), for all GPS satellites and ground stations are estimated as constant values for each day, simultaneously with 13 times 256, or 3328 parameters used to represent the global VTEC distribution. The DCB datum is defined by a zero-mean condition imposed on the satellite bias estimates. P1-C1 bias corrections are taken into account if needed. To convert line-of-sight TEC into vertical TEC, a modified single-layer model mapping function approximating the JPL extended slab model mapping function is adopted. The mapping function is evaluated at geodetic satellite elevation angles (http://www.aiub.unibe.ch/download/CODE/).

4.8.1. BAKO station 3D positional root mean square from GAMIT/GLOBK processes

Table 4-3 BAKO station root mean square

Case- 1 Root mean square without correction of 2nd and 3rd order ionosphere effect				**Case - 2** Root mean square with correction of 2nd and 3rd order ionosphere effect			**Quadratic difference,** i.e., the square root of the differences in the variances		
Year	**N(m)**	**E(m)**	**U(m)**	**N(m)**	**E(m)**	**U(m)**	**N(m)**	**E(m)**	**U(m)**
2001	0.0038	0.0075	0.0087	0.0038	0.0075	0.0087	0.0000	0.0000	0.0000
2002	0.0040	0.0046	0.0087	0.0035	0.0045	0.0086	0.0012	0.0013	0.0021
2003	0.0023	0.0072	0.0080	0.0023	0.0046	0.0080	0.0000	0.0055	0.0000
2004	0.0023	0.0043	0.0086	0.0022	0.0021	0.0084	0.0007	0.0038	0.0018
2005	0.0020	0.0043	0.0079	0.0020	0.0043	0.0079	0.0000	0.0000	0.0000
2006	0.0026	0.0043	0.0081	0.0025	0.0042	0.0079	0.0007	0.0009	0.0018
2007	0.0022	0.0043	0.0080	0.0022	0.0043	0.0080	0.0000	0.0000	0.0000
2008	0.0021	0.0042	0.0082	0.0021	0.0040	0.0079	0.0000	0.0013	0.0022
2009	0.0021	0.0041	0.0081	0.0020	0.0040	0.0079	0.0006	0.0009	0.0018
2010	0.0020	0.0040	0.0079	0.0020	0.0040	0.0079	0.0000	0.0000	0.0000
2011	0.0020	0.0042	0.0079	0.0020	0.0041	0.0077	0.0000	0.0009	0.0018
2012	0.0041	0.0085	0.0094	0.0032	0.0073	0.0064	0.0026	0.0044	0.0069

We have used quadratic differences because it is a better measure statistical accuracy compared to the difference in rms values. The square root of the differences in the variances shows more directly the contribution of the 2nd and 3rd order ionosphere.

Table 4.3 shows the rms values in the three directions (north, east and up). In general, there is a reduction in rms values when we introduced the effects of the higher order terms of ionosphere effects. During 2002 the root mean square of the coordinates were 4mm, 4.6 mm and 8.7 mm respectively in the north, east and up directions while the rms errors have been reduced to 3.5 mm, 4.5 m and 8.6 mm respectively in north, east and up direction by applying the 2nd and 3rd order ionosphere corrections. Significant reductions in rms values come from in year 2002 and 2012 that corresponds to high solar activities of the sun.

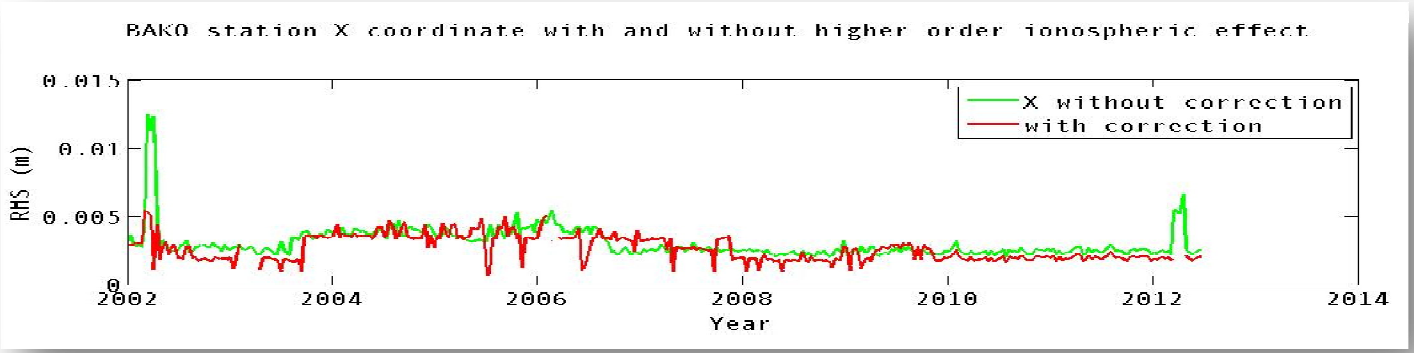

Figure 4-16 BAKO station X coordinate root mean square

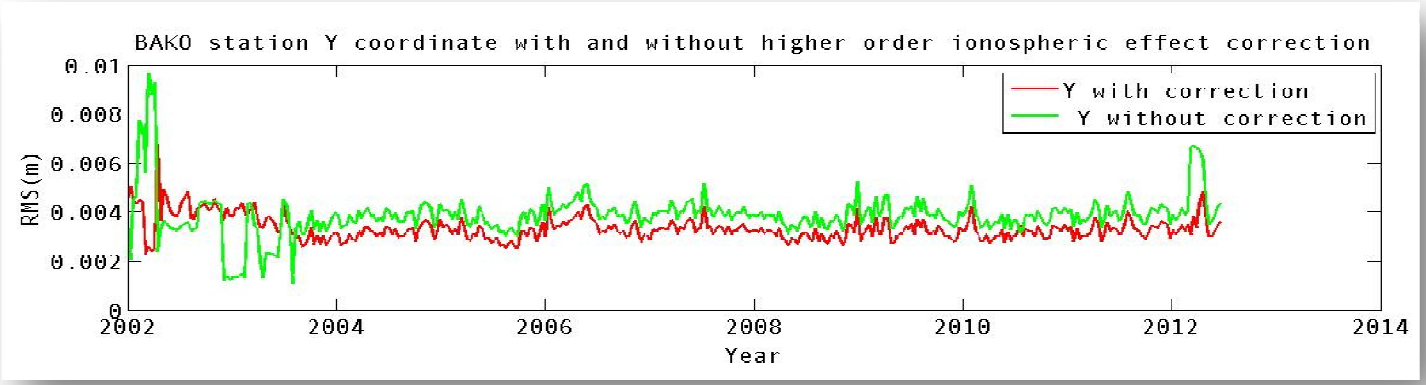

Figure 4-17 BAKO station Y coordinate root mean square

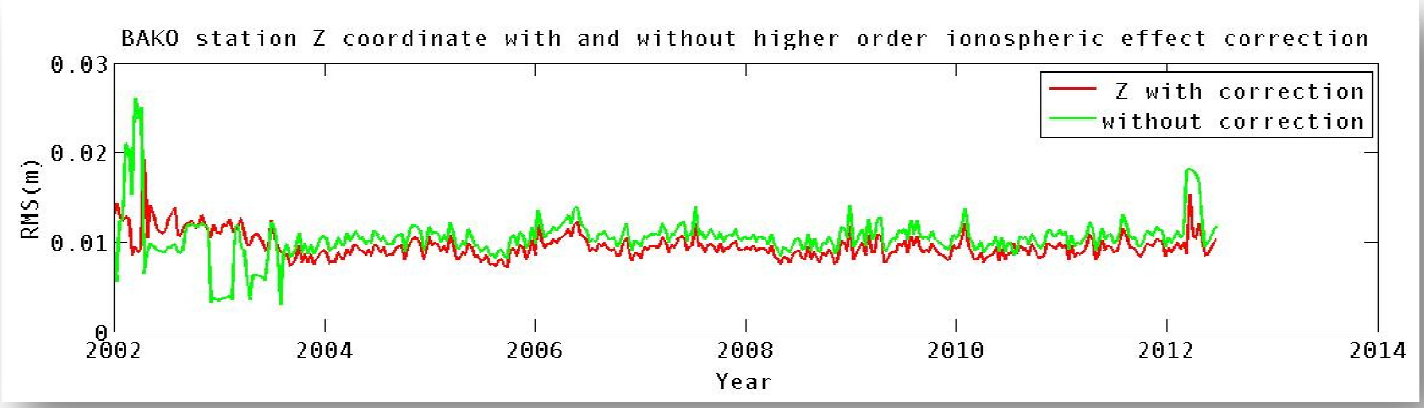

Figure 4-18 BAKO station Z coordinate root mean square

Figure 4.16, 4.17 and 4.18 show the rms values with and without modeling higher order terms during our GPS data processing. The green color represents a root mean square without modeling higher order ionospheric effects and the red color represents a rms values when the higher order terms are modeled in our GPS time

series processing for the period between 2002 to 2012. Again this presentations show a higher noise in year 2002 and 2012 when the higher order terms are not taken into account.

4.8.2. BOGT station 3D position root mean square in GAMIT/GLOBK repeatability

We have also made the same plot now using a different IGS station (BOGT), see Figure 8. This station is clearly located around the equator region.

Table 4-4 BOGT station root mean square

Year	**Case-1** Root mean square without correction (m)			**Case -2** Root mean square with correction (m)			**Quadratic difference,** i.e., the square root of the differences in the variances		
	N(m)	**E(m)**	**U(m)**	**N(m)**	**E(m)**	**U(m)**	**N(m)**	**E(m)**	**U(m)**
2002	0.0500	0.0436	0.0791	0.0347	0.0387	0.0501	0.0360	0.0201	0.0612
2003	0.0500	0.0436	0.0791	0.0347	0.0387	0.0501	0.0046	0.0058	0.0392
2004	0.0500	0.0436	0.0791	0.0347	0.0387	0.0501	0.0032	0.0201	0.0925
2005	0.0500	0.0436	0.0791	0.0347	0.0387	0.0501	0.0094	0.0042	0.0266
2006	0.0500	0.0436	0.0791	0.0347	0.0387	0.0501	0.0144	0.0271	0.1058
2007	0.0500	0.0436	0.0791	0.0347	0.0387	0.0501	0.0109	0.0221	0.0393
2008	0.0500	0.0436	0.0791	0.0347	0.0387	0.0501	0.0098	0.0334	0.0061
2009	0.0500	0.0436	0.0791	0.0347	0.0387	0.0501	0.0429	0.0045	0.0068
2010	0.0500	0.0436	0.0791	0.0347	0.0387	0.0501	0.0357	0.0019	0.0345
2011	0.0500	0.0436	0.0791	0.0347	0.0387	0.0501	0.0174	0.0073	0.0254
2012	0.0500	0.0436	0.06865	0.0347	0.0387	0.0501	0.0266	0.0253	0.0422

Table 4.4 show that during the year 2002 and 2012, the errors in the GPS position coordinates were high the higher order ionospheric effect are not corrected. After the GPS position estimates are corrected for the higher order ionospheric effect, the rms errors were reduced. Also we plotted the time series of the GPS coordinates rms for the period beestween 2002 and 2012 to show the effect the solar cycle on the high positioning mission of the GPS services.

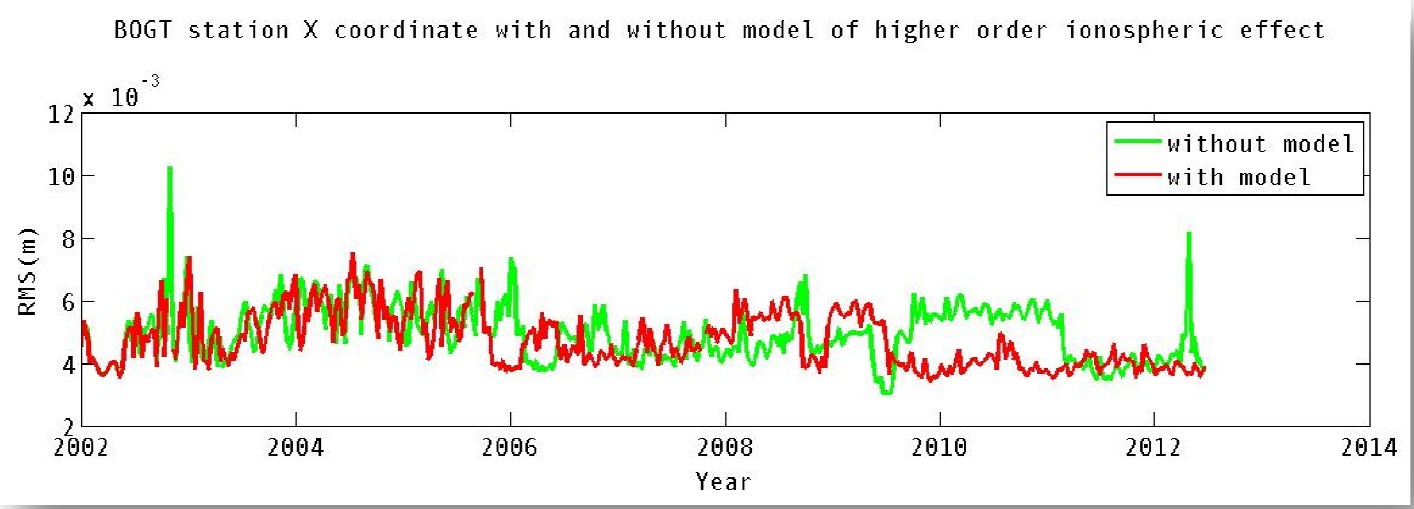

Figure 4-19 BOGT station X coordinate root mean square

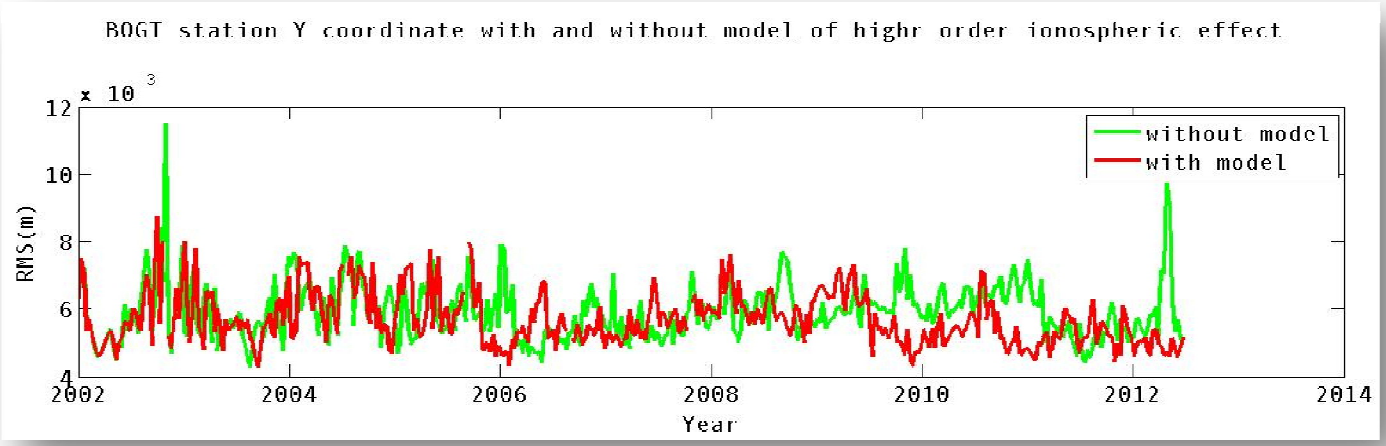

Figure 4-20 BOGT station Y coordinate root mean square

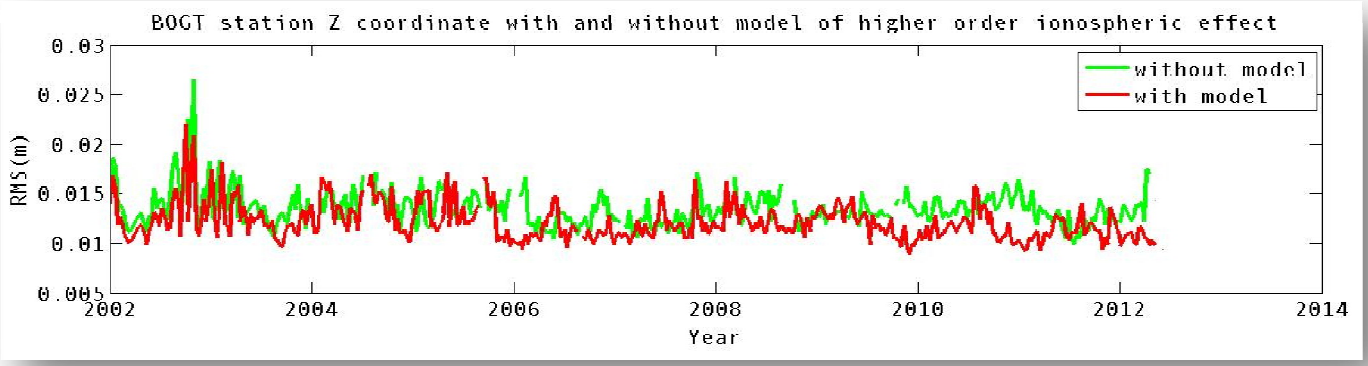

Figure 4-21 BOGT station Z coordinate root mean square

Figures 4.19, 4.20 and 4.21 the green color represents position accuracy without modeling of higher order ionospheric effect while the red color represent when the higher order effects are modeled in our GPS data processing. Again for this equatorial stations the noise where higher around 2002 and 2012. This again presents very high correlations with the solar cycle in 11 years periods.

4.8.3. ADIS 3D position root mean square in GAMIT/GLOBK repeatability

Station ADIS is located in Addis Ababa, Ethiopia near the equator. From Table 4.5, we can see that the noise level associated to the higher order ionospheric effects during 2012.

Table 4-5 ADIS root mean square

Year	**Case-1** RMS without 2nd and 3rd order ionosphere effect correction (m)			**Case-2** RMS with 2nd and 3rd order ionosphere effect correction (m)			**Quadratic difference,** i.e., the square root of the differences in the variances		
	N(m)	**E(m)**	**U(m)**	**N(m)**	**E(m)**	**U(m)**	**N(m)**	**E (m)**	**U (m)**
2008	-0.005	-0.0169	-0.019	-0.0047	-0.0167	-0.018	0.0017	0.0026	0.0061
2009	0.0057	0.0273	0.0193	0.0029	0.0272	0.0092	0.0049	0.0023	0.0170
2010	0.0433	0.0428	-0.0382	0.0421	0.0385	-0.035	0.0101	0.0187	0.0153
2011	-0.0407	-0.024	0.0485	-0.0036	-0.023	0.0413	0.0405	0.0069	0.0254
2012	0.0891	-0.0964	0.1714	0.0753	-0.0441	0.1167	0.0476	0.0857	0.1255

We have been plotted the time series of residual to study diurnal and seasonal effect of ionosphere.

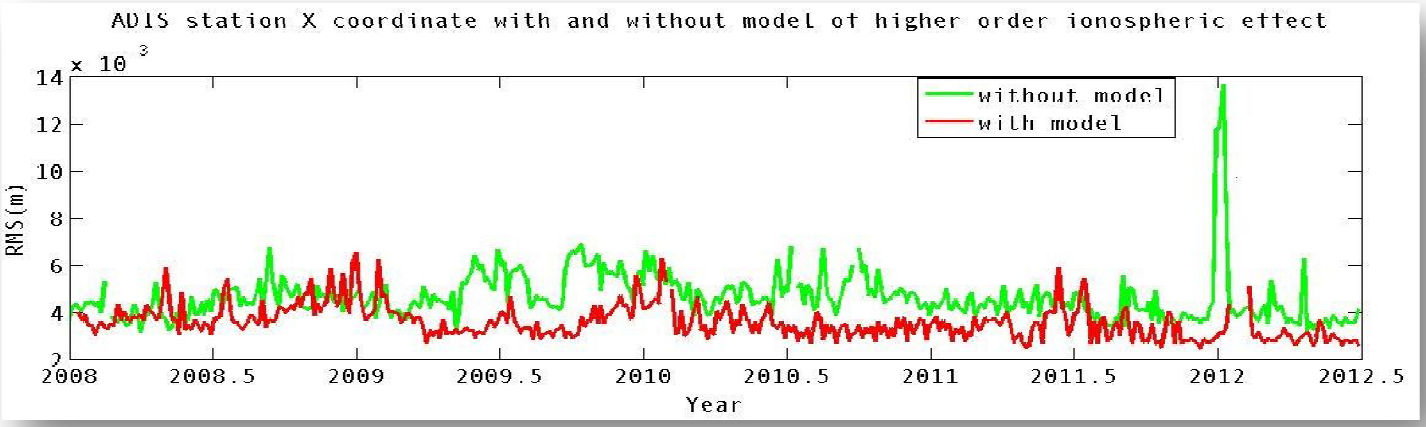

Figure 4-22 ADIS station X coordinate root mean square

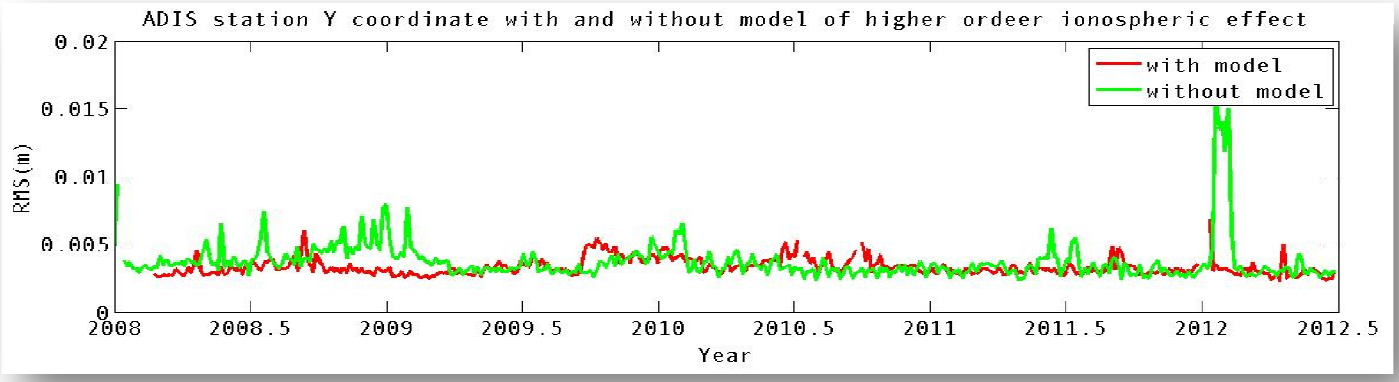

Figure 4-23 ADIS station Y coordinate root mean square

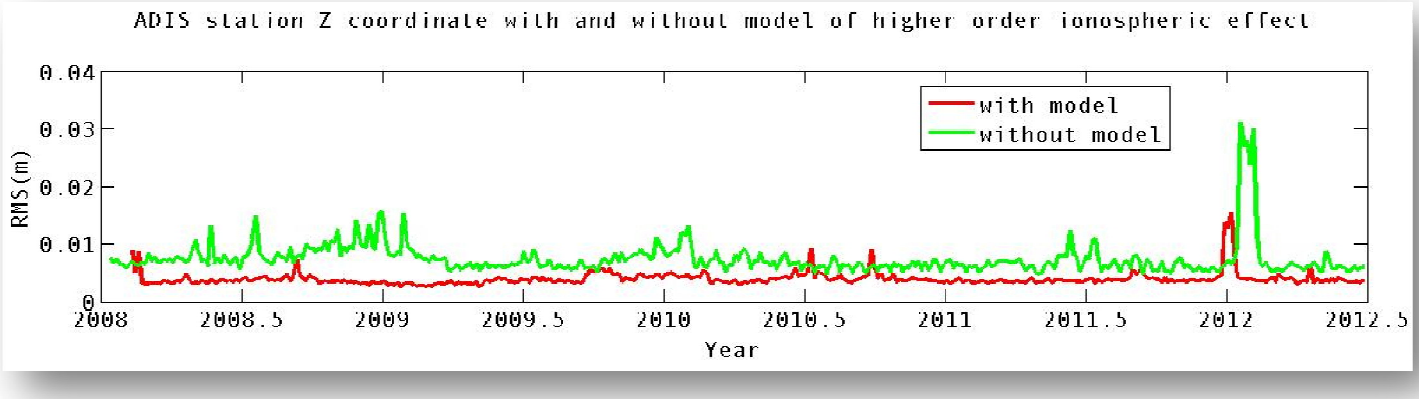

Figure 4-24 ADIS Z coordinate root mean square

In Figures 4.22, 4.23 and 4.24 the green color represents position accuracy without modeling higher order ionospheric effect and the red color with modeled higher order effect correction. The noise level spiked around 2012.

4.9. Signal arrival time measurement and higher order ionospheric time delay

4.9.1. Signal arrival time measurement

The position calculated by a GPS receiver requires the current time, the position of the satellite and the measured delay of the received signal. The position accuracy is primarily dependent on the satellite position and signal delay. To measure the delay, the receiver compares the bit sequence received from the satellite with an internally generated version. By comparing the rising and trailing edges of the bit transitions, modern electronics can measure signal offset to within about one percent of a bit pulse width $\frac{0.01}{1.023*10^6/s}$, or approximately 10 nanoseconds for the C/A code. Since GPS signals propagate at the speed of light, this represents an error of about 3 meters. This component of position accuracy can be improved by a factor of 10 using the higher chip rate P(Y) signal. Assuming the same one percent of bit pulse width accuracy, the high-frequency P(Y) signal results in an accuracy of $\frac{0.01*300{,}000{,}000\ \mathrm{m/s}}{10.23*10^6/s}$ or about 30 centimeter (http://en.wikipedia.org/wiki/Error_analysis).

4.9.2. Higher order ionospheric time delay on L1 and L2 signals

Ionospheric delay of a microwave signal depends on its frequency. It arises from ionized atmosphere. This phenomenon is known as dispersion and can be calculated from measurements of delays for two or more frequency bands, allowing delays at other frequencies to be estimated. Some military and expensive survey-grade civilian receivers calculate atmospheric dispersion from the different delays in the L1 and L2 frequencies, and apply a more precise correction. This can be done in civilian receivers without decrypting the P(Y) signal carried on L2, by tracking the carrier wave instead of the modulated code. To facilitate this on lower cost receivers, a new civilian code signal on L2, called L2C, was added to the Block IIR-M satellites, which was first launched in 2005. It allows a direct comparison of the L1 and L2 signals using the coded signal instead of the carrier wave.

The effects of the ionosphere generally change slowly, and can be averaged over time. It is also possible to remove using differencing techniques for short baselines. Those for any particular geographical area can be easily calculated by comparing the GPS-measured position to a known surveyed location. This correction is also valid for other receivers in the same general location. Several systems send this information over radio or other links to allow L1-only receivers to make ionospheric corrections. The ionospheric data are transmitted via satellite in Satellite Based Augmentation Systems (SBAS) such as Wide Area Augmentation System (WAAS) (available in North America and Hawaii), EGNOS (Europe and Asia) or Multi-functional Satellite Augmentation System (MSAS) (Japan), which transmits it on the GPS frequency using a special pseudo-random noise sequence (PRN), so only one receiver and antenna are required (http://en.wikipedia.org/wiki/Error_analysis)).

4.9.3. L1 and L2 time delay ADIS station

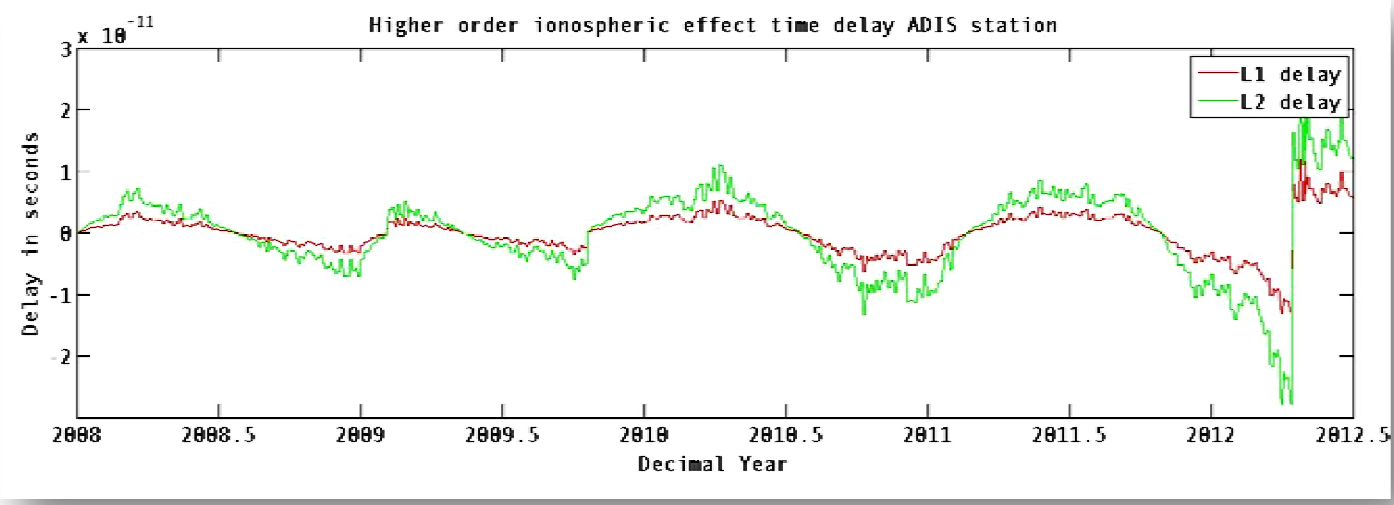

Figure 4-25 L1 and L2 time delay ADIS station

Figure 4.25 show us there are high time delay in L2 during 2012. The reson of high time delay in L2 is the frequency of L2 signal is lower than L1 signale (L1 = 1575.42 MHz and L2 = 1227.6 MHz).

4.9.4. L1 and L2 signal time delay BOGT station

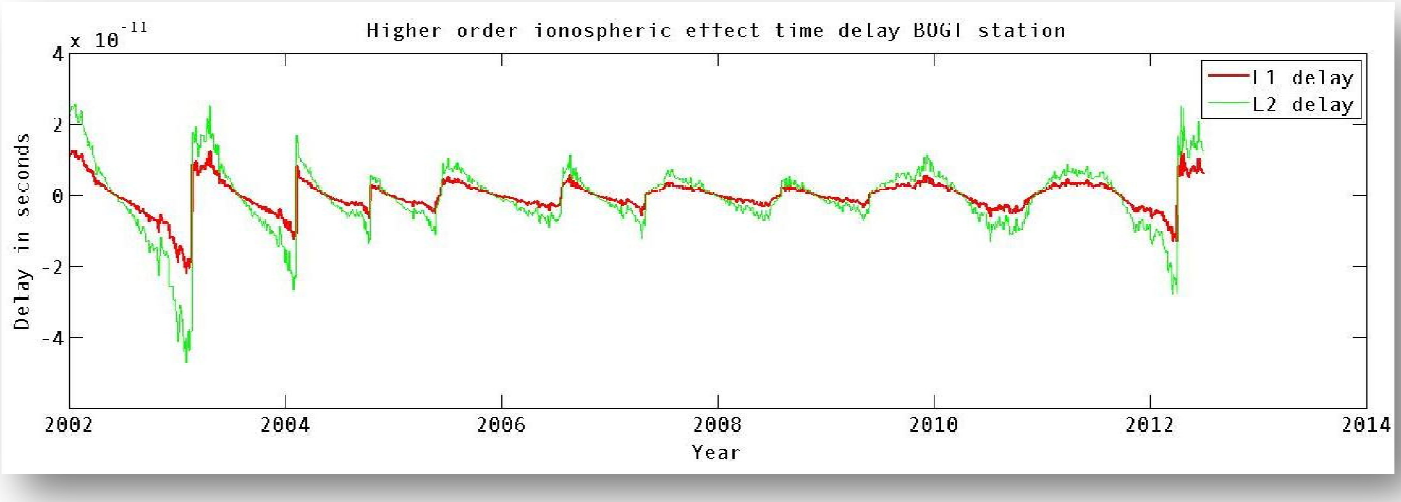

Figure 4-26 L1 and L2 time delay

Figure 4.26 the green color represents higher order ionospheric effect L2 phase delay and the red color represents L1 phase delay. During 2002 and 2012 the delay were high. It shows the solar cycle effect, during these years there were high solar maxima.

4.9.5. L1 and L2 signal time delay BAKO station

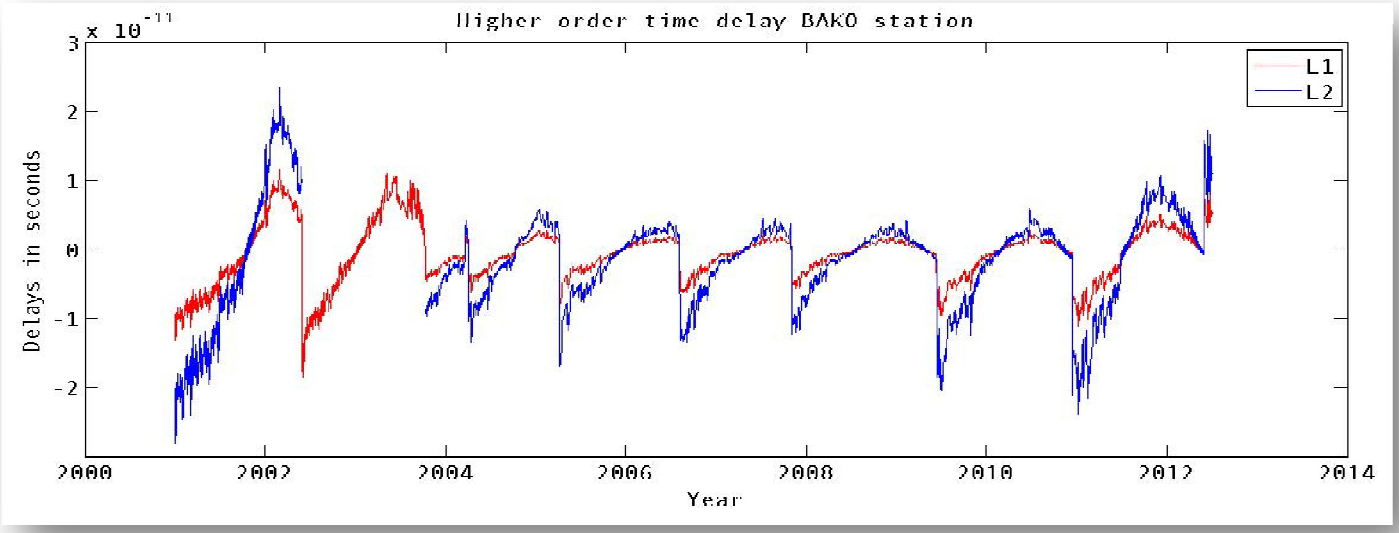

Figure 4-27 L1 and L2 time delay BAKO station

Figure 4.27 blue colors represent time delay due to higher order ionospheric effect in L2 phase signal and the red color represent time delay due to higher order ionospheric effect in L1 phase signal. During 2002 and 2012 the delay were high this is because of high solar activity during these periods.

4.10. Repeatability time series comparison of equatorial region to the North Pole

As we have explained in the objective of the research, we have compared the ionosphere effects of some of GPS stations along the equatorial regions to the North Pole. Therefore, we compared 2012 daily processed GPS data equatorial regions to GPS stations along the North Pole.

4.9.1 ADIS Station: along the Equator

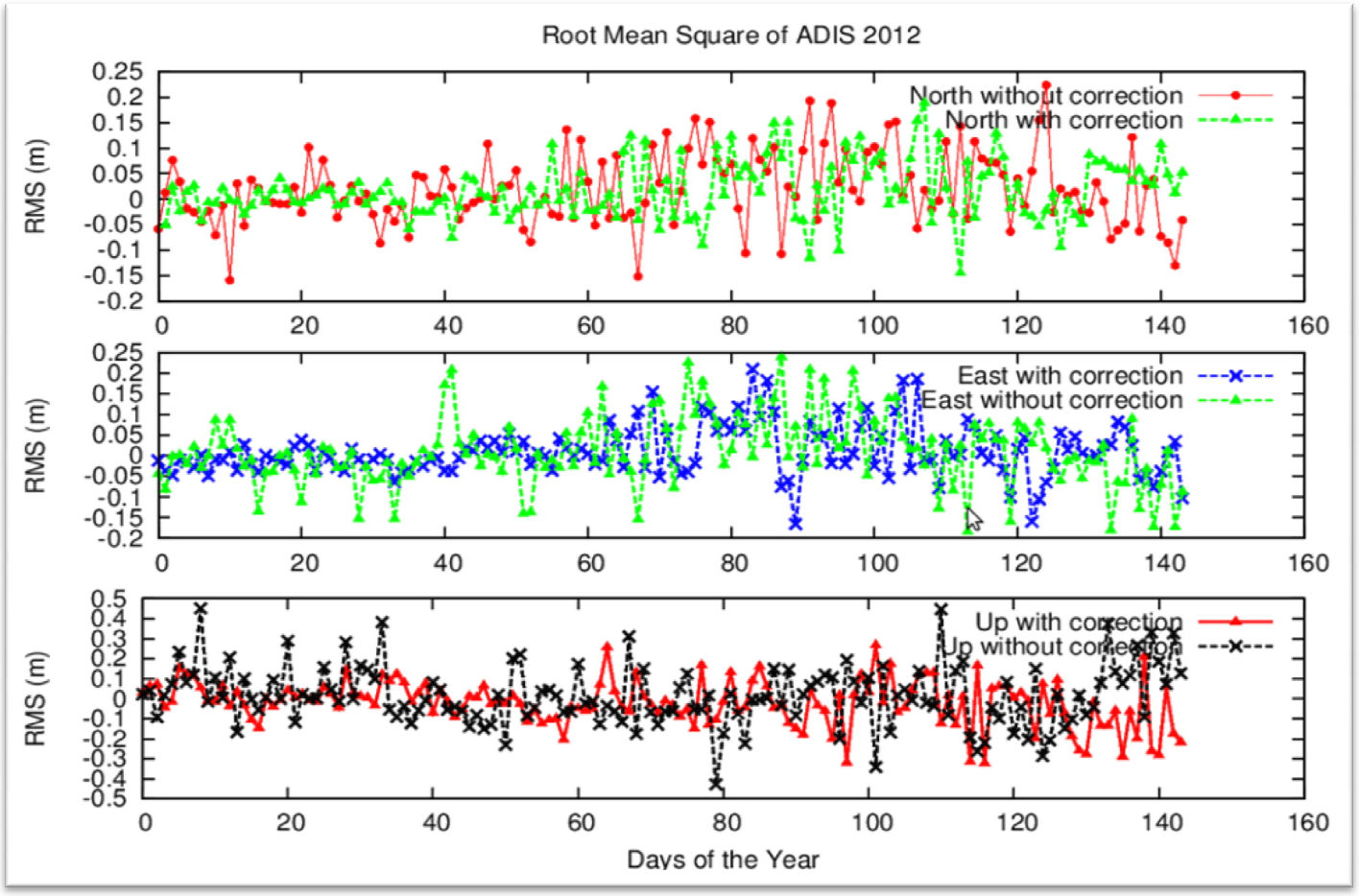

Figure 4-28 Root mean square of ADIS 2012

From Figure 4.28 we observed that, the rms errors in the north, east and up coordinates were high without ionosphere effect correction.

4.9.2. BAKO Station: along the Equator

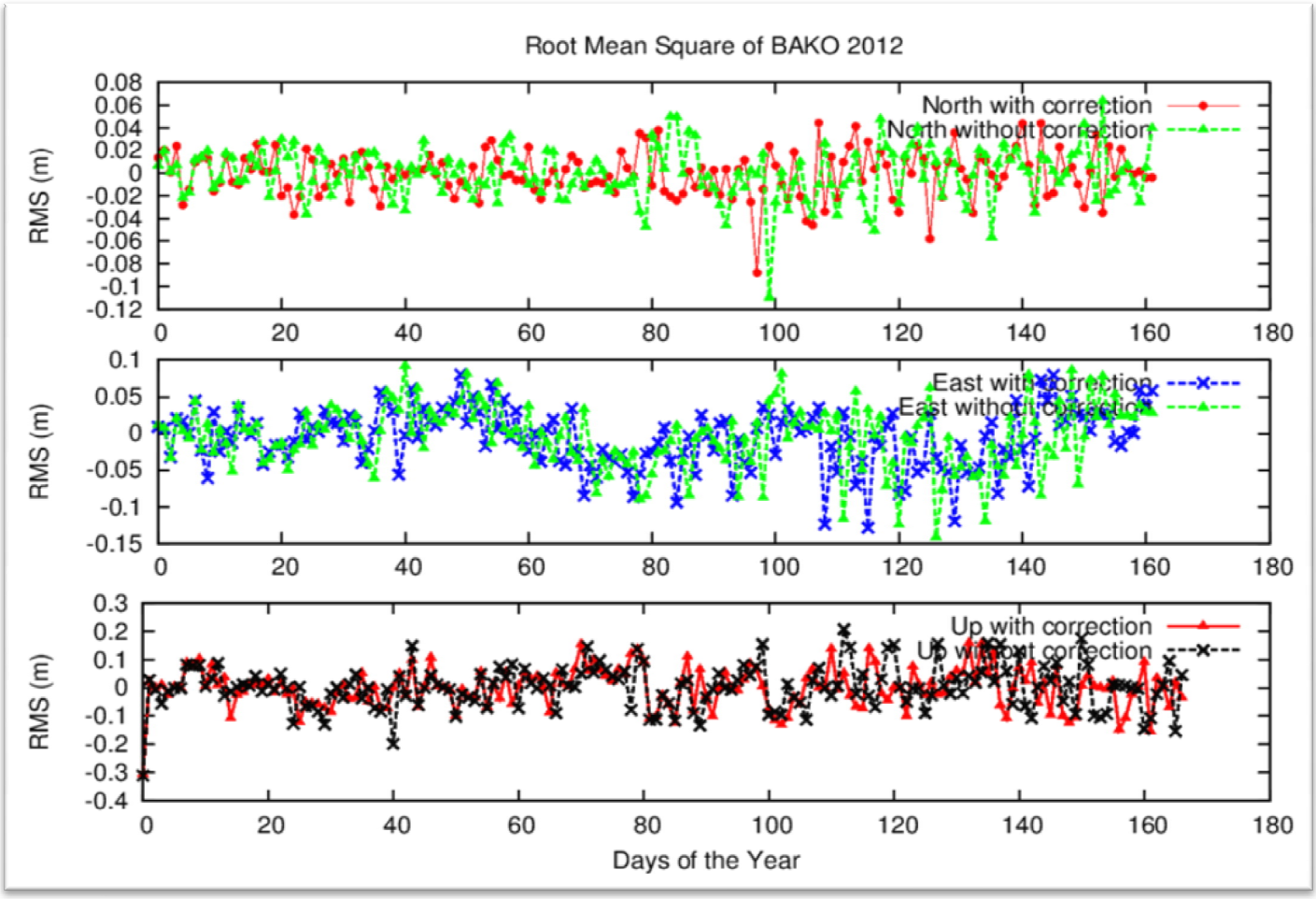

Figure 4-29 Root Mean Square BAKO Station 2012

From Figure 4.29 errors without second and third order ionosphere effect correction were high along north, east and up coordinates. This is also clearly well correlated with the sun spot numbers (see Figure 20.)

4.9.3. FAIR Station: At high northern latitude

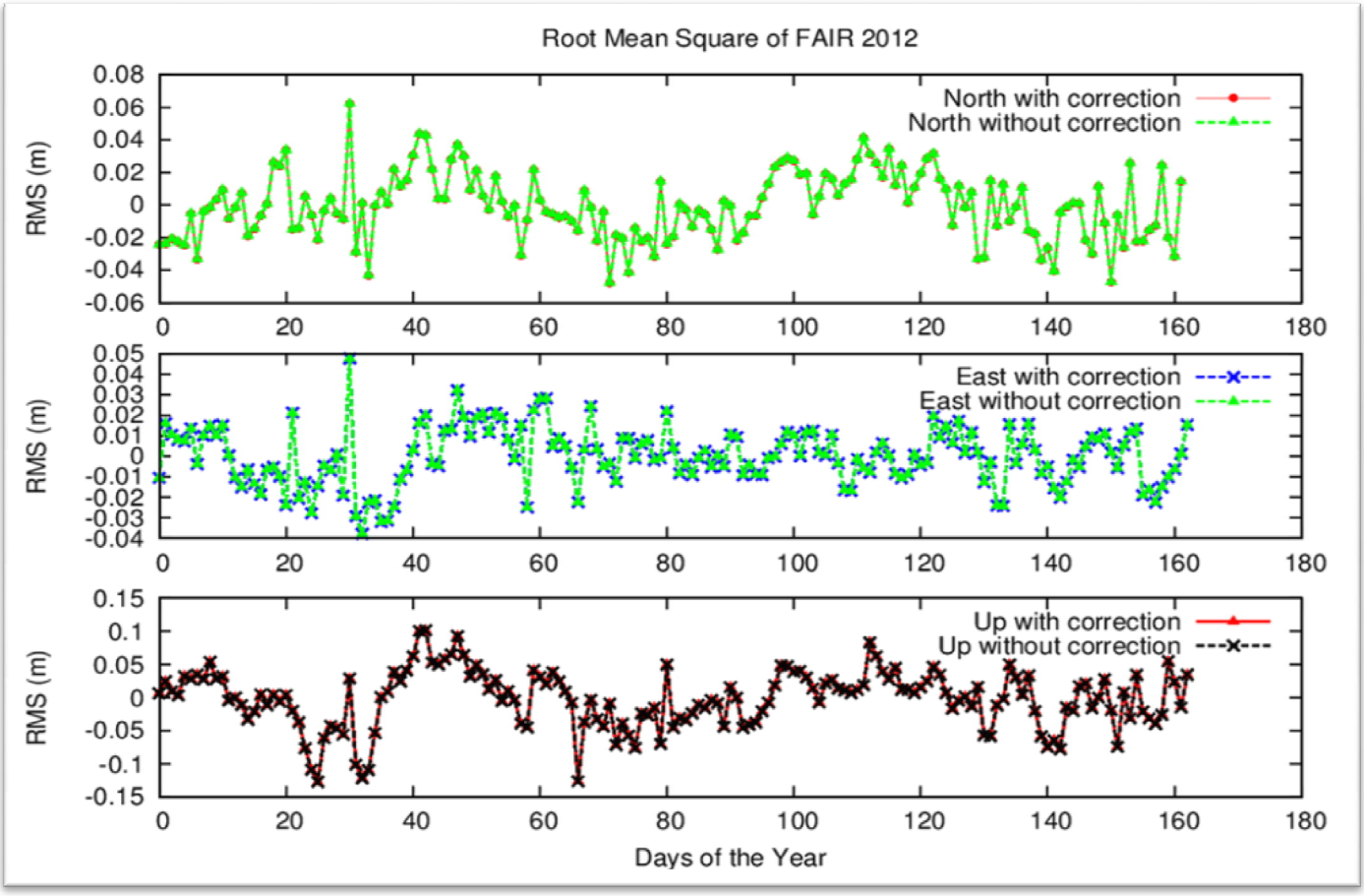

Figure 4-30 Root Mean Square FAIR Station 2012

In Figure 4.30 FAIR station is found at latitude of $64.2673^0\ N$. Errors with second and third order ionosphere effect correction and without correction were almost identical. Therefore, in the equatorial regions there is a higher ionosphere effect than at higher latitude due to the geomagnetic electron jet (EEJ) belt.

Chapter Five

5.1. Conclusion and Recommendation

5.1.1 Conclusion

- After we studied higher order ionospheric effect we found possible solutions to eliminate ionospheric effect. We have used empirical mathematical models, linear combination techniques to model ionospheric effect and different software such as GPS-TEC, QC and IRI-2007 to study the diurnal and seasonal effect of ionosphere.
- We also studied the correlation between geomagnetic field and TEC. Our result shows there is high correlation between geomagnetic field and TEC. Especially the H component of the geomagnetic field has good correlation to the TEC. The reason is, the H component of geomagnetic field is the flow of geomagnetic filed in east-west directions and this field has a direct effect on the Equatorial Electro-Jet (EEJ).
- After processing the data we have analyzed the errors with and without higher order ionospheric effects. The result showed that modeling of higher order ionospheric effects reduces the root mean squares and this effect is more pronounced in higher solar cycles. In higher solar activities (2002 and 2012) the root mean square were in several centimeter levels and when we modeled 2^{nd} and 3^{rd} order ionosphere effect the rms values becomes in reduced.
- High total electron densities found in f layers of ionosphere. Because the f layer it is the upper part of the ionosphere containing its longer portion of spherical shell. In GAMIT/GLOBK software the maximum single layers of ionosphere height set 450 km. We processed and modeled 2^{nd} and 3^{rd} order ionosphere effects at this height and we edited this height from 450 to 350 km. We got different results by varying the height of ionosphere layers (see, more plots on appendices 2.1).
- We have also studied higher order ionospheric effect time delay of L1 and L2 phase signal for ADIS, BAKO, and BOGT stations. The time delays were $-2\ to\ 3\ \times 10^{-11}$seconds to ADIS and BAKO stations and $-4\ to\ 4\ \times 10^{-11}$ second for BOGT station. L2 signal has a higher time delay than L1 this is because of higher noise level of the L2 signal. When the height of ionosphere increases the time delay also increases. Because the more total electron densities delay the signal (see, more plots on appendices 2.2)

5.1.2 Recommendation

- In single frequency receiver the effect of ionosphere is very high so we recommended that this high error must be corrected by using different models like Klobuchar, Global Ionospheric map, International reference of ionosphere model.

- The first order ionosphere effect depends on the total electron content densities. But this error can be avoided by using dual frequency receivers and making linear combinations. However, linear combinations tend to increase the noise level in the combined solution. So we recommended that when we make linear combination we must also take in to account the noise levels for shorter baseline solutions.

- Higher order of ionosphere effect is very small (1% of the total ionosphere error). Even though this small error must be account when we need very accurate positioning.

- Higher order ionosphere effect depends on the slant total electron content, frequencies, geomagnetic field of the earth and the angle between signal wave vector and the geomagnetic field vector at the IPP. It is necessary to incorporate the higher order ionospheric correction (I2 and I3) as a standard term in precise GNSS models. A combined contribution of the I2, I3 effect can reach several millimeter ranges.

Bibliography

1. Alfred Leick, (1992): Delineating Theory for GPS Surveying. American Society of Civil Engineers
2. Attila Grandpierre (December 3, 2004). "On the origin of solar cycle periodicity". Astrophysics and Space Science 243 (2): 393–400. Bibcode 1996Ap&SS.243..393G. doi: 10.1007/BF00644709.
3. Boucher C, Altamimi Z (2001): ITRS, PZ-90 and WGS 84: current realizations and the related transformation parameters. Journal of Geodesy, 75(11): 613–619.
4. C.A.Onwumechili, Okeke, F. N., Agodi Onwumechili, C., & Rabiu, B. A. (1997), Day-to-day variability of geomagnetic hourly amplitudes at low latitudes, Geophysical Journal International, Volume 134, Issue 2, pp. 484-500.
5. Charvátová I. (2000). "Can origin of the 2400-year cycle of solar activity be caused by solar inertial motion?" (PDF). Ann. Geophys. 18 (4): 399–405. Bibcode 2000AnGeo..18..399C. doi:10.1007/s00585-000-0399-x. http://www.ann-geophys.net/18/399 /2000/angeo-18-399-2000.pdf.
6. Charvatova, Hejda (2008-9) (PDF). Possible role of the Solar inertial motion in climatic changes. CA: Bill Howell.
7. Datta-Barua, S., Walter, T., Blanch, J., and Enge, P.: Bounding higher order ionosphere errors for the dual-frequency GPS user, Radio Sci., 43, RS5010, doi: 10.1029/2007RS003772, 2008.
8. Dr. Gopi (2008), GPS-TEC analysis application, Institute for Scientific Research, Boston College, 140 Commonwealth Avenue, Chestnut Hill, MA - 02467, U.S.A
9. E. Pallé (2010). The Earth as a Distant Planet: A Rosetta stone for the Search of Earth-Like Worlds (Astronomy and Astrophysics Library). Berlin: Springer. pp. 316–317. ISBN 1-4419 1683-0.
10. Feairheller S, Clark R (2006): Other satellite navigation systems. In: Kaplan ED, Hegarty CJ (eds): Understanding GPS – principles and applications, 2nd edition. Artech House, Norwood: 595–634.
11. H. Schwentek and W. Elling (July 1984). "A possible relationship between spectral bands in sunspot number and the space-time organization of our planetary system". Solar Physics 93 (2): 403–13. Bibcode 1984SoPh...93...403S. doi: 10.1007/BF02270851.
12. Hein GW, Pany T (2002): Architecture and signal design of the European satellite navigation system Galileo – status December 2002. Journal of Global Positioning Systems, 1(2): 73–84.
13. O. Colombo, Hernandez-Pajares M., Juan J.M., Sanz J., J. Talaya. (1999, 2000), Resolving carrier-phase ambiguities on-the-fly, at more than 100Km from the nearest reference, with the help of ionospheric tomography (Best paper award, Group of Astronomy and Geomatics, Universitat Politècnica de Catalunya (gAGE/UPC) , Barcelona, Spain
14. Héroux P, Gao Y, Kouba J, Lahaye F, Mireault Y Collins P, Macleod K, Tétreault P, Chen K (2004). Products and applications for precise point positioning–moving towards real-time. In: ION GNSS 17

International Technical meeting of the satellite division, Long Beach, California, pp. 1832-1843.Hofmann-Wellenhof B, Lichtenegger H, Collins J (2001): GPS – theory and practice, 5th edition. Springer, Wien New York.

15. Hofmann-Wellenhof B, Lichtenegger H, Collins J (2008): GPS – GNSS – Global Navigation Satellite Systems, Springer, Wien New York.

16. Kim, B. C. and Tinin, M. V.: Contribution of ionospheric irreg- ularities to the error of dual-frequency GNSS positioning, J. Geodesy., 81, 189–199, doi: 10.1007/s00190-006-0099-8, 2007.

17. KOUBA, J. and P. HEROUX (2001): GPS precise point positioning using IGS orbit products, GPS Solutions, 5 (2), 12-28. KOUBA, J. and T. SPRINGER (2001): New IGS Station and Satellite Clock Combination, GPS Solutions, 4 (4), 31-36.

18. Komjathy, A., R.B. Langley, and D. Bilitza (1998). "Ingesting GPS-Derived TEC Data into the International Reference Ionosphere for Single Frequency Radar Altimeter Ionospheric Delay Corrections." Advances in Space Research, Vol. 22, No. 6, pp. 793-801.

19. Memarzadeh, Yahya, (2009), Ionospheric modeling for precise GNSS applications Delft institute of Earth Observation and Space systems (DEOS), PhD thesis, Delft University of Technology, ISBN-10 90-902468-5 ISBN-13 978-90-902468-5-7 .

20. Menzel, Whipple, and de Vaucouleurs (1970), "Survey of the Universe", NUWC-NPT Technical Report,

21. Roßbach U (2001): Positioning and navigation using the Russian satellite system GLO NASS. Schriftenreihe der Universität der Bundeswehr München, vol 71.

22. Günter Seeber, Univ. Prof. Dr.-Ing. (2003), Satellite geodesy : foundations, methods, and applications 2nd completely rev. and extended edition, ISBN 3-11-017549-5, Germany

23. Parkinson, J. Spilker Jr., P. Axelrad and P. Enge (Jan 1, 1996), Global Positioning System: Theory and Applications, 2-Volume Set (Vol. 163/164) (Progress in Astronautics & Aeronautics), AIAA, ISBN-10: 1563471078 ISBN-13: 978-1563471070

24. Swann J (2006): Will GPS and Galileo have the same or interoperable reference systems? In: Lachapelle G, Petovello M (eds): GNSS Solutions: Reference systems, UTC leap second, and L2C receivers? Inside GNSS, 1(1): 20–24.vstendal

25. Wang, Z., Wu, Y., Zhang, K., and Meng, Y.: Triple-frequency method for high-order ionospheric refractive error modelling in GPS modernization, Journal of Global Positioning Systems, 4, 91–295, available at: http://www.gmat.unsw.edu.au/wang/jgps/ v4n12/v4n12p36.pdf, 2005.

26. Wanninger, L., E. Sard´ n, and R. Warnant (1994), Determination of the Total Ionospheric Electron Content with GPS—Difficulties and their Solution, Proceedings of Beacon Satellite Symposium ’94, edited by Dpt. of Physics of University of Aberystwyth.

27. Yunck, T.P. (1996), Orbit Determination. In Parkinson & Spilker, Jr. (Eds.), Global positioning systems: Theory and applications. Progress in Astronautics and Aeronautics, Volume 163, American Institute of Aeronautics and Astronautics, Inc.

28. Z. G. Elmas et al, (2011): Higher order ionospheric effects in GNSS positioning, Institute of Engineering Surveying and Space Geodesy (IESSG), The University of Nottingham, Triumph Road, Nottingham, NG7 2TU, UK.

29. IGS Central Bureau (2007) The IGS is a voluntary federation of many worldwide agencies that pool resources and permanent GNSS station data. URL: http://igscb.jpl.nasa.gov/faqs.html#id2845337

30. Rose India (2012) Sources of errors in GNSS URL:www.roseindia.net/software-tutorials/detail/19656

31. Wikipedia, the free encyclopedia(2012) Error analysis for the Global Positioning System URL: http://en.wikipedia.org/wiki/Error_analysis_for_the_Global_P

32. Wikipedia, the free encyclopedia (2012) Solar flare URL: http://en.wikipedia.org/wiki/Solar_flare

33. Wikipedia, the free encyclopedia (2012) Earth magnetic field URL: http://en.wikipedia.org/wiki/Earth's_magnetic_field

34. Journal of geophysical research (2006) Equatorial Electrojet URL: http://info.geomag.us/equatorial_electrojet.html

35. GNSS Research Group (2013) Ionosphere : Tutorial URL: http://gnss.be/ionosphere_tutorial.php#x2-70000

Appendices

Appendices1.

1.1. GAMIT/GLOBK processing procedures

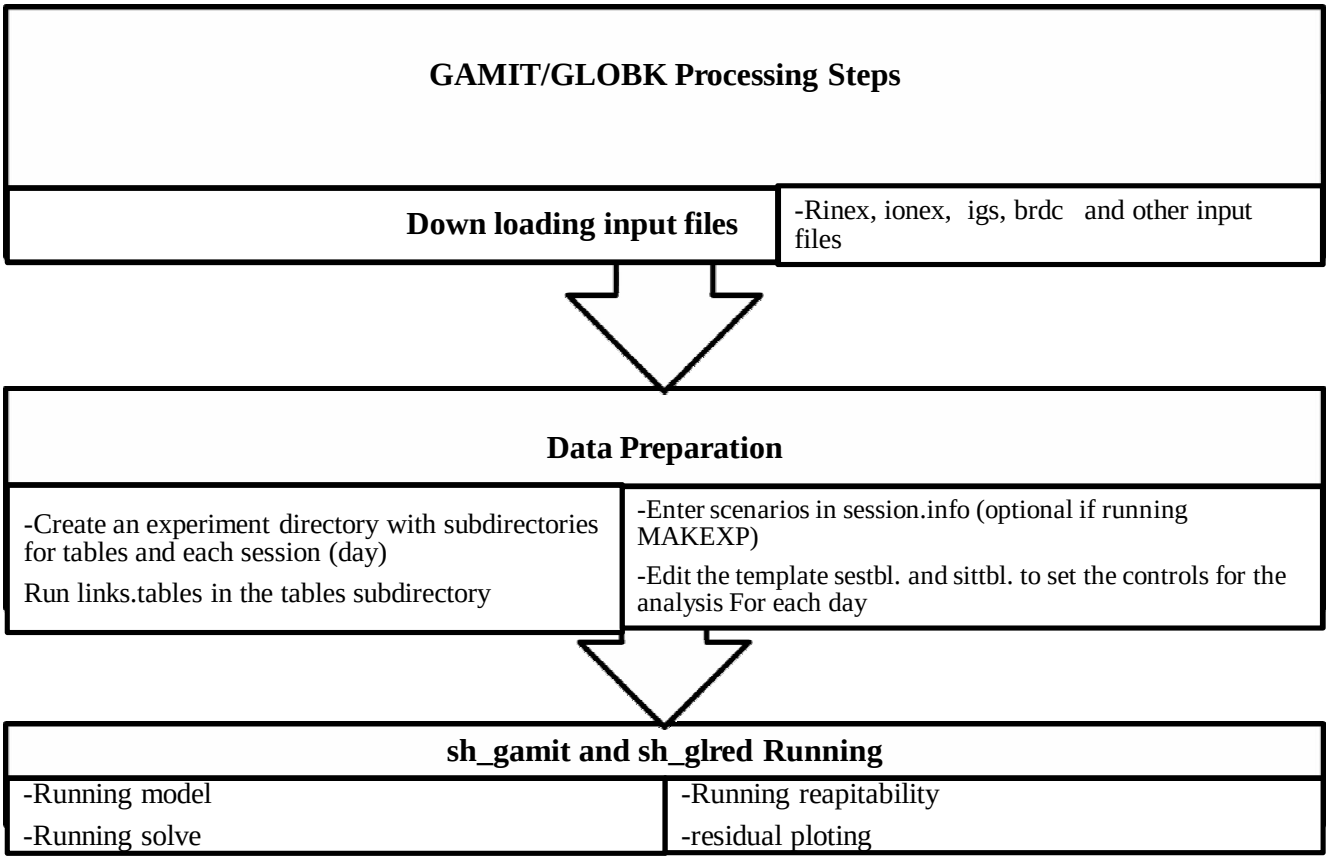

Detail Processing Steps

- mkdir (filename) we used this command to create directory and we put the file name of the directory.
- cp –r /directory/ this command is to copy all input data to our directory
- sh_setup -yr year (for example sh_setup –yr 2002) this script create tables.
- cd ../tables this command is to change the directory from previous directory to tables
- cp –r /directory/ this command to copied process.defaults, sites., defaults, sittbl., itrf08.apr and sestbl.
- sh_upd_stnfo -l sd this script will create 'station.info.new', using from the SOPAC station.info only the sites listed in sites.defaults. After checking, rename it to 'station.info' (overwriting the no-longer-useful SOPAC station.info).

- sh_gamit_Bob -expt expt -s 2008 001 365 -pres ELEV -orbit IGSF -copt x k p z -dopts c ao –noftp this script is to process daily data of 2008 without 2nd and 3rd order ionosphere model
- sh_gamit_Bob -expt expt -s 2008 001 365 -pres ELEV -orbit IGSF -copt x k p z -dopts c ao –noftp –ion this script is to process daily data of 2008 with 2nd and 3rd order ionosphere model
- sh_glred –s 2002 001 2002 365 –expt expt –opt H G E this script provides an efficient way to generate time series from a combination of regional and global data. The input is a specified set of regional and/or global networks, a total span of days to be processed, and the number of days to be combined in each solution. The script then collects H-files from your GAMIT processing and external sources, runs glred and glorg to produce a solution for each group, and generates repeatability plots.
- Now we created two directories tables and vsoln
- Being on vsoln, type ls ../????/glbf/h*.glx > expt.gdl
- glred 6 globk_comb.part globk_comb.log expt.gdl globk_comb.cmd this script is to run repeatability expt.gdl binary file will be created
- sh_plotcrd -f globk_comb.org -s long-res -o 1 -vert -col 1 -x 2000.0 2005.0 this script plots the residuals from 2000 to 2005 repeatability (GAMIT Documentation, 2010).

Running sh_gamit and sh_glreg

Using sh_gamit

The most complex feature of sh_gamit is the procedure by which raw and RINEX files are gathered for each day of a survey. The simplest situation is when you have all of the data on your local system in RINEX form and placed into the /rinex directory under the experiment directory before you start. In this case, you should leave blank all of the variables associated with collecting additional data: /raw, /rawfnd, /rnxfnd in process.defaults and the ftpraw and ftprnx tokens of sites.defaults. If you need to acquire global RINEX files from an IGS data center, you may specify the stations using ftprnx in sites.defaults. Sh_gamit will invoke sh_get_rinex for the CDDIS, SOPAC, and UNAVCO archives and ftp to your /rinex directory all stations specified that are available. A more complicated situation arises when you have a mixture of raw and RINEX data, which may be archived in multiple directories on your system or at a remote data center. The /rawfnd and /rnxfnd variables of process.defaults specify a path to multiple-level raw and RINEX directories which will be searched for any data files available for the day being processed. In this case, sh_gamit will create links within the experiment /raw and /rinex directories to the files in the /rawfnd and /rnxfnd paths.

Any case-folding or renaming necessary to create standard file names for raw files will be done for the links in /raw, leaving the original names in /rawfnd unchanged. Whatever the mix of raw and RINEX files

available, sh_gamit will compare the lists of X-, RINEX, and raw files available, and perform translations only when the product file is not available. If you wish to force retranslation of raw to RINEX, you must remove the product files before you start. X-files are remade whenever there is a change in session information (-sessinfo in the command line, or a change in the session.info file) or when you specify –remakex Y.

You can command sh_gamit to processing sessions spanning UTC day boundaries so long as you set the session information appropriately with -sesfo in the command line (or change sint, nepc, and stime in process.defaults) and have rx_doy_plus and rx_doy_minus each set to 1 (default) so that RINEX files from both days will be downloaded (if necessary) and linked into the day directory. The most awkward aspect is the orbits. If the overlap into the shortest day is only a few hours, then you can safely extrapolate from the primary day both the navigation files (for the satellite clocks) and the precise orbit files (SP3) converted to a G-file and integrated for the full span of the data) without losing accuracy, at least for regional networks. There is a danger, however, that a satellite will have experienced a “burn” or clock event not accounted for by the navigation or SP3 files. A safer procedure, and one which is necessary if the session extends many hours into an adjacent day, is to merge the navigation file and SP3 files for the two days. For the navigation message, you can simply concatenate the two brdc files, naming the resulting file with the day number you wish to use for the processing. For the precise orbits, you can run sh_get_orbits or sh_sp3fit with SP3 files for both days specified to get a G-file fit to the GAMIT (arc) orbit that best matches the SP3-file values over the two days. With this procedure, any discontinuities any the orbit will manifest themselves in a poor fit, and the satellite removed automatically from the G-file. For example, for a session spanning days 71 and 72 of 2009, you can run in the /igs directory

sh_get_orbits -yr 2009 -doy 71 -ndays 2 -multiday -max_fit_tol 0.1

which will produce gigsf9.071 with a set of initial conditions and radiation pressure parameters at 12:00 UTC on day 71 using the IGS final SP3 files for days 71 and 72. A satellite will be excluded from the G-file if the rms of its fit is greater than 10 cm (the sh_gamit default is 20 cm, but there is no default for sh_get_orbits.) You can check the consistency of the orbits by examing the output file sp3fit_igsf9071.rms.

If you have previously downloaded the SP3 files for days 71 (GPS week 1522 day 4) and 72 (GPS week 1522 day 5) then the command would be

sh_sp3fit -f igs15524.sp3 igs15525.sp3 -o igsf -d 2009 71 -m 0.1

If the larger part of your session is on the second day, then you may prefer to process the data in the day directory for the second day. In this case, you will need to manually rename (or link) a G-file produced for 12:00 UTC on the first day so that its name corresponds to the second day.

Using sh_glred

This script provides an efficient way to generate time series from a combination of regional and global data. The input is a specified set of regional and/or global networks, a total span of days to be processed, and the number of days to be combined in each solution. The script then collects H-files from your GAMIT processing and external sources, runs glred and glorg to produce a solution for each group, and generates repeatability plots. The search areas for H-files may include GAMIT day directories, any number of other local directory trees, and the MIT and SOPAC archives. Sh_glred is executed from the experiment-level directory, but runs in a solution directory below it, specified by glbpth in process.defaults. By changing this name you can generate multiple parallel solution directories. Although sh_glred can generate the command files (globk_comb.cmd and glorg_comb.cmd) if they are not present, we recommend that you create them manually by copying the versions in gg/tables into the solution directory and editing them for your task. The most common changes are for the apriori files and for the stations to be used in the solution and for the stations and constraints to be used in defining the reference frame.

Sh_glred is not designed to generate repeatabilities from daily binary h-files that have already been combined or to estimate velocities from H-files spanning several years.

Once you have edited appropriately the command files, you can start the processing from within the experiment directory:

sh_glred -s <yr1 doy1 yr2 doy2> -expt <expt> -net <networks> -local

-netext <char> -yrext <year> -ncomb <num> -stnfo <station.info> -cmd

-opt <A F H L U G E K C R>

where -s is used to specify the start (yr1 doy1) and stop (yr2 doy2) year and day-of-year for the processing, -expt is the 4-character experiment name for the H-files in local day directories (ddd[char]) , and -net indicates the external H-files to be included. The options are MIT for the global MIT processing, igs all (shorthand for igs[1-6]) for the SOPAC global processing, or some combination of the regional solutions in the SOPAC archive: California (bard net[1-c]), Basin and Range (ban[1-3] ebr[1-2]), northwest North America(pan[1-

5], akda), southwest US (swu1), eastern US (neu1), and western Eurasia (eura emed). If -local is specified, the script will process only days within the span for which local data are available; otherwise, it will process all days within the span for which it can find external H-files. The days to be processed can also be specified explicitly using -d yr doy1 doy2 doy3 ..., or with -r days to indicate that processing should commence a certain number of days (days) before the current date and continue until there are no more local or external files to include. The local directories are searched by default with the day-of-year, but can be restricted by specifying a network suffix (e.g, 035r) with -netext or a year prefix (e.g. 1997_) with -yrext. The optional argument -ncomb is used to specify the number of days to include in each combination. The default is 1 day, but you can also use the script to produce weekly or monthly averages of local or global files. The argument (-stnfo) is the name of the station.info or SINEX file to be read by program hfupd; the default is ../tables/station.info.

The following processing tasks are available, listed in the order in which they are performed:

<R> Remove old h*.gl? files from the glfpth directory prior to starting.

<F> Ftp global h-files from the SOPAC archive, search names given by <networks> .

<H> Run htoglb on all ascii files present or linked within glfpth (usually procdir/glbf).

<LA> Link locally archived ascii H-files (all h[net|expt]?.yyddd) for inclusion in the combination.

<LB> Link locally archived binary H-files (all hyymmdd????_[net|expt].gl?) for inclusion

in the combination. Searches are from hfnd down, where hfnd is by default

procdir/glbf but may be specified as multiple paths in process.defaults.

<LC> Link locally generated combined binary H-files (*.GLX)

<U> Run hfupd on binary h-files (not yet tested).

<G> Run glred for combination or repeatabilities.

<E> Run ensum and sh_baseline for plots.

<C> At the end compress the ascii H-files, remove any links, and copy the ascii and binary H-files to glbpth/ascii_yyyy and glbpth/bin_yyyy, respectively, where glbpth is specified by process.defaults [default glbf]

<A> Do all options.

The script uses command files named globk_comb.cmd and glorg_comb.cmd, which it looks for in the solution (e.g. /gsoln) directory. If you wish to alter any of the globk or glorg commands, for example to constrain orbits in a regional solution, change the default EOP constraints, or omit the glorg solution, you can run sh_glred initially with only the –cmd option to create the command files for editing.

Output H-files from the combination are named HYYMMDD_[expt][netext].GLX and written in to the solution directory. The script creates a separate .gdl file for each day with a similar name, each pointing to the combined GLX H-file in the solution directory. When ensum is run, it will create SUM. and VAL. files by concatenating all .org files present, so you can run sh_glred separately for different time spans and create plots that combine the spans (for details see GAMIT Documentation 2010).

Appendices2.

2.1. More figures on different heights of ionosphere layers root mean square

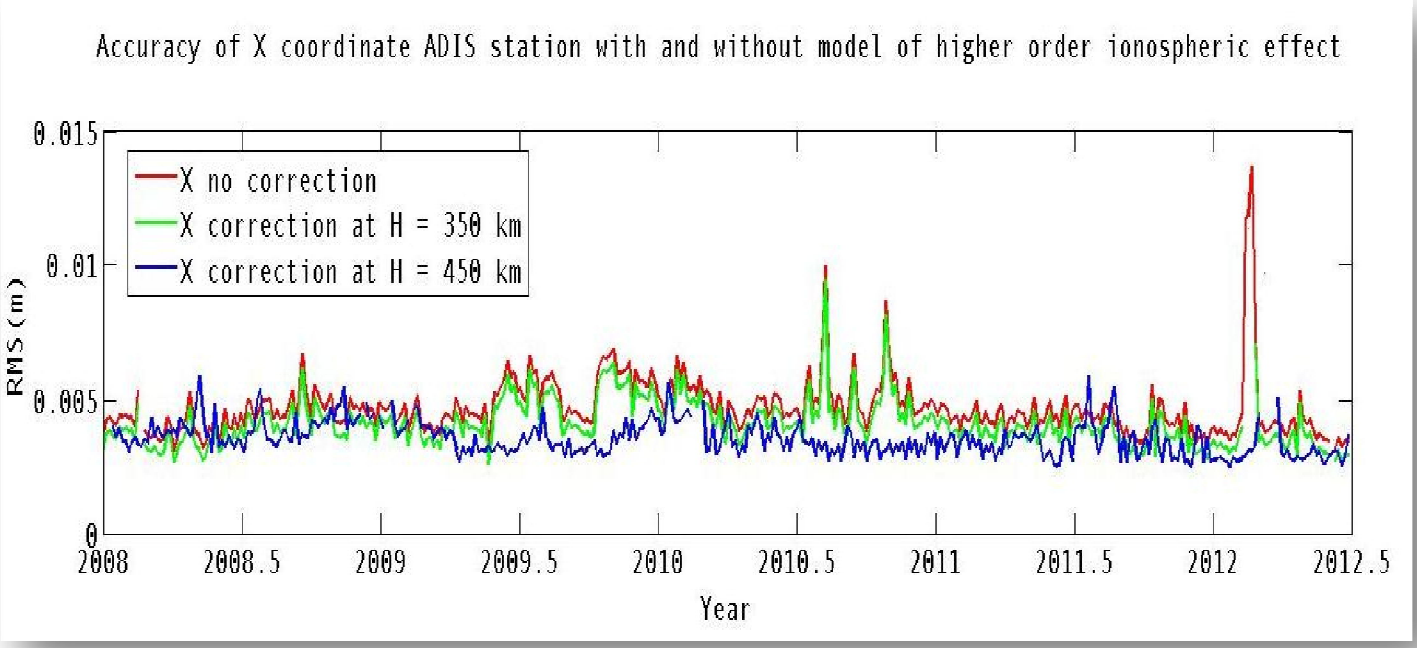

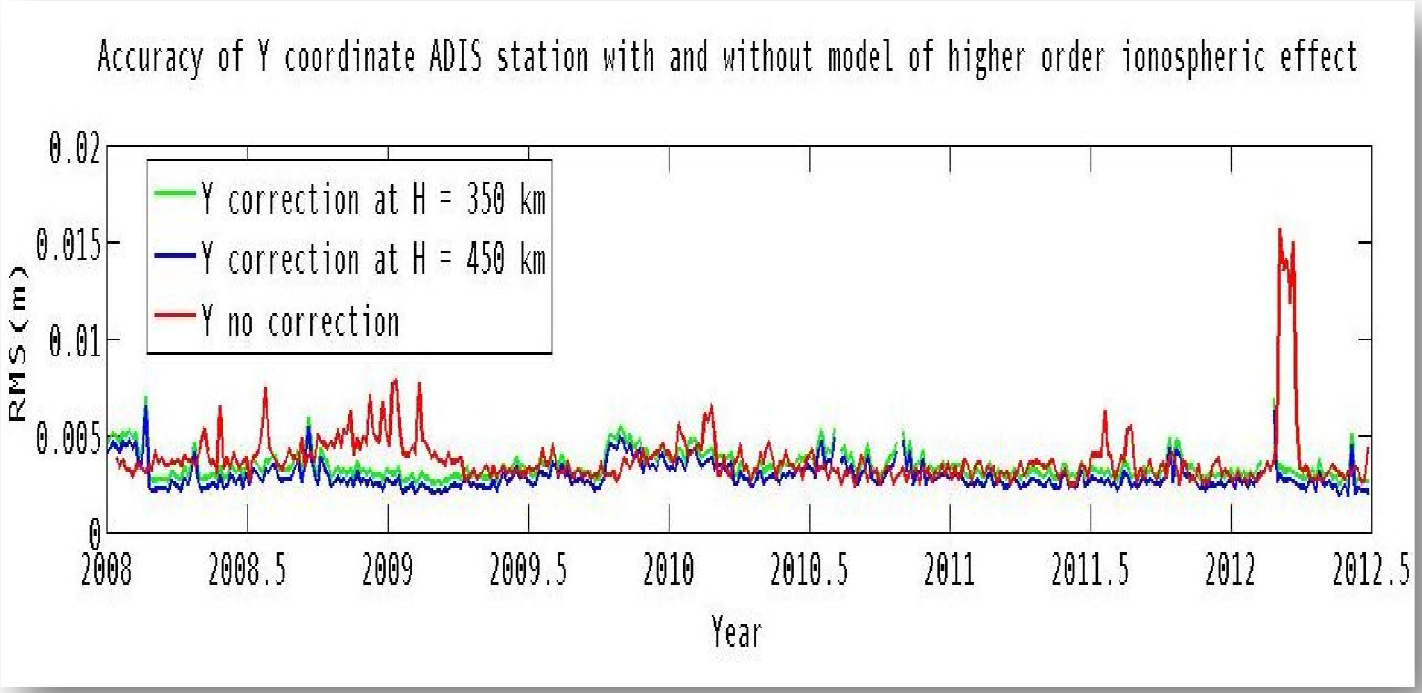
Accuracy of Y coordinate ADIS station with and without model of higher order ionospheric effect
Y correction at H = 350 km
Y correction at H = 450 km
Y no correction
RMS(m)
0.02
0.015
0.01
0.005
0
2008
2008.5
2009
2009.5
2010
2010.5
2011
2011.5
2012
2012.5
Year

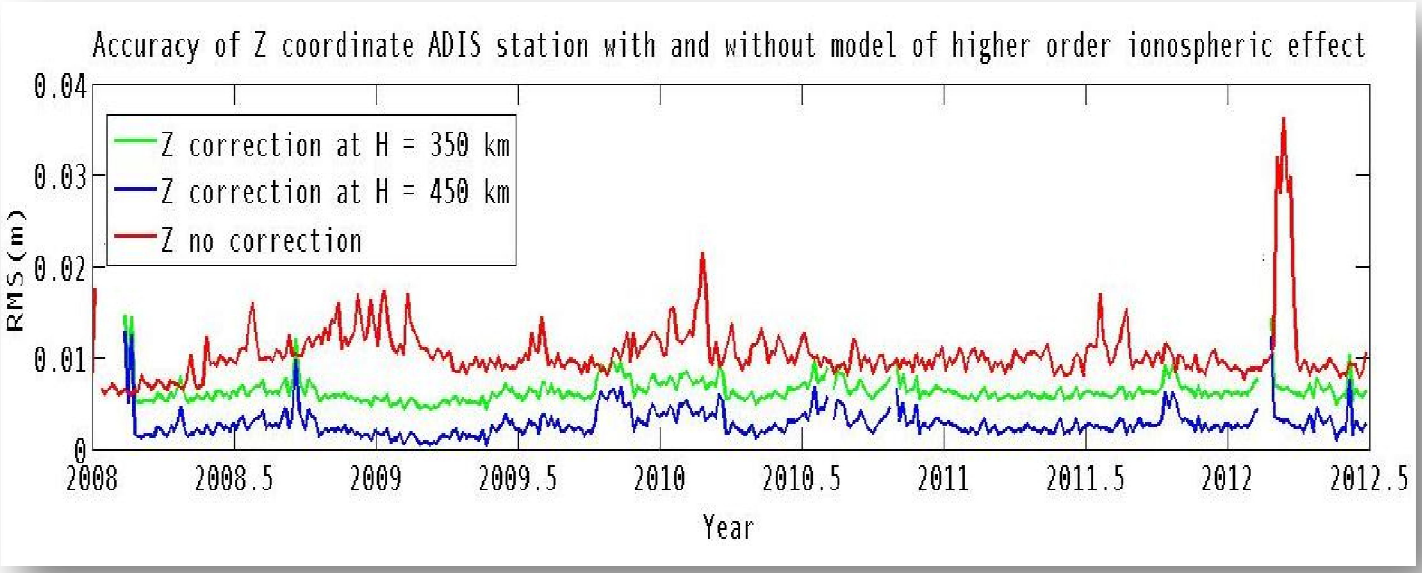
Accuracy of Z coordinate ADIS station with and without model of higher order ionospheric effect
Z correction at H = 350 km
Z correction at H = 450 km
Z no correction
RMS(m)
0.04
0.03
0.02
0.01
0
2008
2008.5
2009
2009.5
2010
2010.5
2011
2011.5
2012
2012.5
Year

2.2. More figure on higher order ionospheric effect time delay at different height of ionosphere laye

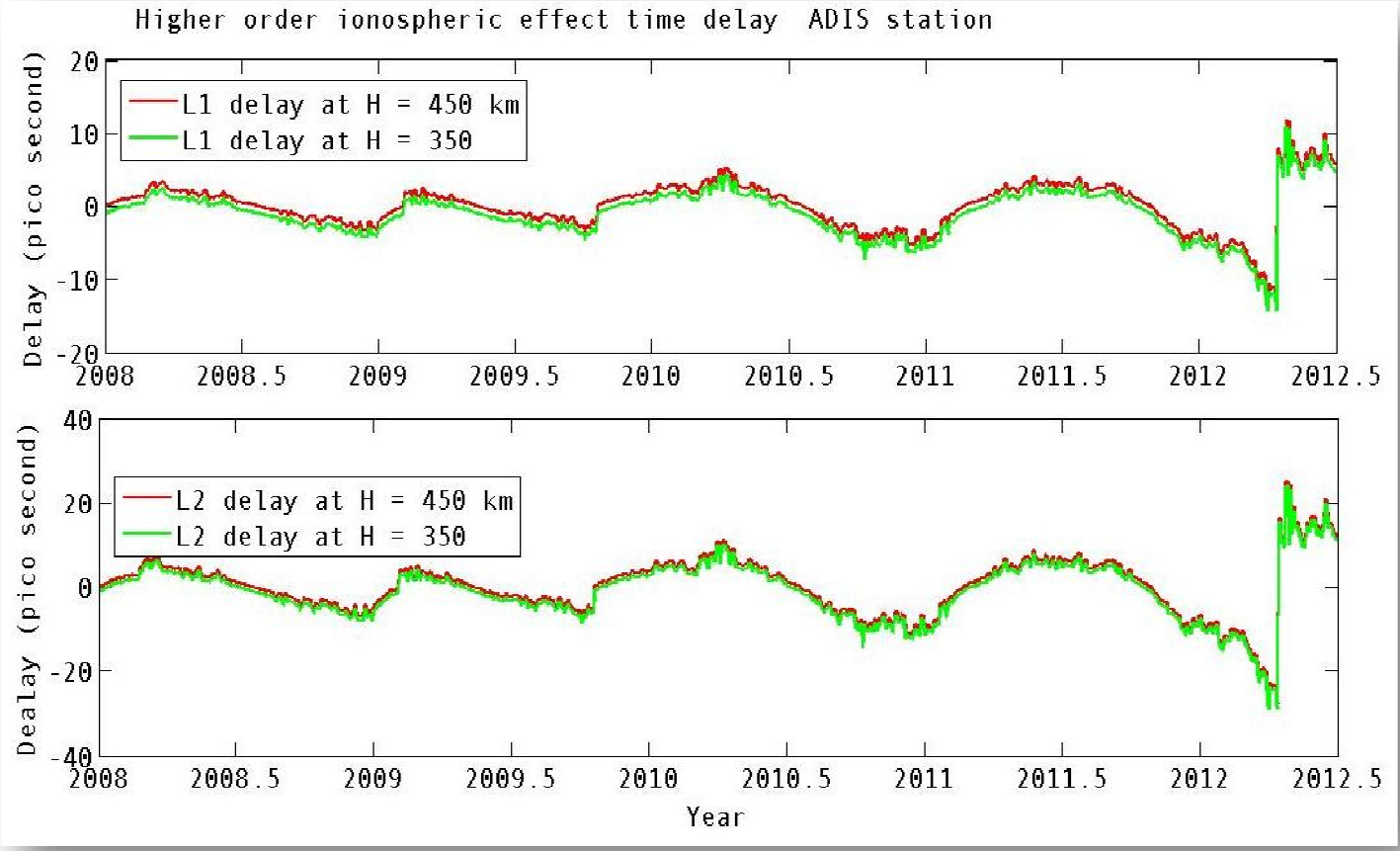

2.3. More figures on TEC

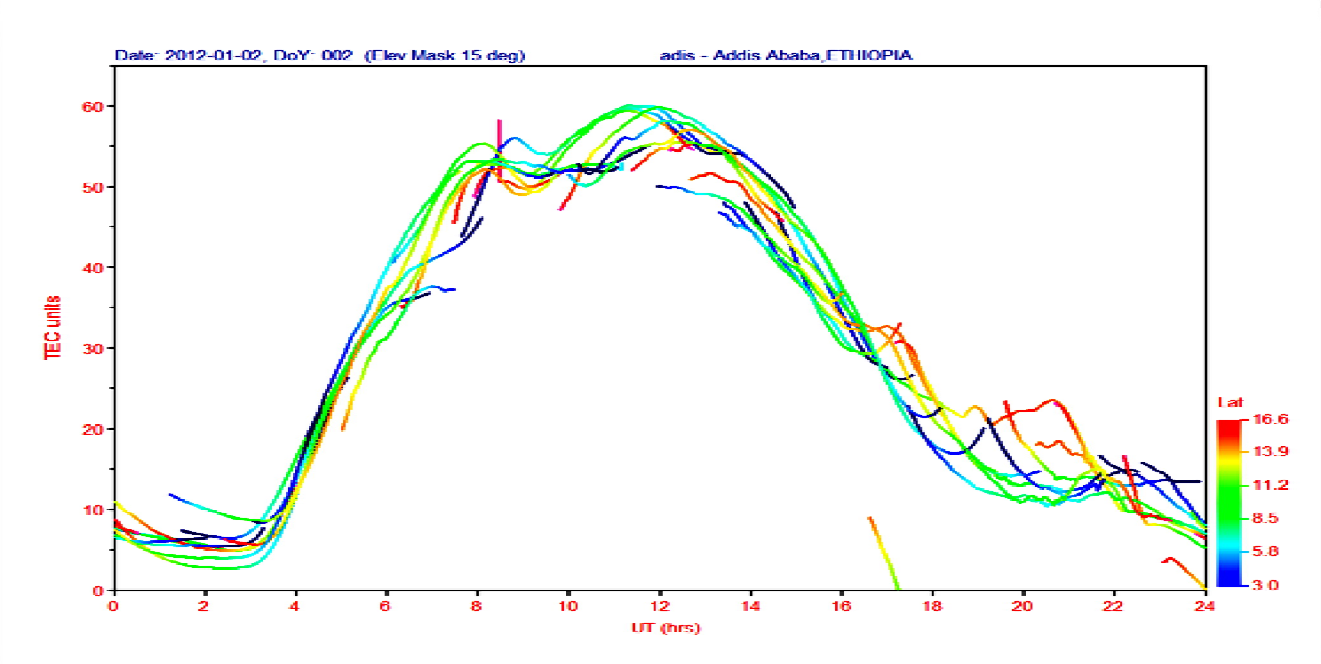

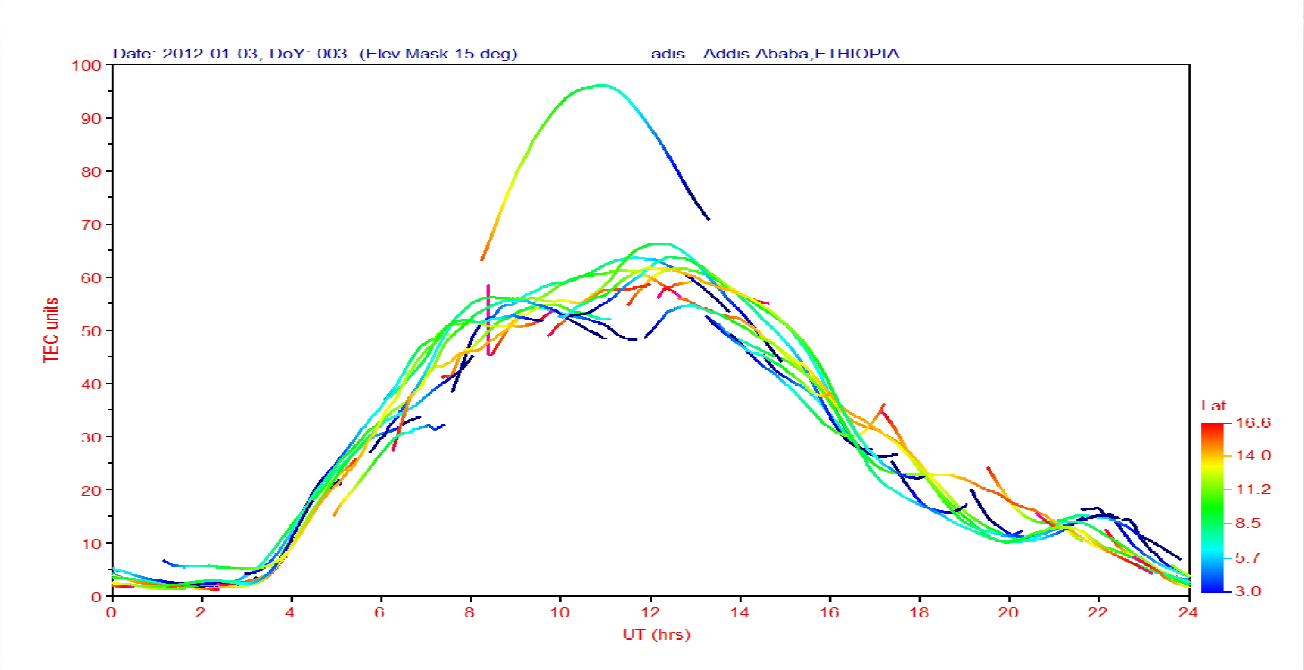

Declaration

"This thesis is my original work and has not been presented for a degree in any other university, and that all sources of material used for the thesis have been duly acknowledged."

SUBMITTED BY:

Asmamaw Chanie Yehun _____ _____

Signature Date

CONFIRMATION:

_____ _____ _____

Advisor(s) Signature Date